Level statistics of real eigenvalues in non-Hermitian systems

Zhenyu Xiao,[1] Kohei Kawabata,[2] Xunlong Luo,[3] Tomi Ohtsuki,[4] and Ryuichi Shindou[1,*]

[1]*International Center for Quantum Materials, Peking University, Beijing 100871, China*
[2]*Department of Physics, Princeton University, Princeton, New Jersey 08540, USA*
[3]*Science and Technology on Surface Physics and Chemistry Laboratory, Mianyang 621907, China*
[4]*Physics Division, Sophia University, Chiyoda-ku, Tokyo 102-8554, Japan*

(Received 5 July 2022; revised 9 November 2022; accepted 28 November 2022; published 19 December 2022)

Symmetries associated with complex conjugation and Hermitian conjugation, such as time-reversal symmetry and pseudo-Hermiticity, have a great impact on the eigenvalue spectra of non-Hermitian random matrices. Here, we show that time-reversal symmetry and pseudo-Hermiticity lead to universal level statistics of non-Hermitian random matrices on and around the real axis. From the extensive numerical calculations of large random matrices, we obtain the five universal level-spacing and level-spacing-ratio distributions of real eigenvalues, each of which is unique to the symmetry class. Furthermore, we analyze spacings of real eigenvalues in physical models, such as bosonic many-body systems and free fermionic systems with disorder and dissipation. We clarify that the level spacings in ergodic (metallic) phases are described by the universal distributions of non-Hermitian random matrices in the same symmetry classes, while the level spacings in many-body localized and Anderson localized phases show the Poisson statistics. We also find that the number of real eigenvalues shows distinct scalings in the ergodic and localized phases in these symmetry classes. These results serve as effective tools for detecting quantum chaos, many-body localization, and real-complex transitions in non-Hermitian systems with symmetries.

DOI: 10.1103/PhysRevResearch.4.043196

I. INTRODUCTION

An understanding of spectral correlations under symmetries is useful in classifying phases of matter [1]. In closed quantum systems, the spectral statistics of nonintegrable systems typically coincide with those of Hermitian random matrices with symmetries, which serves as an effective tool for detecting quantum chaos [2–5]. The spectral statistics also provide a measure of the Anderson transitions [6–9] and many-body-localization (MBL) transitions [10–13]. When a disordered many-body Hermitian system is in the ergodic phase, the statistics of spacing between its eigenenergy levels are described by the Wigner-Dyson distribution of Hermitian random matrices. The Wigner-Dyson distribution is universally classified by time-reversal symmetry (TRS). Hermitian random matrices without and with TRS, whose sign is $+1$ and -1, respectively, belong to the Gaussian unitary, orthogonal, and symplectic ensembles, each of which exhibits distinct spectral statistics.

While state-of-the-art quantum experiments facilitate probing quantum many-body physics including MBL [13,14], energy gain and loss naturally exist in these optical systems, removing the Hermiticity condition from their many-body Hamiltonians. Consequently, open quantum systems described by non-Hermitian operators have attracted growing interest. Researchers have studied the non-Hermitian physics of optical phenomena [15–24], topological phases [25–35], and Anderson and many-body localization [36–49]. These works have led to a remarkable advance in spectral properties of non-Hermitian operators [50–65]. Still, it remains to be fully explored how symmetries influence the universal spectral properties of non-Hermitian operators.

The level statistics analyses of Hermitian systems cannot be directly applied to non-Hermitian systems. Due to the absence of Hermiticity, the 10-fold Hermitian symmetry classification [66] is enriched into a 38-fold symmetry classification [32,67,68]. The eigenvalues of non-Hermitian systems are distributed in the two-dimensional (2D) complex plane. The statistics of complex level spacings s_α, defined as the distance between the closest eigenvalues in the complex plane (i.e., $s_\alpha \equiv \min_\beta |E_\alpha - E_\beta|$ for all complex eigenvalues E_α, E_β with $\alpha \neq \beta$), were previously studied to capture the spectral correlations of non-Hermitian systems [50,59,60,62,63]. Non-Hermitian random matrices without any symmetry show a universal distribution of the spacing of complex eigenvalues, known as the Ginibre distribution [50]. An introduction of the transposition version of TRS, $H = \mathcal{U}_T^\dagger H^T \mathcal{U}_T$, $\mathcal{U}_T^* \mathcal{U}_T = \pm 1$, which is called TRS† [32], changes the distribution into two distinct distributions, depending on the sign of $\mathcal{U}_T^* \mathcal{U}_T = \pm 1$ [59]. This is similar to the threefold Wigner-Dyson distribution for Hermitian random matrices. Meanwhile, an introduction of TRS, $H = \mathcal{U}_T^\dagger H^* \mathcal{U}_T$, $\mathcal{U}_T^* \mathcal{U}_T =$

*rshindou@pku.edu.cn

TABLE I. Tenfold symmetry classification based on time-reversal symmetry (TRS), time-reversal symmetry† (TRS†), and pseudo-Hermiticity (pH). TRS and pH are equivalent to particle-hole symmetry† (PHS†) and chiral symmetry (CS), respectively. For the columns of given symmetry, the blank entries mean the absence of symmetry. For TRS and TRS†, ±1 stands for the sign of the symmetry. If H belongs to the symmetry class in the first column, iH belongs to the equivalent symmetry class in the second column. The column "soft gap" gives the small $y = \mathrm{Im}(E)$ behavior of the density $\rho_c(x, y)$ of complex eigenvalues if there is a soft gap around the real axis $y = 0$. The column "$\delta(y)$" indicates whether there is a δ-function peak on the real axis $y = 0$. In the presence of the δ-function peak, the columns "$\langle r\rangle$" and "χ," respectively, show the mean spacing ratio and spectral compressibility of real eigenvalues [see Eqs. (11) and (23) for their definitions] obtained from 4000×4000 random matrices in the generalized Gaussian ensemble. The standard deviation of $\langle r\rangle$ is estimated by the bootstrap method [69] and labeled in parentheses; for example, the standard deviation is 0.0004 for "0.4194(4)."

Symmetry class	Symmetry class (equiv)	TRS (PHS†)	TRS†	pH (CS)	Soft gap	$\delta(y)$	$\langle r\rangle$	χ
A	A							
A + η	AIII			√	$\lvert y\rvert$	√	0.4194(4)	0.83
AI	D†	+1			$\lvert y\rvert$	√	0.4858(3)	0.59
AII	C†	−1			$\lvert y\rvert^2$			
AI†	AI†		+1					
AII†	AII†		−1					
AI + η_+	BDI†	+1	+1	√	$-\lvert y\rvert\ln(\lvert y\rvert)$	√	0.4451(4)	0.73
AI + η_-	DIII†	+1	−1	√	$\lvert y\rvert$	√	0.4943(4)	0.58
AII + η_+	CII†	−1	−1	√	$\lvert y\rvert$	√	0.3708(7)	1.11
AII + η_-	CI†	−1	+1	√	$\lvert y\rvert$			

±1, does not alter the spacing distribution away from the real axis [50]. In fact, unlike TRS†, TRS only relates an eigenvalue with its complex conjugate, so that it has no impact on the correlation between two neighboring eigenvalues away from the real axis. This fact makes the role of symmetries in the universality classes of non-Hermitian random matrices elusive.

In this paper, we show that TRS leads to universal level statistics on and around the real axis. In addition to TRS, we also identify the relevant symmetries that give rise to universal level statistics of real eigenvalues in non-Hermitian random matrices. The universal level statistics provide an effective tool for detecting quantum chaos in open quantum systems with the symmetries. In the 38-fold symmetry classification of non-Hermitian random matrices, we show that there exist seven symmetry classes in which eigenstates with real eigenvalues preserve all the symmetries of the symmetry class, whereas eigenstates away from the real axis break some symmetries. They are a class only with pseudo-Hermiticity (class A + η; class AIII), classes with TRS whose sign is either ±1 (classes AI and AII), and classes with both TRS and pseudo-Hermiticity (classes AI + $\eta_\pm$ and AII + $\eta_\pm$); see Table I. In the last classes, TRS commutes or anticommutes with pseudo-Hermiticity. The subscript of $\eta_\pm$ denotes the commutation (+) or anticommutation (−) relation between TRS and pseudo-Hermiticity. Note that random matrices with particle-hole symmetry ($H = -\mathcal{U}_P^\dagger H^T \mathcal{U}_P$) and/or sublattice symmetry ($H = -\mathcal{U}_S^\dagger H \mathcal{U}_S$) do not give rise to the universal level statistics of real eigenvalues because only states with zero eigenvalue respect the symmetries.

The density of states (DOS) of non-Hermitian random matrices and physical Hamiltonians is generally defined in the complex plane, $\rho(E \equiv x + iy)$. Based on analytical and numerical analyses, we find that in five out of the seven symmetry classes, the DOS in the complex plane has a δ-function peak on the real axis. They are class A + η, class AI (equivalent to the real Ginibre ensemble [37,53,54,57,58]), class AI + η_+, class AI + η_-, and class AII + η_-. In these symmetry classes, the DOS $\rho(E = x + iy)$ is decomposed into two parts,

$$\rho(E = x + iy) = \rho_c(x, y) + \rho_r(x)\delta(y), \tag{1}$$

where $\rho_c(x, y)$ is the density of complex eigenvalues away from the real axis, and $\rho_r(x)$ is the density of real eigenvalues. Since only the states with real eigenvalues respect the full symmetries in these symmetry classes, $\rho_r(x)$ plays a role similar to the DOS in Hermitian systems. We show that the level statistics of real eigenvalues obtained from non-Hermitian random matrices, such as the level-spacing and level-spacing-ratio distributions, are different from those obtained from Hermitian random matrices and belong to the five distinctive universality classes according to the symmetries. It is also notable that TRS or pseudo-Hermiticity does not necessarily lead to $\rho_r(x) \neq 0$ in the DOS. We find that no real eigenvalues appear generally in class AII, which is consistent with the absence of real eigenvalues in the Ginibre symplectic ensemble [50]. We further generalize the absence of real eigenvalues to class AII + η_-.

We use random matrix analysis and exact diagonalization to identify universal level statistics of real eigenvalues for the five non-Hermitian symmetry classes. To demonstrate the universality of the level statistics, we apply the analysis to many-body and noninteracting physical Hamiltonians with disorder and non-Hermiticity. In physical systems that belong to the five symmetry classes, a finite density $\rho_r(x)$ of real eigenvalues enables comparison with those of non-Hermitian random matrices. We introduce non-Hermitian terms into interacting spin and hard-core boson models, such that many-body Hamiltonians belong to classes A + η, AI, and AI + $\eta_\pm$. By the exact diagonalization, we calculate their many-body eigenenergies and their spacing distributions on the real axis. In these four symmetry classes, the level statistics in the ergodic phases follow those of non-Hermitian random matrices in the corresponding symmetry classes. On the other hand, in class AII + η_+, the level statistics of a dissipative free

fermionic system deviate from those of non-Hermitian random matrices in class AII + η_+. We attribute this discrepancy to the unconventional level interaction between real eigenvalues, which is unique to non-Hermitian random matrices in class AII + η_+.

The reality of the spectrum in non-Hermitian Hamiltonians was studied extensively [15]. References [54,56] showed that the number of real eigenvalues is proportional to the square root of the matrix size for non-Hermitian random matrices in class AI, and several previous works [33,36,37,49,55,59] found that a nonzero proportion of real eigenvalues can appear in non-Hermitian physical systems with TRS. However, how the number of real eigenvalues scales with the system size in physical systems, and its relationship with random matrix theory, are still unknown. We find that the average number $\bar{N}_{\rm real}$ of real eigenvalues show distinctive scalings with respect to the dimensions N of Hilbert space in the five symmetry classes. We clarify $\bar{N}_{\rm real} \propto \sqrt{N}$ in the ergodic (metallic) phase and $\bar{N}_{\rm real} \propto N$ in the localized phases. Our results show that the level statistics analyses are powerful tools for detecting quantum chaos and MBL in non-Hermitian systems.

This paper is organized as follows. In Sec. II, we begin by reviewing the symmetry classification of non-Hermitian matrices, and we introduce level-spacing and level-spacing-ratio distributions of real eigenvalues for non-Hermitian random matrices. We numerically obtain the real-eigenvalue spacing and spacing-ratio distributions from large non-Hermitian random matrices. Analyzing small random matrices, we clarify the nature of effective interactions between two neighboring eigenvalues on the real axis, and we use them to explain the behavior of large random matrices. We also show the scaling of the number of real eigenvalues with respect to the dimensions of random matrices. In Sec. III, we use a hard-core boson model and interacting spin models to demonstrate the universality of the real-eigenvalue spacing and spacing-ratio distribution functions. We argue that the level statistics of real eigenvalues are useful for detecting different many-body phases in interacting disordered systems. We uncover that in the MBL phase, the number of real eigenvalues shows a nonuniversal scaling with respect to the dimensions of Hilbert space. We provide an explanation for the nonuniversal scaling. In Sec. IV, we apply the analysis to non-Hermitian noninteracting fermionic models in two and three dimensions. We find that the number of real eigenvalues shows distinctive universal scaling properties with respect to the matrix dimensions in the metal and localized phases. Section V is devoted to the conclusion and discussion.

II. RANDOM MATRICES

A. Non-Hermitian symmetry classes

The 38-fold symmetry class of non-Hermitian Hamiltonians is given by the following antiunitary symmetries [32]:

$$\begin{aligned}
&\text{time-reversal symmetry (TRS)}:\\
&\mathcal{U}_{\mathcal{T}_+} H^* \mathcal{U}_{\mathcal{T}_+}^\dagger = H, \quad \mathcal{U}_{\mathcal{T}_+}\mathcal{U}_{\mathcal{T}_+}^* = \pm 1,\\
&\text{particle-hole symmetry (PHS)}:\\
&\mathcal{U}_{\mathcal{P}_-} H^T \mathcal{U}_{\mathcal{P}_-}^\dagger = -H, \quad \mathcal{U}_{\mathcal{P}_-}\mathcal{U}_{\mathcal{P}_-}^* = \pm 1,\\
&\text{time-reversal symmetry}^\dagger\ (\text{TRS}^\dagger):\\
&\mathcal{U}_{\mathcal{P}_+} H^T \mathcal{U}_{\mathcal{P}_+}^\dagger = H, \quad \mathcal{U}_{\mathcal{P}_+}\mathcal{U}_{\mathcal{P}_+}^* = \pm 1,\\
&\text{particle-hole symmetry}^\dagger\ (\text{PHS}^\dagger):\\
&\mathcal{U}_{\mathcal{T}_-} H^* \mathcal{U}_{\mathcal{T}_-}^\dagger = -H, \quad \mathcal{U}_{\mathcal{T}_-}\mathcal{U}_{\mathcal{T}_-}^* = \pm 1,
\end{aligned} \tag{2}$$

and unitary symmetries:

$$\begin{aligned}
&\text{pseudo-Hermiticity (pH)}:\\
&\mathcal{U}_\eta H^\dagger \mathcal{U}_\eta^\dagger = H, \quad \mathcal{U}_\eta^2 = 1,\\
&\text{chiral symmetry (CS)}:\\
&\mathcal{U}_\mathcal{C} H^\dagger \mathcal{U}_\mathcal{C}^\dagger = -H, \quad {\mathcal{U}_\mathcal{C}}^2 = 1,\\
&\text{sublattice symmetry (SLS)}:\\
&\mathcal{U}_\mathcal{S} H \mathcal{U}_\mathcal{S}^\dagger = -H, \quad {\mathcal{U}_\mathcal{S}}^2 = 1,
\end{aligned} \tag{3}$$

where $\mathcal{U}_{\mathcal{T}_\pm}$, $\mathcal{U}_{\mathcal{P}_\pm}$, $\mathcal{U}_\eta$, $\mathcal{U}_\mathcal{C}$, and $\mathcal{U}_\mathcal{S}$ are unitary matrices. When H respects TRS (pH), iH respects PHS† (CS), and vice versa. In this sense, TRS and PHS† are unified, so are pH and CS [31]. TRS relates an eigenvalue z with its complex conjugate z^*. If $\boldsymbol{v}$ is a right eigenvector of a Hamiltonian H with TRS for an eigenvalue z ($H\boldsymbol{v} = z\boldsymbol{v}$), $\mathcal{U}_\mathcal{T}^T \boldsymbol{v}^*$ is another right eigenvector of H with the eigenvalue z^* ($H\,\mathcal{U}_\mathcal{T}^T \boldsymbol{v}^* = z^* \mathcal{U}_\mathcal{T}^T \boldsymbol{v}^*$). Likewise, pseudo-Hermiticity (pH) relates an eigenvalue z with its complex conjugate z^*, PHS† and CS relate an eigenvalue z with $-z^*$, and PHS and SLS relate an eigenvalue z with $-z$. On the other hand, TRS† imposes a constraint on each eigenvector.

When a symmetry relates an eigenvalue z with $z' \neq z$, and $|z - z'|$ is much larger than the mean level-spacing, such symmetry is expected to have no influence on the local eigenvalue correlation around z. For example, neither TRS nor PHS changes the nearest-spacing distribution of non-Hermitian random matrices for general complex eigenvalues [59]. This is similar to Hermitian random matrices with PHS or CS; for example, the eigenvalue spacing distribution away from zero energy in class D is the same as that in class A [66].

The spectral correlation on or around the real axis depends on TRS, pH, and their combination (TRS†). From TRS, pH, and TRS†, a tenfold symmetry classification is derived, as shown in Table I. This tenfold class includes seven symmetry classes that have at least one symmetry associated with complex conjugation (TRS) or Hermitian conjugation (pH): a class with pH (class A + η), classes with TRS whose sign can be ± 1 (classes AI and AII), and classes with both pH and TRS, where the sign of TRS is ± 1 and TRS commutes with pH (classes AI + η_+ and AII + η_+) or TRS anticommutes with pH (classes AI + η_- and AII + η_-). According to the 38-fold symmetry classification of non-Hermitian systems [32], these symmetry classes are equivalent to classes AIII, D†, C†, BDI†, DIII†, CII†, and CI† (see Table I). The tenfold symmetry class in Table I is also equivalent to the Hermitian conjugate of the non-Hermitian Altland-Zirnbauer class (i.e., AZ† class) in Ref. [32].

B. Level statistics of real eigenvalues for non-Hermitian random matrices

We consider non-Hermitian random matrices $\mathcal{H}$ in symmetry classes A + η, AI, AII, AI + $\eta_\pm$, and AII + $\eta_\pm$ in the

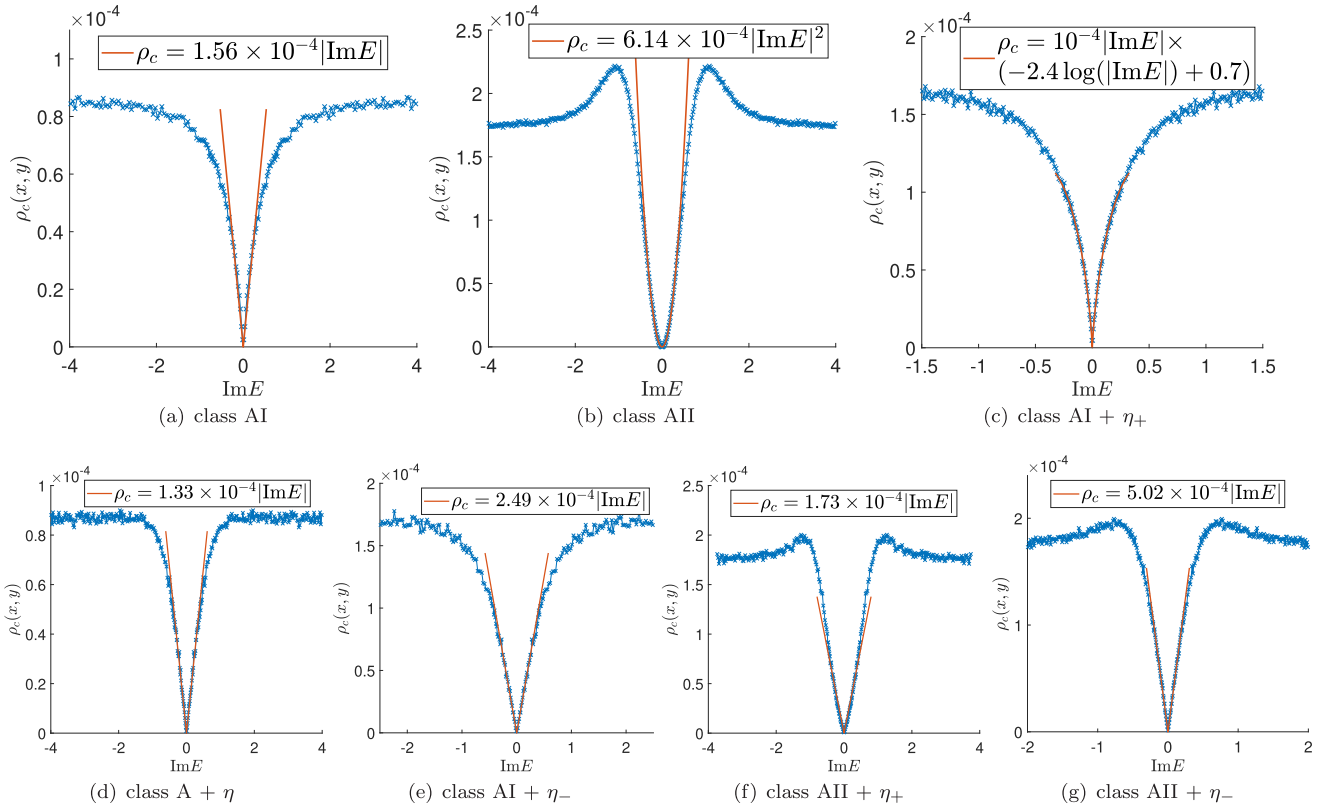

FIG. 1. Density $\rho_c(x, y)$ of complex eigenvalues of non-Hermitian random matrices in the Gaussian ensemble for classes (a) AI, (b) AII, (c) AI + η_+, (d) A + η, (e) AI + η_-, (f) AII + η_+, and (g) AII + η_-. Here, $\rho_c(x, y)$ is shown as a function of $y = \mathrm{Im}(E)$ for fixed $x = \mathrm{Re}(E)$ near the real axis of complex energy E (i.e., $y \simeq 0$). For classes AI, AI + $\eta_\pm$, A+ η, and AII + η_+, the density of states $\rho(E = x + iy) \equiv \rho_c(x, y) + \delta(y)\rho_r(x)$ is separated into the density $\rho_c(x, y)$ of complex eigenvalues and the density $\rho_r(x)$ of real eigenvalues. For classes AII and AII +η_-, no real eigenvalues appear, and we have $\rho(x + iy) \equiv \rho_c(x, y)$. The data of $\rho(x + iy)$ are obtained from diagonalizations of 5000 samples of 4000 × 4000 random matrices in each symmetry class. Note that $\rho_c(x, y)$ is almost independent of $x = \mathrm{Re}(E)$ when E is away from the boundary of a circle inside which the complex eigenvalues E distribute. All the 'log' in the figures are the natural log (ln).

Gaussian ensemble with the following probability distribution function $p(\mathcal{H})$:

$$p(\mathcal{H}) = C_N^{-1} e^{-\beta \mathrm{Tr}(\mathcal{H}^\dagger \mathcal{H})}, \tag{4}$$

where β is a positive constant and C_N is a normalization constant. Without loss of generality, we choose $\beta = 1/2$ for the rest of this paper. Non-Hermitian matrices $\mathcal{H}$ are required to belong to symmetry classes in Table I (see Appendix B for details). Diagonalizations of large random matrices show that eigenvalues are distributed almost uniformly in a circle except around the real axis and its circumference (not shown here). This distribution is consistent with the circular law of the Ginibre ensemble [50]. For non-Hermitian random matrices in classes A + η, AI, AI + $\eta_\pm$, and AII + η_+, a subextensive number of eigenvalues are real, and the DOS $\rho(x, y)$ has a δ-function peak on the real axis:

$$\rho(E = x + iy) = \rho_c(x, y) + \rho_r(x)\delta(y).$$

In numerical diagonalizations, real eigenvalues and complex eigenvalues are clearly distinguished, although real eigenvalues can artificially have tiny imaginary parts due to machine inaccuracy of a numerical subroutine program. In fact, with proper normalization, the apparent imaginary parts of real eigenvalues of Hermitian matrices are less than a certain error bound [70]. Meanwhile, to avoid regarding real eigenvalues as complex due to the machine inaccuracy, we choose a cutoff C larger than the error bound. The probability that complex eigenvalues are mistaken as real depends on the dimensions N of the matrix. With our choice of the cutoff C, this probability is estimated to be negligible for $N < 10^4$, where N in this paper is typically less than 10^4 [70].

The density $\rho_c(x, y)$ of complex eigenvalues in all seven symmetry classes vanishes toward the real axis and hence has a soft gap around the real axis (see Fig. 1). The size of the gap is of the same order as a mean level-spacing of eigenvalues in the complex plane. When $|y|$ is much smaller than the mean eigenvalue spacing, we have $\rho_c(x, y) \sim |y|$ in classes AI, A + η, AI + η_-, AII + η_+, and AII + η_-, while $\rho_c(x, y) \sim |y|^2$ in class AII and $\rho_c(x, y) \sim -|y|\ln|y|$ in class AI + η_+ (Fig. 1). These small y behaviors are consistent with the small matrix analysis discussed in Sec. II C. The logarithmic correction in class AI + η_+ seems to be due to TRS† with the sign +1 [52,59].

The number of real eigenvalues of non-Hermitian real random matrices (symmetry class AI) was previously studied [37,53,54,57,58]. However, a systematic study on the other symmetry classes is still lacking. In this paper, we find that the averaged number $\bar{N}_{\mathrm{real}}$ of real eigenvalues of $N \times N$ non-Hermitian random matrices is proportional to the square-root of the dimensions of the matrices in all five symmetry classes

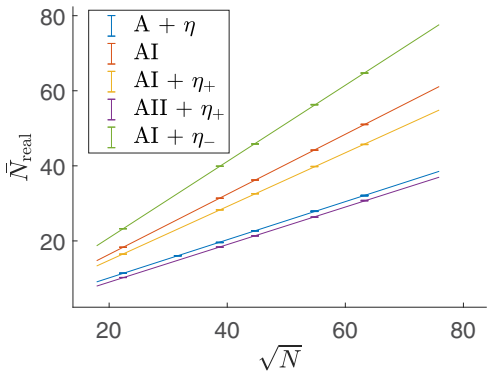

FIG. 2. Average number $\bar{N}_{\rm real}$ of real eigenvalues of non-Hermitian random matrices in the Gaussian ensemble as a function of $\sqrt{N}$ for the five symmetry classes. Here, N is the dimensions of random matrices. The error bars in the plot stand for twice the standard deviation of $\bar{N}_{\rm real}$. The standard deviation $\sigma_{N_{\rm real}}$ is estimated by $N_{\rm sample}\sigma^2_{N_{\rm real}} \equiv \sum_{i=1}^{N_{\rm sample}} (N^{(i)}_{\rm real} - \bar{N}_{\rm real})^2/(N_{\rm sample}-1)$, where $N^{(i)}_{\rm real}$ is the number of real eigenvalues in the ith random matrix, and $N_{\rm sample}$ is the number of random matrices in the ensemble. $N_{\rm sample}$ is at least 5000 for each matrix size. The plot clearly demonstrates the square-root scaling $\bar{N}_{\rm real} \sim \sqrt{N}$ in all five symmetry classes.

(see Fig. 2),

$$\bar{N}_{\rm real} \propto \sqrt{N}. \tag{6}$$

This subextensive number of real eigenvalues enables level statistics analyses on the real axis, where the symmetries associated with complex conjugation must have important effects as in the Hermitian case [9].

Furthermore, we obtain the universal distribution functions of spacings of real eigenvalues. Let $\lambda_1, \lambda_2, \ldots, \lambda_{N_{\rm real}}$ be all the real eigenvalues of given $\mathcal{H}$ in descending order. We define a normalized spacing of the real eigenvalues as

$$s_i \equiv \frac{\lambda_{i+1} - \lambda_i}{\langle \lambda_{i+1} - \lambda_i \rangle}. \tag{7}$$

Here, $\langle \cdots \rangle$ stands for the average over the ensemble, and $\langle \lambda_{i+1} - \lambda_i \rangle$ is evaluated by the average density of real eigenvalues at $x = (\lambda_i + \lambda_{i+1})/2$,

$$\langle \lambda_{i+1} - \lambda_i \rangle = \frac{1}{\overline{\rho}_r\left(\frac{1}{2}(\lambda_{i+1} + \lambda_i)\right)}, \tag{8}$$

where $\overline{\rho}_r(x)$ is the averaged density of real eigenvalues,

$$\overline{\rho}_r(x) \equiv \sum_{\lambda_i \in \mathcal{R}} \langle \delta(x - \lambda_i) \rangle, \tag{9}$$

with the set $\mathcal{R}$ of real eigenvalues. Here, $\overline{\rho}_r(x)$ is estimated by the average over the Gaussian ensemble. To exclude a fluctuation due to finite sampling numbers, we follow Refs. [4,71] and replace the δ function in Eq. (9) with the Gaussian distribution, $\exp[-(x-\lambda_i)^2/(2\sigma^2)]/(\sqrt{2\pi}\sigma)$ with $\sigma = n\bar{s}$. Here, $\bar{s}$ is the mean level-spacing on the real axis, and n is an $O(1)$ constant. We verify the validity of this numerical approach by using different n in the range from 2 to 5 and also replacing the δ function with the uniform distribution

$$\frac{1}{4\sigma} \times 1_{[\lambda_i - 2\sigma, \lambda_i + 2\sigma]}(x) = \begin{cases} \frac{1}{4\sigma} & (x \in [\lambda_i - 2\sigma, \lambda_i + 2\sigma]), \\ 0 & (x \notin [\lambda_i - 2\sigma, \lambda_i + 2\sigma]). \end{cases} \tag{10}$$

We confirm that $\overline{\rho}_r(x)$ is barely influenced by the approximation scheme, where the maximal difference of $\overline{\rho}_r(x)$ between the different approximation methods is around or smaller than 1%. Note also that we exclude the real eigenvalues around the edges of the spectrum when studying the distribution of the spacings of real eigenvalues, because $\overline{\rho}_r(x)$ near the edges changes sharply and the estimated $\overline{\rho}_r(x)$ might have larger error bars.

The spacing ratio of real eigenvalues [10,11,72] is also a useful quantity to characterize the level statistics on the real axis. It is defined by

$$r_i \equiv \min\left(\frac{\lambda_{i+1} - \lambda_i}{\lambda_i - \lambda_{i-1}}, \frac{\lambda_i - \lambda_{i-1}}{\lambda_{i+1} - \lambda_i}\right), \tag{11}$$

satisfying $0 \leqslant r_i \leqslant 1$. Since r_i is a dimensionless quantity and free from the normalization, it is easier to numerically obtain the distribution of r_i than of s_i.

In each of the five symmetry classes (i.e., classes A + η, AI, AI + η_+, AII + η_+, and AI + η_-), we numerically calculate the level-spacing distribution $p(s)$ and the level-spacing-ratio distribution $p_r(r)$ of real eigenvalues, both of which converge to the characteristic functions (Fig. 3). Here, $p_r(r)$ and $p(s)$ in class AII + η_+ converge more slowly than those in the other symmetry classes and do not converge even at the maximal matrix size [$N = 4000$; see Figs. 3(d) and 3(i)].

To improve the convergence, we also introduce a generalized Gaussian ensemble with the following probability distribution function $p'(\mathcal{H})$:

$$p'(\mathcal{H}) = C^{-1}_{N,(\beta_1,\beta_2)} e^{-{\rm Tr}\,[\beta_1 (\mathcal{H}+\mathcal{H}^\dagger)^2 - \beta_2 (\mathcal{H}-\mathcal{H}^\dagger)^2]}, \tag{12}$$

where β_1 and β_2 control the fluctuations of Hermitian and anti-Hermitian parts of $\mathcal{H}$, respectively. For $\beta_1 = \beta_2$, $p'(\mathcal{H})$ reduces to $p(\mathcal{H})$ in the Gaussian ensemble. For $\beta_1 \neq \beta_2$, the eigenvalues $E = x + iy$ of $\mathcal{H}$ distribute almost uniformly in the ellipse in the complex plane,

$$\frac{x^2}{a^2} + \frac{y^2}{b^2} = 1, \tag{13}$$

with $a/b = \beta_2/\beta_1$ [56]. In each symmetry class, random matrices in the generalized Gaussian ensemble show the same universal behaviors, such as soft gaps around the real axis and the square-root scaling of the average number $\bar{N}_{\rm real}$ of real eigenvalues. We find that in each symmetry class, for a matrix size N, the average number $\bar{N}'_{\rm real}$ of real eigenvalues in the generalized Gaussian ensemble with β_1 and β_2 is approximately scaled by $\bar{N}_{\rm real}$ in the Gaussian ensemble with the same matrix size as

$$\bar{N}'_{\rm real} \simeq \sqrt{\frac{\beta_2}{\beta_1}} \bar{N}_{\rm real} \tag{14}$$

for $\bar{N}_{\rm real}, \bar{N}'_{\rm real} \ll N$. We also find that for $\bar{N}'_{\rm real} \simeq \bar{N}_{\rm real}$, $p(s)$ and $p_r(r)$ in the two ensembles are close to each other (see Appendix C for details). Thus, $p(s)$ and $p_r(r)$ converge much

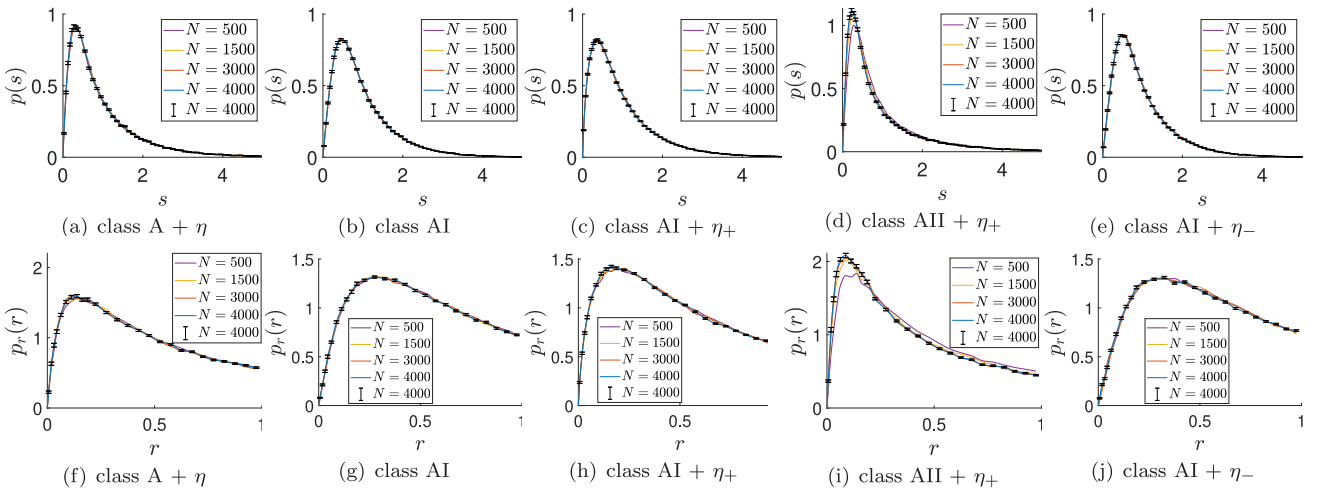

FIG. 3. Level-spacing distributions $p(s)$ of real eigenvalues of $N \times N$ non-Hermitian random matrices in the Gaussian ensemble for (a) class A + η, (b) class AI, (c) class AI + η_+, (d) class AII + η_+, and (e) class AI + η_-. Level-spacing-ratio distributions $p_r(r)$ of real eigenvalues of $N \times N$ non-Hermitian random matrices in the Gaussian ensemble for (f) class A + η, (g) class AI, (h) class AI + η_+, (i) class AII + η_+, and (j) class AI + η_-. For each N and for each symmetry class, $p(s)$ and $p_r(r)$ are averaged over at least 5000 random matrices in the ensemble. The black points for $p(s)$ and $p_r(r)$ are obtained from 4000×4000 random matrices, where the standard deviation error bars are evaluated by the bootstrap method [69]. The error bars for the smaller matrices are smaller than the error bars for $N = 4000$ and not shown.

faster in the generalized Gaussian ensemble with $\beta_2 > \beta_1$. We choose $\beta_2/\beta_1 = 16$ in the following.

In each symmetry class, the error bars of $p(s)$ and $p_r(r)$ of non-Hermitian random matrices in the generalized Gaussian ensemble with a larger matrix size ($N > 1000$) overlap with each other. Both $p(s)$ and $p_r(r)$ converge to the characteristic universal functions in the limit of the large matrix size (Figs. 4 and 5). $p(s)$ for classes A + η, AI + η_+, and AII + η_+ in different ensembles was previously calculated in Ref. [73], although the sizes of the matrices are small and $p(s)$ in Ref. [73] does not seem to reach the universal function forms shown in Fig. 4. $p(s)$ and $p_r(r)$ in the limit of the large matrix size can distinguish the different symmetry classes among the five symmetry classes. We confirm the universality of $p(s)$ and $p_r(r)$ in each symmetry class by comparisons with $p(s)$ and $p_r(r)$ in the Bernoulli ensemble (see Appendix B for details). This comparison illustrates that both of the level-spacing and level-spacing-ratio distributions of real eigenvalues are universal and unique in each symmetry class. In Secs. III and IV, we compare $p(s)$ and $p_r(r)$ obtained in the random matrix theory with those obtained from physical models.

Note that the level-spacing distributions $p(s)$ in the different symmetry classes share the same asymptotic behaviors. For $s \gg 1$, we have

$$\ln p(s) \propto -s \tag{15}$$

in all five symmetry classes. On the other hand, for $s \ll 1$, we have (see the insets of Fig. 4)

$$p(s) \propto \begin{cases} -s\ln s & (\text{class AI} + \eta_+), \\ s & (\text{other four classes}). \end{cases} \tag{16}$$

As a comparison, the level-spacing distributions of Hermitian random matrices satisfy $\ln p(s) \propto -s^2$ for $s \gg 1$ and $p(s) \propto s^\beta$ for $s \ll 1$, where the Dyson index $\beta = 1, 2, 4$ characterizes the Gaussian orthogonal, unitary, and symplectic ensembles, respectively [1]. The small-s behavior of $p(s)$ and its difference with Hermitian random matrices are well understood by analyses of effective small matrices (see Sec. II C for details). In the large-s regime, the tail of $p(s)$ in the non-Hermitian case is much heavier than that in the Hermitian case. This difference in the large-s behavior shows that the correlation between two neighboring real eigenvalues decays more quickly in non-Hermitian random matrices than Hermitian ones. When the distance between two neighboring real eigenvalues of a non-Hermitian random matrix is larger, more complex eigenvalues surround them and weaken the correlation between the two real eigenvalues.

For reference, in the Hermitian random matrix theory, the level-spacing-ratio distribution $p_r(r)$ is well approximated by [72]

$$p_r(r) \simeq \frac{1}{C_\beta} \frac{(r + r^2)^\beta}{(1 + r + r^2)^{(1+\frac{3}{2}\beta)}} \theta(1 - r), \tag{17}$$

where $\theta(r)$ is the step function, C_β is a normalized constant, and $\beta = 1, 2, 4$ is the Dyson index. By contrast, if all real eigenvalues are uncorrelated and follow the Poisson statistics, $p_r(r)$ is given by

$$p_r(r) = \frac{2}{(1 + r)^2} \theta(1 - r). \tag{18}$$

None of these level-spacing-ratio distributions $p_r(r)$ of Hermitian matrices can describe any of our universal $p_r(r)$ of non-Hermitian random matrices in Fig. 5, showing the unique non-Hermitian nature of our universal distribution functions.

Notably, the mean value of the level-spacing ratios

$$\langle r \rangle = \int_0^1 p_r(r) r dr \approx 0.371 \tag{19}$$

in class AII + η_+ is smaller than

$$\langle r \rangle_{\text{Poisson}} = -1 + \ln 4 \approx 0.386 \tag{20}$$

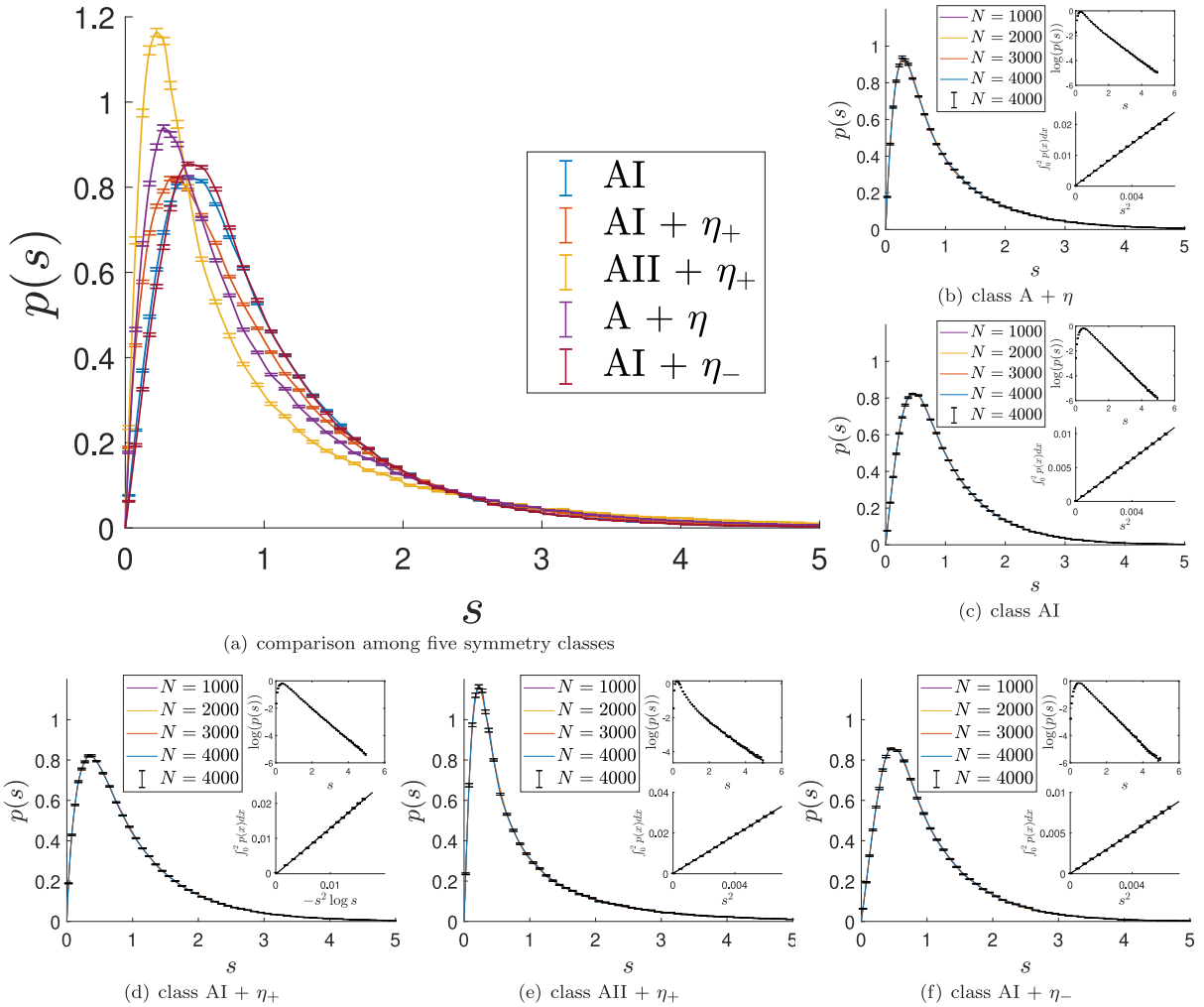

(a) comparison among five symmetry classes

(b) class A + η

(c) class AI

(d) class AI + η_+

(e) class AII + η_+

(f) class AI + η_-

FIG. 4. Level-spacing distributions $p(s)$ of real eigenvalues of $N \times N$ non-Hermitian random matrices in the generalized Gaussian ensemble for (a) all five symmetry classes, (b) class A + η, (c) class AI, (d) class AI + η_+, (e) class AII + η_+, and (f) class AI + η_-. For each N and for each symmetry class, the spacing distribution function is averaged over at least 5000 random matrices in the ensemble. The black points with the error bars are $p(s)$ obtained from 4000×4000 random matrices, where the standard deviation error bars are evaluated by the bootstrap method [69]. The error bars for the smaller matrices are smaller than those for $N = 4000$ and not shown. In each symmetry class, $p(s)$ of random matrices with different sizes N ($N > 1000$) almost overlap with each other. Insets: Asymptotic behaviors of the distribution function for $s \gg 1$ and for $s \ll 1$. For small s, the cumulative distribution function $\int_0^s p(s')ds'$ is plotted as a function of either s^2 or $-\ln(s)s^2$. For $s \gg 1$, $\ln(p(s))$ is linear in s, indicating the Poisson-like tail. The comparison of $p(s)$ among the five symmetry classes shows that $p(s)$ for classes AI and AI + η_- are close to each other, and that $p(s)$ for the other three classes are clearly distinguished from $p(s)$ for classes AI and AI + η_-. All the 'log' in the figures are the natural log (ln).

of uncorrelated levels. By contrast, $\langle r \rangle$ of non-Hermitian random matrices in the other four symmetry classes are all larger than $\langle r \rangle_{\text{Poisson}}$ (see Table I and Fig. 5). In the Hermitian random matrix theory, the mean values of level-spacing ratios in the Gaussian orthogonal, unitary, and symplectic ensembles are [72]

$$\langle r \rangle_{\text{GOE}} \approx 0.531, \ \langle r \rangle_{\text{GOE}} \approx 0.600, \ \langle r \rangle_{\text{GSE}} \approx 0.674, \quad (21)$$

all of which are larger than $\langle r \rangle_{\text{Poisson}} \approx 0.386$. In addition, $\langle r \rangle$ increases with the Dyson index $\beta = 1, 2, 4$ that describes the strength of the level repulsion [1]. Thus, $\langle r \rangle < \langle r \rangle_{\text{Poisson}}$ in class AII + η_+ indicates unusual level interactions on the real axis unique to this symmetry class.

To further clarify the nature of the interactions between real eigenvalues in each symmetry class, we also calculate the variance Σ_2 of the number N_W of real eigenvalues in an interval on the real axis [9],

$$\Sigma_2 \equiv \langle N_W^2 \rangle - \langle N_W \rangle^2. \quad (22)$$

We have $\Sigma_2 \propto \ln\langle N_W \rangle$ in Hermitian random matrix theory, while we have $\Sigma_2 = \langle N_W \rangle$ for uncorrelated real numbers (i.e., Poisson statistics). The spectral compressibility,

$$\chi \equiv \lim_{N_W \to \infty} \frac{d\Sigma_2}{d\langle N_W \rangle}, \quad (23)$$

quantifies the level interaction between real eigenvalues. For Hermitian random matrices, the level repulsion is stronger, leading to $\chi = 0$. On the other hand, we have $\chi_{\text{Poisson}} = 1$ for the uncorrelated real spectrum. In the intermediate regime, such as the metal-insulator transition points in Hermitian

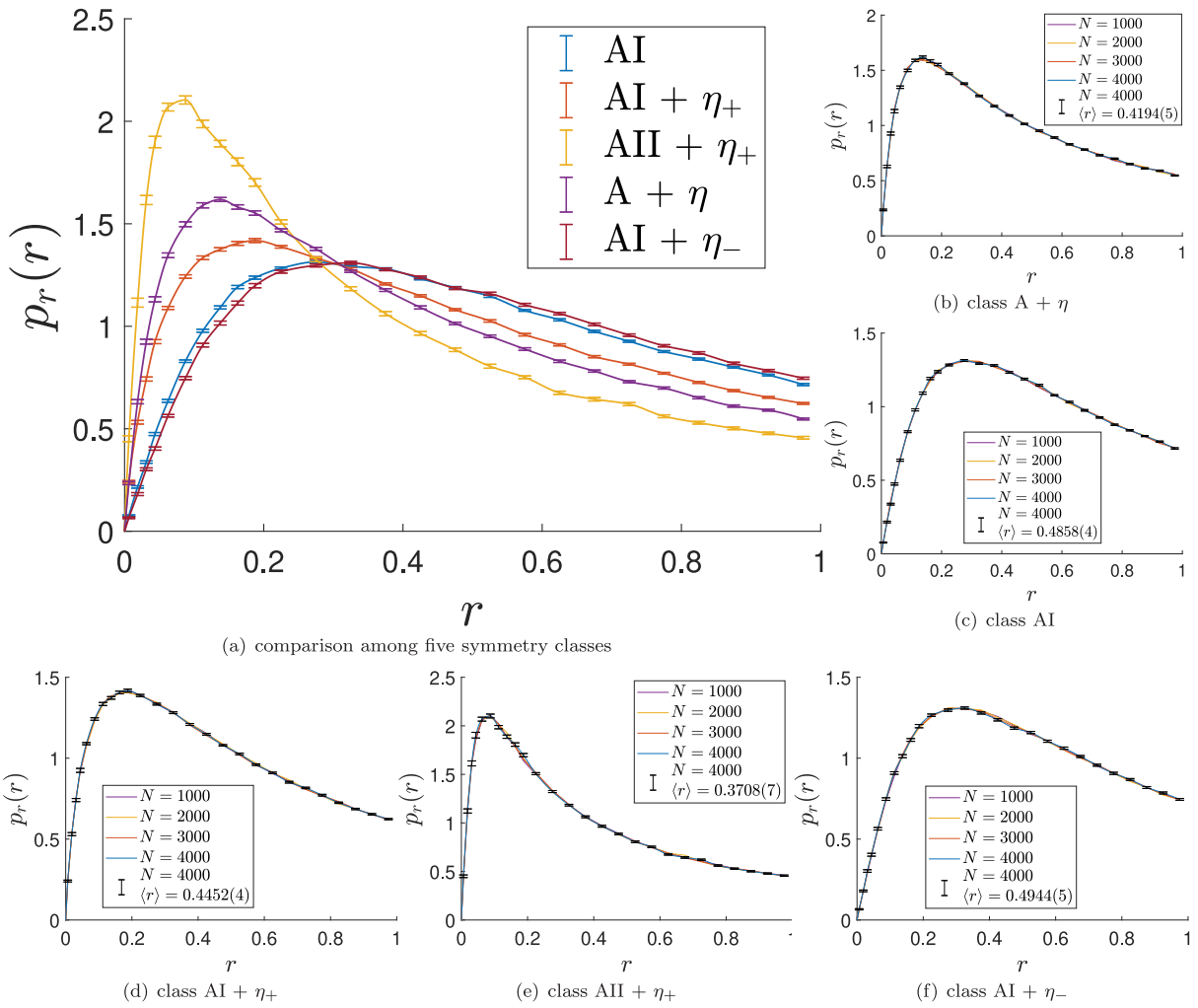

(a) comparison among five symmetry classes
(b) class A + η
(c) class AI
(d) class AI + η_+
(e) class AII + η_+
(f) class AI + η_-

FIG. 5. Level-spacing-ratio distributions $p_r(r)$ of real eigenvalues of $N \times N$ non-Hermitian random matrices in the generalized Gaussian ensemble for (a) all five symmetry classes, (b) class A + η, (c) class AI, (d) class AI + η_+, (e) class AII + η_+, and (f) class AI + η_-. For each N and for each symmetry class, the level-spacing-ratio distribution function is averaged over at least 5000 random matrices in the ensemble. The black points with the error bars are $p_r(r)$ obtained from 4000×4000 random matrices, where the standard deviation error bars are evaluated by the bootstrap method [69]. The error bars for the smaller matrices are smaller than the error bars for $N = 4000$ and not shown. In each symmetry class, $p_r(r)$ of random matrices with different sizes N ($N \geqslant 1000$) almost overlap with each other. The mean value $\langle r\rangle = \int_0^1 p_r(r)dr$ of the spacing ratios and its standard deviation are given for $N = 4000$ for each symmetry class. The comparison of $p_r(r)$ among the five symmetry classes shows that $p_r(r)$ distinguishes between different symmetry classes.

disordered systems, the level repulsion is weaker than the random matrices but stronger than the Poisson statistics, resulting in $0 < \chi < 1$ [9]. For non-Hermitian random matrices in each of the five symmetry classes, we find

$$\Sigma_2 \propto \langle N_W \rangle, \tag{24}$$

meaning that the spectral compressibility χ gives a universal constant unique to each symmetry class (see Table I and Appendix E for details).

Remarkably, we have $\chi \approx 1.11 > \chi_{\text{Poisson}} = 1$ in class AII + η_+, again indicating the unusual level interactions. As shown by $p(s) \propto s \to 0$ for $s \to 0$, the interaction is repulsive in the small-s regime even for class AII + η_+, although the level repulsion is much smaller than $p(s) \propto s^4$ of Hermitian random matrices in class AII (i.e., Gaussian symplectic ensemble). Hence, from our numerical results of $\langle r\rangle < \langle r\rangle_{\text{Poisson}}$ and $\chi > \chi_{\text{Poisson}}$, the attractive interaction should appear in the finite-s regime and dominate the repulsive interaction in the small-s regime on average. This is also compatible with the large peak of $p(s)$ and $p_r(r)$ compared with the other symmetry classes (see Figs. 4 and 5). A distinctive feature of class AII + η_+ is the simultaneous presence of TRS and TRS†, whose signs are -1. While TRS† with the sign -1 leads to the Kramers degeneracy of generic complex eigenvalues and the consequent strong level repulsion, TRS with the sign -1 leads to the strong level repulsion around the real axis, as shown by the absence of real eigenvalues in class AII. The combination of TRS and TRS† seems to result in the unusual interactions between neighboring levels (Kramers pairs) on the real axis that are repulsive in the small-s regime but attractive in the larger-s regime. This is a possible reason for $\langle r\rangle < \langle r\rangle_{\text{Poisson}}$ and $\chi > \chi_{\text{Poisson}}$. In Sec. II C, we use effective small matrices to analyze the interactions between neighboring real eigenvalues, and we find that the degrees of freedom of the attractive

interaction in class AII + η_+ are much larger than those of the other symmetry classes.

Note also that no real eigenvalues generally appear in classes AII and AII + η_-. This should be due to TRS with the sign -1, which only enforces the Kramers degeneracy on the real axis. If a real eigenvalue is present in these symmetry classes, a Kramers partner with the same real eigenvalue should always appear. While this Kramers pair is robust against Hermitian perturbations, it is sensitive to non-Hermitian perturbations and forms a complex-conjugate pair in the complex plane. Consequently, real eigenvalues are unstable in these symmetry classes. On the contrary, in class AII + η_+, all eigenvalues including complex ones exhibit Kramers degeneracy because of the additional presence of TRS† with the sign -1. Consequently, the Kramers pair on the real axis is robust even against certain degrees of non-Hermitian perturbations, which leads to the subextensive number of real eigenvalues. This is different from class AII + η_-, where only TRS† with the sign $+1$ is present and no such robust Kramers degeneracy is allowed generally. We also discuss the absence of real eigenvalues in classes AII and AII + η_- by effective small matrices in Sec. II C.

C. Effective small matrix analysis

Interactions between two neighboring eigenvalues can be qualitatively understood by effective small matrices [59]. When two eigenvalues get close to each other by the change of parameters, the interactions between them can be studied by nearly degenerate perturbation theory [4]. The strength of the interactions is generally determined by symmetry such as TRS and pH. To see the influence of symmetry in each of the seven symmetry classes, we consider the two adjacent eigenvalues that are either both real or complex conjugate to each other. Then, we project the variation of a full Hamiltonian onto a smaller space spanned by eigenvectors that belong to the two adjacent eigenvalues. The small Hamiltonians thus obtained take forms of either a 2×2 matrix or a 4×4 matrix, depending on the presence of the Kramers degeneracy. The symmetry classes of the small matrices are the same as the full Hamiltonians.

The small matrices in the seven symmetry classes are of the following forms:

$$\mathcal{H}^{(s)}_{\rm AI}=\begin{pmatrix} a_0+a_1 & a_2+a_3\\ a_2-a_3 & a_0-a_1\end{pmatrix},$$

$$\mathcal{H}^{(s)}_{\rm A+\eta}=\begin{pmatrix} a_0+a_1 & a_3+ia_2\\ -a_3+ia_2 & a_0-a_1\end{pmatrix},$$

$$\mathcal{H}^{(s)}_{\rm AI+\eta_+}=\begin{pmatrix} a_0+a_1 & a_2\\ -a_2 & a_0-a_1\end{pmatrix},$$

$$\mathcal{H}^{(s)}_{\rm AII}=\begin{pmatrix} a_0+ia_1 & a_3+ia_2\\ -a_3+ia_2 & a_0-ia_1\end{pmatrix},$$

$$\mathcal{H}^{(s)}_{\rm AI+\eta_-}=\begin{pmatrix} a_0+a_1 & 0 & a_2+a_5 & a_4-a_3\\ 0 & a_0+a_1 & a_4+a_3 & a_2-a_5\\ a_2-a_5 & -a_4+a_3 & a_0-a_1 & 0\\ -a_4-a_3 & a_2+a_5 & 0 & a_0-a_1\end{pmatrix},$$

$$\mathcal{H}^{(s)}_{\rm AII+\eta_-}=\begin{pmatrix} a_0 & a_2+ia_1\\ -a_2+ia_1 & a_0\end{pmatrix},$$

$$\mathcal{H}^{(s)}_{\rm AII+\eta_+}=\begin{pmatrix} a_0+a_1 & 0 & a_2+ia_5 & a_4+ia_3\\ 0 & a_0+a_1 & -a_4+ia_3 & a_2-ia_5\\ -a_2+ia_5 & a_4+ia_3 & a_0-a_1 & 0\\ -a_4+ia_3 & -a_2-ia_5 & 0 & a_0-a_1\end{pmatrix},$$

where $a_0, a_1, \ldots, a_{m+n}$ are real random variables. The eigenvalues of the small matrices are written in a unified form as

$$\lambda = a_0 \pm \sqrt{X-Y},$$
$$X \equiv \begin{cases} \sum_{i=1}^{m} a_i^2 & (m\neq 0),\\ 0 & (m=0),\end{cases}$$
$$Y \equiv \sum_{i=m+1}^{m+n} a_i^2 \qquad (25)$$

for the seven symmetry classes (see Appendix A for details). The two eigenvalues of each of these matrices are either both real or complex conjugate to each other. For $m=0$ (classes AII and AII + η_-), they are always complex conjugate to each other, meaning the absence of real eigenvalues. For $m>0$, the probability of two real eigenvalues is finite and equal to the probability for $X \geqslant Y$. This explains the presence and absence of the δ-function peak on the real axis in the DOS in the seven symmetry classes. In Appendix A, we analytically obtain the level statistics of real eigenvalues and the DOS around the real axis for the above effective small matrices in the seven symmetry classes.

The finite probability of the real eigenvalues of the random matrices leads to the square-root scaling of $\bar{N}_{\rm real}$. According to the circular law [50], the uniform distribution of complex eigenvalues within the circle of radius R suggests that the number of complex eigenvalues near the real axis within an energy window of a mean complex energy spacing $\bar{s}_c$ is scaled by $\sqrt{N}$,

$$N\times\frac{2R\bar{s}_c}{\pi R^2}=2\sqrt{\frac{N}{\pi}}\propto\sqrt{N}, \qquad (26)$$

with $\pi R^2/\bar{s}_c^2 = N$. The complex eigenvalues near the real axis can be regarded as complex-conjugate pairs of eigenvalues, each of which is described by the small random matrices. Due to the finite probability of $X>Y$, a complex-conjugate pair of the eigenvalues near the real axis is converted into real eigenvalues with a finite probability. This gives the square-root scaling, $\bar{N}_{\rm real}\sim\sqrt{N}$.

For $X<Y$, the two eigenvalues are complex conjugate to each other. Thereby, X and Y in Eq. (25) give an attractive and repulsive interaction between the two eigenvalues, respectively. The increase of X (Y) will decrease (increase) the distance between the two eigenvalues along the imaginary axis. In symmetry classes A + η, AI, AI + η_+, AII + η_+, and AI + η_-, we have $m>0$, and both attractive and repulsive interactions are present. By contrast, in classes AII and AII

TABLE II. Degrees of freedom of Hermitian and anti-Hermitian parts of traceless effective small random matrices H for the seven symmetry classes. For each class, the traceless parts of the small matrix are decomposed into the Hermitian and anti-Hermitian parts, the degrees of which are denoted by m and n, respectively. If H belongs to the symmetry class in the first column, iH belongs to the equivalent symmetry class in the second column.

Symmetry class	Equivalent symmetry class	Real degree of freedom m	Imaginary degree of freedom n
AI	$\mathrm{D}^\dagger$	2	1
A + η	AIII	1	2
AI + η_+	$\mathrm{BDI}^\dagger$	1	1
AII	$\mathrm{C}^\dagger$	0	3
AI + η_-	$\mathrm{DIII}^\dagger$	3	2
AII + η_-	$\mathrm{CI}^\dagger$	0	2
AII + η_+	$\mathrm{CII}^\dagger$	1	4

+ η_-, we have $m = 0$, and thus no attractive interaction is present (see Table II).

The DOS around the real axis is determined by the interaction between the two complex-conjugate eigenvalues. When the attractive interaction along the imaginary axis is absent ($m = 0$ in classes AII and AII + η_-), the two eigenvalues are less likely to appear around the real axis than the other symmetry classes. The repulsion between the two eigenvalues becomes larger for larger n. In fact, our analysis of the small matrices in the Gaussian ensemble gives

$$\rho_c(x+iy) \propto \begin{cases} |y|^2 & \text{(class AII)}, \\ |y| & \text{(class AII} + \eta_-\text{)}. \end{cases} \tag{27}$$

In the presence of the attractive interaction ($m > 0$ in classes A + η, AI, AI + η_+, AII + η_+, and AI + η_-), the larger attractive interaction converts the complex-conjugate pair of eigenvalues near the real axis onto two real eigenvalues. As a result, a subextensive number of eigenvalues of the full matrix appear on the real axis. In fact, our analysis of the small matrices in the Gaussian ensemble gives (see Appendix A for detailed derivations)

$$\rho_c(x,y) \propto \begin{cases} -|y|\ln|y| & \text{(class AI} + \eta_+\text{)}, \\ |y| & \text{(other four classes)} \end{cases} \tag{28}$$

for small $|y|$. These small-$|y|$ behaviors of $\rho_c(x, y)$ from the small matrix analyses are consistent with the numerical results of large random matrices shown in Fig. 1.

For $X > Y$, the two eigenvalues are real. Thereby, X and Y in Eq. (25), respectively, give a repulsive and attractive interaction between the pair of two real eigenvalues. The increase of X (Y) increases (decreases) the distance between the two eigenvalues along the real axis. We analytically calculate the spacing distribution function of the two real eigenvalues for the small matrices in the five symmetry classes with $m > 0$ (see Appendix A for detailed derivations). For small s, the real-eigenvalue spacing distribution is obtained as

$$p(s) \propto \begin{cases} -s\ln s & \text{(class AI} + \eta_+\text{)}, \\ s & \text{(other four classes)}. \end{cases} \tag{29}$$

Note that $p(s)$ from the small matrix analyses and that from large random matrices are not exactly the same, while they share the same asymptotic behavior for small s for each of the five symmetry classes. Note also that in class AII + η_+, the degrees of freedom of the attractive interaction Y (i.e., $n = 4$) are much larger than the degrees of freedom m of the repulsive interaction X (i.e., $m = 1$). This is consistent with $\langle r\rangle < \langle r\rangle_{\text{Poisson}}$ and $\chi > 1$ in class AII + η_+ for large random matrices (see Sec. II B for details).

III. DISSIPATIVE MANY-BODY SYSTEMS

In the previous section, we study the general behavior of the level statistics of non-Hermitian random matrices in symmetry classes AI, A + η, AI + η_+, AI + η_-, and AII + η_+. The DOS in these symmetry classes shows a δ-function peak on the real axis. The number of real eigenvalues is scaled by the square-root of the dimensions of the matrices.

In this section, we study many-body disordered Hamiltonians that belong to symmetry classes AI, A + η, AI + η_+, and AI + η_-. We calculate the level-spacing distributions, level-spacing-ratio distributions, and the numbers of real eigenvalues in the weak disorder regime (ergodic phase) and the strong disorder regime (MBL phase). In the weak disorder regime, we show that the level-spacing and level-spacing-ratio distributions of real eigenvalues match well with those of non-Hermitian random matrices in the same symmetry classes. In addition, we find that the number of real eigenvalues in the weak disorder regime is scaled by the square root of the dimensions of the many-body Hamiltonians, which is also consistent with the random matrix theory. In the strong disorder regime, we show that the many-body model in class AI is characterized by nonuniversal scalings of the number of real eigenvalues and its standard deviation. We also provide a phenomenological explanation for this nonuniversal behavior.

A. Hard-core boson system

We consider the following one-dimensional (1D) hard-core boson model with the nonreciprocal hopping [36,41]:

$$\mathcal{H}_{\text{HN}} = \sum_{i=1}^{L_x} \{t(e^g c_{i+1}^\dagger c_i + e^{-g} c_i^\dagger c_{i+1}) + U n_{i+1} n_i + h_i n_i\}. \tag{30}$$

Here, c_i is a boson annihilation operator at site i, $n_i = c_i^\dagger c_i$ is its number operator, and the periodic boundary conditions are imposed (i.e., $c_{L_x+1} = c_1$). Every site is allowed to be occupied by no more than one boson under the local hard-core boson constraint. g controls the degree of nonreciprocity and non-Hermiticity, and h_i is the random potential at site i that distributes uniformly in $[-W/2, W/2]$ with $W \geqslant 0$. On the occupation-number basis, $\mathcal{H}_{\text{HN}}$ satisfies

$$\mathcal{H}_{\text{HN}} = \mathcal{H}_{\text{HN}}^* \tag{31}$$

and belongs to class AI. This model can be mapped to an interacting spin model with a random magnetic field and realized, for example, in ultracold atoms [14,28,41].

The Hermitian limit ($g = 0$) of the model was previously studied [11–13,74–77], where the level-spacing

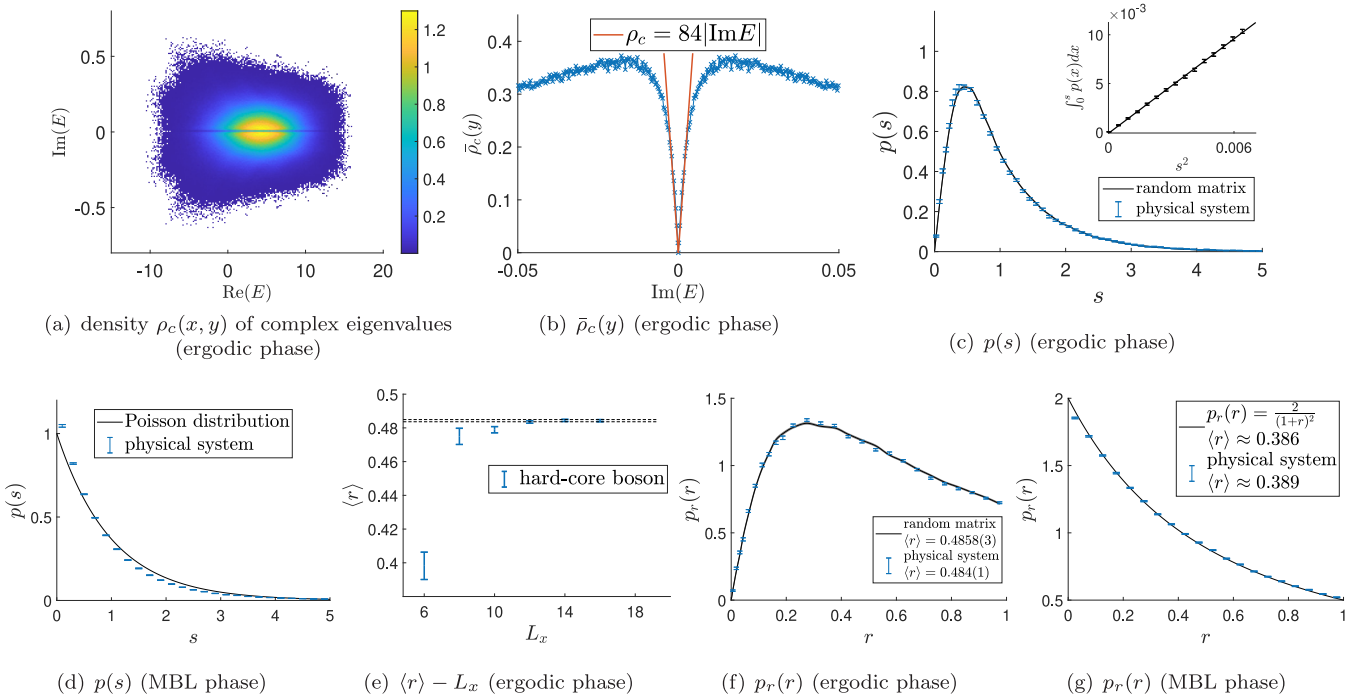

(a) density $\rho_c(x, y)$ of complex eigenvalues (ergodic phase) (b) $\bar{\rho}_c(y)$ (ergodic phase) (c) $p(s)$ (ergodic phase)

(d) $p(s)$ (MBL phase) (e) $\langle r\rangle - L_x$ (ergodic phase) (f) $p_r(r)$ (ergodic phase) (g) $p_r(r)$ (MBL phase)

FIG. 6. (a) Heat map of the density $\rho_c(x, y)$ of complex eigenvalues of the hard-core boson model in the weak disorder regime ($W = 2$, $L_x = 16$). (b) Integrated density of complex eigenvalues, $\bar{\rho}_c(y) \equiv \frac{1}{10}\int_{-1}^{9} \rho_c(x, y)dx$. As seen from the heat map, $-1 < E < 9$ is well within the ergodic phase for $W = 2$. (c) Level-spacing distribution $p(s)$ of real eigenvalues within the energy window $-1 < E < 9$ in the weak disorder regime of the hard-core boson model, and its comparison with $p(s)$ obtained from non-Hermitian random matrices in symmetry class AI (black line). Inset: Asymptotic behavior of $\int_0^s p(s')ds'$ for $s \ll 1$. The consistency between $p(s)$ from the hard-core boson model and $p(s)$ from the random matrices justifies that $-1 < E < 9$ for $W = 2$ is well within the ergodic phase. (d) $p(s)$ in the many-body localized phase (all the real energies E, $W = 30$), and its comparison with the Poisson distribution. (e) Mean value of level-spacing ratios $\langle r\rangle = \int_0^1 p_r(r)dr$ as a function of system size L_x. The average is taken in the ergodic phase ($W = 2$, $-1 < E < 9$, $L_x = 16$). (f) Level-spacing-ratio distribution $p_r(r)$ of real eigenvalues in the ergodic phase ($W = 2$, $-1 < E < 9$, $L_x = 16$) and its comparison to $p_r(r)$ obtained from non-Hermitian random matrices in class AI. (g) $p_r(r)$ in the many-body localized phase and its comparison with $p_r(r)$ of uncorrelated real numbers. The mean value $\langle r\rangle$ of each level-spacing-ratio distribution is also shown in the figures. (c)–(g) The error ranges are evaluated by the bootstrap method [69]. The error ranges of the distributions of random matrices are much smaller than those of the hard-core boson model and are not shown here or in the following figures (i.e., Figs. 8, 13, and 17; see also Figs. 4 and 5).

distribution obtained by the exact diagonalization is one of the most powerful tools for detecting the MBL. To identify the ergodic and MBL phases in the non-Hermitian case ($g \neq 0$), Ref. [41] used a scaling of the proportion of the number of real eigenvalues, entanglement entropy, and level-spacing distribution in the complex plane. The proportion of the number of real eigenvalues increases as the disorder strength increases. Furthermore, Ref. [41] conjectured that complex eigenvalues collapse onto the real axis and that the proportion of real eigenvalues becomes approximately 1 when the system undergoes a transition from the ergodic to MBL phases. Meanwhile, the scaling relationship between $\bar{N}_{\mathrm{real}}$ and N in the ergodic phase was not clarified.

We study the weak (strong) disorder regime of this model at the half-filling of the boson number with the parameters $t = 1$, $g = 0.1$, $U = 2$, $W = 2$ ($W = 30$). At the half-filling, the boson number M is the same as the half of the lattice site number L_x, (i.e., $M = L_x/2$). At least 400 different disorder realizations of Eq. (30) are diagonalized for each system size (the maximal system size is $L_x = 16$) and for each disorder strength.

In the weak disorder regime (ergodic phase), we find that $\rho(x + iy)$ has a δ-function peak on the real axis, $\rho(x + iy) = \rho_c(x, y) + \delta(y)\rho_r(x)$, and $\rho_c(x, y)$ shows a soft gap $\rho_c(x, y) \propto |y|$ around the real axis $y = 0$ [Figs. 6(a) and 6(b)]. We calculate the level-spacing distribution $p(s)$ and level-spacing-ratio distribution $p_r(r)$ of the real eigenvalues from an energy range around the center of the many-body spectrum. We exclude real eigenvalues near the edges of the spectrum from the statistics. For the system sizes $L_x \geqslant 12$, the error bars of the mean values of the level-spacing ratio with different system size L_x already overlap with each other [see Fig. 6(e)]. This indicates that the level statistics in the ergodic phase reach the convergence for $L_x \geqslant 12$.

We find that the level-spacing distribution and level-spacing-ratio distribution of real eigenvalues are well described by those obtained from non-Hermitian random matrices in class AI [Figs. 6(c) and 6(f)]. For reference, we compare the Kolmogorov-Smirnov distances between $p(s)$, $p_r(r)$ of our hard-core boson model in the ergodic phase and those from the non-Hermitian random matrices in the five symmetry classes in Appendix D. The comparison further confirms the consistency between the random matrix theory

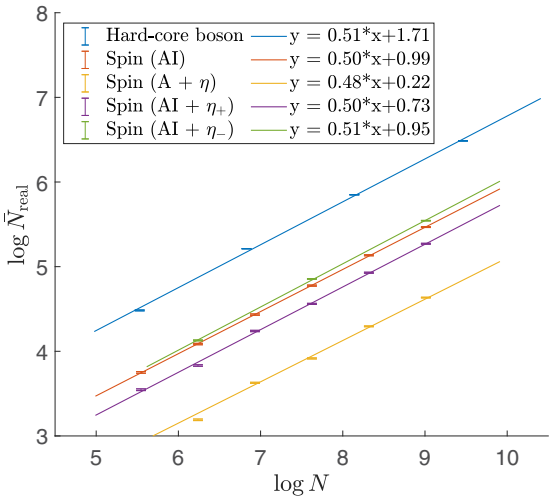

FIG. 7. Average number $\bar{N}_{\text{real}}$ of all the real eigenvalues as a function of the dimensions N of the Hilbert space for the many-body bosonic models in the weak disorder regimes ($W = 2$ or $W_x = W_y = W_z = W_D = 1$). The square-root scaling $\bar{N}_{\text{real}} \propto \sqrt{N}$ suggests that all the real eigenvalues of the bosonic models in the weak disorder regimes are consistent with the random matrix theory and hence well within the ergodic phase. All the 'log' in the figures are the natural log (ln).

and the physical Hamiltonian. We also calculate the number N_{real} of all the real many-body eigenenergies and its average $\bar{N}_{\text{real}}$ over the different disorder realizations. We find that $\bar{N}_{\text{real}}$ is scaled by the square root of the dimensions N of the many-body Hamiltonian, $\bar{N}_{\text{real}} \sim \sqrt{N}$ (Fig. 7), which is also consistent with the random matrix theory.

In the strong disorder regime (MBL phase), by contrast, almost all the eigenvalues are real, and thus we have $\bar{N}_{\text{real}} \sim N$. While the level-spacing-ratio distribution $p_r(r)$ of real eigenvalues is the same as $p_r(r)$ of uncorrelated real eigenvalues [Eq. (18)], the level-spacing distribution $p(s)$ of real eigenvalues is slightly different from the Poisson distribution. This slight difference is due to the finite-size effect and will vanish if the disorder strength or the system size is increased.

B. Interacting spin system

We consider the following 1D Heisenberg spin models with random magnetic fields, random energy gain (loss), or random imaginary Dzyaloshinskii-Moriya (DM) interaction:

$$\begin{aligned}
\mathcal{H}_{\text{I}} &= \sum_{i=1}^{L_x} J\boldsymbol{S}_i \cdot \boldsymbol{S}_{i+1},\\
\mathcal{H}_1 &= \mathcal{H}_{\text{I}} + \sum_i \left\{h_x^{(i)} S_x^{(i)} + i h_y^{(i)} S_y^{(i)} + h_z^{(i)} S_z^{(i)}\right\},\\
\mathcal{H}_2 &= \mathcal{H}_{\text{I}} + \sum_i \left\{i h_x^{(i)} S_x^{(i)} + i h_y^{(i)} S_y^{(i)} + h_z^{(i)} S_z^{(i)}\right\},\\
\mathcal{H}_3 &= \mathcal{H}_{\text{I}} + \sum_i \left\{i h_y^{(i)} S_y^{(i)} + h_z^{(i)} S_z^{(i)}\right\},\\
\mathcal{H}_4 &= \mathcal{H}_{\text{I}} + \sum_{i=1}^{L_x} \left\{iD_x^{(i)}\left(S_y^{(i)} S_z^{(i+1)} - S_z^{(i)} S_y^{(i+1)}\right)\right.\\
&\quad \left. + iD_z^{(i)}\left(S_y^{(i)} S_x^{(i+1)} - S_x^{(i)} S_y^{(i+1)}\right)\right\}. \qquad (32)
\end{aligned}$$

Here, $\boldsymbol{S}_i \equiv (S_x^{(i)}, S_y^{(i)}, S_z^{(i)}) \equiv \frac{1}{2}(\sigma_x^{(i)}, \sigma_y^{(i)}, \sigma_z^{(i)})$ is the spin-1/2 operators at site i with the periodic boundary conditions (i.e., $\boldsymbol{S}_{L_x+1} = \boldsymbol{S}_1$). The lattice site number L_x for $\mathcal{H}_4$ is chosen to be an odd integer to respect TRS whose sign is -1 [see also Eq. (40) below]. $h_x^{(i)}$, $h_y^{(i)}$, and $h_z^{(i)}$ are real random numbers that describe random magnetic fields or random energy gain and loss. $h_\mu^{(i)}$ ($\mu = x, y, z$) distributes independently and uniformly in $[-W_\mu/2, W_\mu/2]$ with $W_\mu \geqslant 0$. $D_x^{(i)}$ and $D_z^{(i)}$ are real random numbers (random imaginary DM interactions) that distribute independently and uniformly $[-W_D/2, W_D/2]$ with $W_D \geqslant 0$. These non-Hermitian terms can be realized, for example, in continuously measured cold atomic systems [78,79].

The random spin model $\mathcal{H}_1$ satisfies

$$\mathcal{H}_1 = \mathcal{H}_1^* \qquad (33)$$

and thus belongs to symmetry class AI. $\mathcal{H}_2$ satisfies

$$\mathcal{H}_2 = \left(\prod_i^{L_x} \sigma_z^{(i)}\right) \mathcal{H}_2^\dagger \left(\prod_i^{L_x} \sigma_z^{(i)}\right) \qquad (34)$$

and belongs to symmetry class A + η. $\mathcal{H}_3$ satisfies

$$\mathcal{H}_3 = \mathcal{H}_3^*, \qquad (35)$$

$$\mathcal{H}_3 = \left(\prod_i^{L_x} \sigma_z^{(i)}\right) \mathcal{H}_3^\dagger \left(\prod_i^{L_x} \sigma_z^{(i)}\right) \qquad (36)$$

with

$$\left(\prod_i^{L_x} \sigma_z^{(i)}\right) = \left(\prod_i^{L_x} \sigma_z^{(i)}\right)^*, \qquad (37)$$

and thus belongs to symmetry class AI + η_+. $\mathcal{H}_4$ satisfies

$$\mathcal{H}_4 = \mathcal{H}_4^*, \qquad (38)$$

$$\mathcal{H}_4 = \left(\prod_i^{L_x} \sigma_y^{(i)}\right) \mathcal{H}_4^\dagger \left(\prod_i^{L_x} \sigma_y^{(i)}\right). \qquad (39)$$

When L_x is an odd integer, the unitary matrix satisfies

$$\left(\prod_i^{L_x} \sigma_y^{(i)}\right) = -\left(\prod_i^{L_x} \sigma_y^{(i)}\right)^*, \qquad (40)$$

and hence the TRS operator and pH operator anticommute with each other. Thus, $\mathcal{H}_4$ belongs to class AI + η_- for odd L_x.

We study the weak disorder regimes of the four 1D Heisenberg models with the parameters $J = 1$, $W_x = W_y = W_z = W_D = 1$ and with the different system sizes (the maximal size is $L_x = 13$). From the DOS $\rho(E = x + iy) = \rho_c(x, y) + \delta(y)\rho_r(x)$, the soft gap of $\rho_c(x, y)$ around the real axis $y = 0$ is universally observed with the same asymptotic behavior for small y [Figs. 8(e)–8(h)]. For different L_x (L_x of $\mathcal{H}_4$ changes only for odd numbers), the number $\bar{N}_{\text{real}}$ of real eigenvalues shows the square-root scaling with respect to the dimensions N of the many-body Hamiltonians, $\bar{N}_{\text{real}} \propto \sqrt{N}$ (Fig. 7), which is consistent with the random matrix theory.

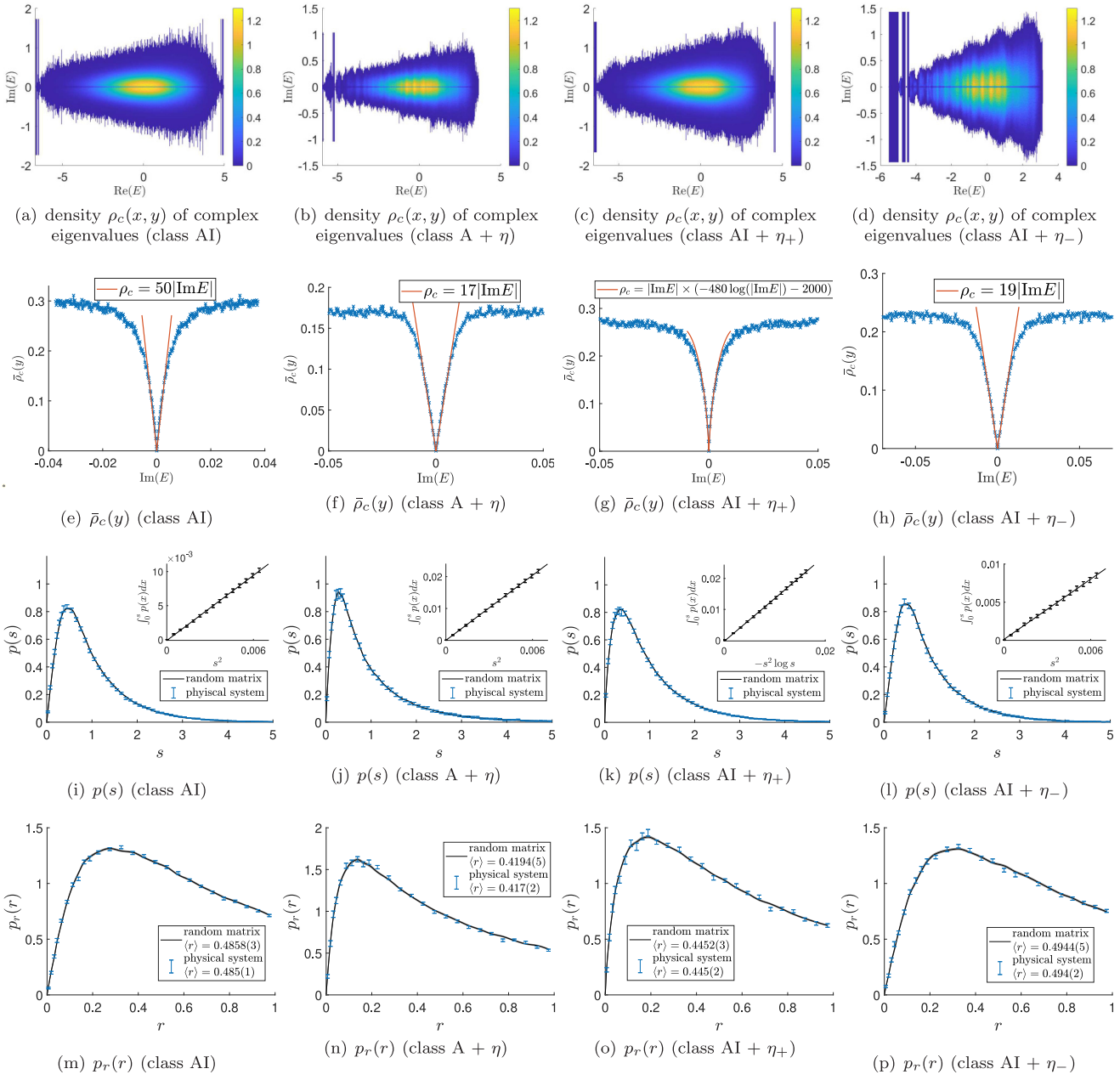

(a) density $\rho_c(x, y)$ of complex eigenvalues (class AI)
(b) density $\rho_c(x, y)$ of complex eigenvalues (class A + η)
(c) density $\rho_c(x, y)$ of complex eigenvalues (class AI + η_+)
(d) density $\rho_c(x, y)$ of complex eigenvalues (class AI + η_-)
(e) $\bar{\rho}_c(y)$ (class AI)
(f) $\bar{\rho}_c(y)$ (class A + η)
(g) $\bar{\rho}_c(y)$ (class AI + η_+)
(h) $\bar{\rho}_c(y)$ (class AI + η_-)
(i) $p(s)$ (class AI)
(j) $p(s)$ (class A + η)
(k) $p(s)$ (class AI + η_+)
(l) $p(s)$ (class AI + η_-)
(m) $p_r(r)$ (class AI)
(n) $p_r(r)$ (class A + η)
(o) $p_r(r)$ (class AI + η_+)
(p) $p_r(r)$ (class AI + η_-)

FIG. 8. (a)–(d) Heat maps of the density $\rho_c(x, y)$ of complex eigenvalues of the non-Hermitian interacting spin models in the weak disorder regimes ($W_x = W_y = W_z = W_D = 1$, $L_x = 13$) for (a) class AI, (b) class A + η, (c) class AI + η_+, and (d) class AI + η_-. (e)–(h) Integrated density of complex eigenvalues, $\bar{\rho}_c(y) = \frac{1}{5}\int_{-2.5}^{2.5} \rho_c(x, y)dx$, in the weak disorder regimes. From the heat maps, $-2.5 < E < 2.5$ for $W_x = W_y = W_z = W_D = 1$ is well within the ergodic phase for all the spin models. (i)–(l) Level-spacing distributions $p(s)$ of real eigenvalues in the weak disorder regimes of the interacting spin models, and their comparison to $p(s)$ from non-Hermitian random matrices in the same symmetry classes (red line). Insets: Asymptotic behavior of $\int_0^s p(s')ds'$ for $s \ll 1$. (m)–(p) Level-spacing-ratio distributions $p_r(r)$ of real eigenvalues in the weak disorder regimes of the interacting spin models, and their comparison to $p_r(r)$ from non-Hermitian random matrices in the same symmetry classes. The mean value $\langle r\rangle = \int_0^1 p_r(r)dr$ of each level-spacing-ratio distribution is shown in the figures. The statistics are taken in the weak disorder regime ($W_x = W_y = W_z = W_D = 1$ and $-10 < E < 10$ in all four spin models). The consistency between $p(s)$ [$p_r(r)$] from the spin models and $p(s)$ [$p_r(r)$] from the random matrices justifies that all eigenstates with real energy $-10 < E < 10$ in the weak disorder regime are in the ergodic phases. (i)–(p) The error ranges are evaluated by the bootstrap method [69]. All the 'log' in the figures are the natural log (ln).

Both level-spacing statistics and level-spacing-ratio statistics of real eigenvalues for each spin model show the same distributions as in the random matrices in the same symmetry class [Figs. 8(i)–8(l) and 8(m)–8(p)]. These results indicate that the square-root scaling of $\bar{N}_{\mathrm{real}}$ universally holds true in the ergodic phases of interacting disordered systems. It should be noted that many-body eigenstates in the ergodic phases are extended in many-body Hilbert space, while single-particle eigenstates in the metal phase, which are studied in Sec. IV, are extended in the spatial coordinate space.

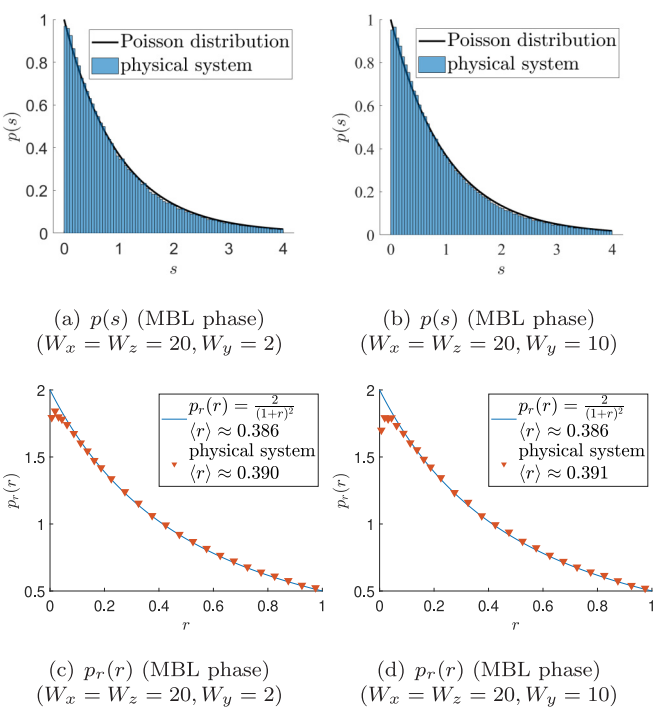

(a) $p(s)$ (MBL phase) $(W_x = W_z = 20, W_y = 2)$

(b) $p(s)$ (MBL phase) $(W_x = W_z = 20, W_y = 10)$

(c) $p_r(r)$ (MBL phase) $(W_x = W_z = 20, W_y = 2)$

(d) $p_r(r)$ (MBL phase) $(W_x = W_z = 20, W_y = 10)$

FIG. 9. Level-spacing distributions $p(s)$ of real eigenvalues in the strong disorder regimes of the non-Hermitian spin model $\mathcal{H}_1$ for (a) $W_x = W_z = 20$, $W_y = 2$ and (b) $W_x = W_z = 15$, $W_y = 10$. Level-spacing-ratio distributions $p_r(r)$ of real eigenvalues in the strong disorder regimes of $\mathcal{H}_1$ for (c) $W_x = W_z = 20$, $W_y = 2$ and (d) $W_x = W_z = 15, W_y = 10$. The statistics are taken from all the real eigenvalues of $\mathcal{H}_1$.

Moreover, we study the strong disorder regimes of $\mathcal{H}_1$ in class AI with the parameters $J = 1$, $W_x = W_z = 20$, $W_y = 2$ or $J = 1$, $15 \leqslant W_x = W_z \leqslant 40$, $W_y = 10$. We find that $\mathcal{H}_2$ and $\mathcal{H}_3$ in the strong disorder regimes show the level statistics of real eigenvalues similar to those of $\mathcal{H}_1$ in the strong disorder regimes (not shown). W_x and W_z in $\mathcal{H}_1$ describe Hermitian local disorder while W_y describes anti-Hermitian local disorder. When the Hermitian disorder dominates over the anti-Hermitian disorder ($W_x = W_z = 20$, $W_y = 2$), almost all the eigenvalues are real, where we have $\bar{N}_{\text{real}} \propto N$. The level-spacings and level-spacing ratios of real eigenvalues satisfy the Poisson distribution [Fig. 9(a)] and the distribution in Eq. (18) [Fig. 9(c)].

When the anti-Hermitian disorder is of the same order as the Hermitian disorders ($W_y = 10$, $10 \leqslant W_x = W_z \leqslant 40$), the number N_{real} of real eigenvalues fluctuates largely from sample to sample. The standard deviation of N_{real}, $\sigma^2_{\bar{N}_{\text{real}}} \equiv \langle N^2_{\text{real}} \rangle - \langle N_{\text{real}} \rangle^2$, grows exponentially with the system size L_x, and $\sigma_{N_{\text{real}}}$ is much larger than $\bar{N}_{\text{real}} \equiv \langle N_{\text{real}} \rangle$ (Fig. 10). Notably, we find that the scalings of $\bar{N}_{\text{real}}$ and $\sigma_{N_{\text{real}}}$ with respect to the dimensions N of the Hamiltonian are characterized by nonuniversal powers, such as $\bar{N}_{\text{real}} \sim N^{\alpha}$ (see Figs. 10 and 11). The powers of both $\bar{N}_{\text{real}}$ and $\sigma_{N_{\text{real}}}$ increase when the Hermitian disorders become larger.

The nonuniversal powers α in the scalings of $\bar{N}_{\text{real}}$ and $\sigma_{N_{\text{real}}}$ can be explained with a hypothesis that the MBL phase in the non-Hermitian case exhibits an emergent integrability as in the Hermitian case [12,13]. Suppose that the many-body non-

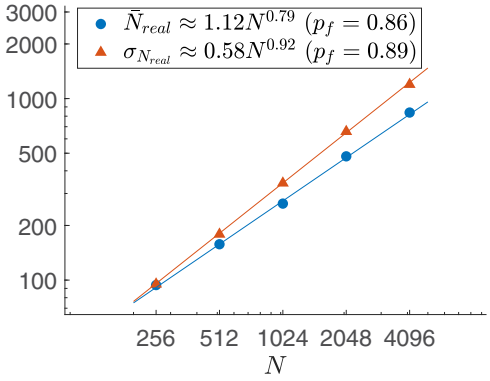

FIG. 10. Average number $\bar{N}_{\text{real}}$ of all the real eigenvalues and its standard deviation $\sigma_{N_{\text{real}}}$ in the non-Hermitian interacting spin model $\mathcal{H}_1$ as functions of the dimensions N of the Hilbert space. The Hermitian and anti-Hermitian disorder strengths are chosen to be on the same order ($W_x = W_z = 15$, $W_y = 10$). p_f is an estimation of the probability p in Eq. (45) by the linear regression on $\ln\bar{N}_{\text{real}}$ with $\ln N$ or $\ln\sigma_{N_{\text{real}}}$ with $\ln N$.

Hermitian Hamiltonian in the MBL phase can be effectively expanded in terms of L_x mutually commuting bit operators $\tau_z^{(i)}$ $(i = 1, 2, \ldots, L_x)$ as

$$\mathcal{H}_1^{\text{MBL}} = \sum_{i=1}^{L_x} \tau_z^{(i)} + \sum_{i,j} J_{ij} \tau_z^{(i)} \tau_z^{(j)} + \sum_{ijk} K_{ijk} \tau_z^{(i)} \tau_z^{(j)} \tau_z^{(k)} + \cdots . \tag{41}$$

Here, we have $[\tau_z^{(i)}, \tau_z^{(j)}] = [\mathcal{H}_1^{\text{MBL}}, \tau_z^{(i)}] = 0$ for all i and j. The bit operator $\tau_z^{(i)}$ is a two-by-two non-Hermitian matrix. $\mathcal{H}_1^{\text{MBL}}$ respects TRS and belongs to class AI. Given that the

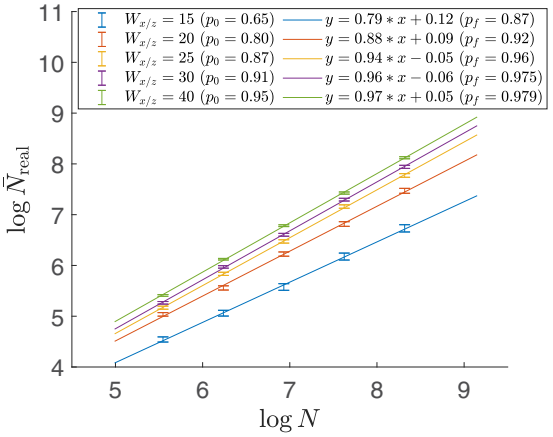

FIG. 11. Average number $\bar{N}_{\text{real}}$ of real eigenvalues as a function of the dimensions N of the Hilbert space of the interacting spin model $\mathcal{H}_1$. The Hermitian disorder strength and anti-Hermitian disorder strength are of the same order: the anti-Hermitian disorder strength is fixed to $W_y = 10$, while the Hermitian disorder strength is changed from $W_{x/z} = 15$ to 40. p_0 is the probability that an eigenvalue of the local disordered Hamiltonian $h_x^{(i)}\sigma_x^{(i)} + ih_y^{(i)}\sigma_y^{(i)} + h_z^{(i)}\sigma_z^{(i)}$ becomes real. p_f is an estimation of the probability p in Eq. (45) by the linear regression on $\ln\bar{N}_{\text{real}}$ with $\ln N$. All the 'log' in the figures are the natural log (ln).

coefficients such as J_{ij} and K_{ijk} are real numbers, the bit operator must also be real $(\tau_z^{(i)})^* = \tau_z^{(i)}$:

$$\tau_z^{(i)} = \begin{pmatrix} a_0^{(i)} + a_1^{(i)} & a_2^{(i)} + a_3^{(i)} \\ a_2^{(i)} - a_3^{(i)} & a_0^{(i)} - a_1^{(i)} \end{pmatrix} \tag{42}$$

with real numbers $a_\alpha^{(i)}$ $(\alpha = 0, 1, 2, 3)$. The real numbers of different i and different components are almost independent of one another in the strong disorder regime. When $\mathcal{H}_1$ is dominated by the on-site random terms $(W_x, W_y, W_z \gg J)$, the bit operator is given by the random magnetic fields at each lattice site, $a_0^{(i)} = 0$, $a_1^{(i)} = h_z^{(i)}/2$, $a_2^{(i)} = h_x^{(i)}/2$, and $a_3^{(i)} = h_y^{(i)}/2$. For $(a_1^{(i)})^2 + (a_2^{(i)})^2 > (a_3^{(i)})^2$, the bit operator $\tau_z^{(i)}$ has real eigenvalues,

$$\lambda_{\pm 1}^{(i)} = a_0 \pm \sqrt{\left(a_1^{(i)}\right)^2 + \left(a_2^{(i)}\right)^2 - \left(a_3^{(i)}\right)^2}.$$

For $(a_1^{(i)})^2 + (a_2^{(i)})^2 < (a_3^{(i)})^2$, the bit operator has complex eigenvalues,

$$\lambda_{\pm \mathrm{i}}^{(i)} = a_0 \pm i\sqrt{\left(a_3^{(i)}\right)^2 - \left(a_1^{(i)}\right)^2 - \left(a_2^{(i)}\right)^2}.$$

From them, a many-body eigenvalue of $\mathcal{H}_1^{\mathrm{MBL}}$ is given by

$$E(\{\beta_j\}) = \sum_{j=1}^{L_x} \lambda_{\beta_j}^{(j)} + \sum_{i,j} J_{ij} \lambda_{\beta_i}^{(i)} \lambda_{\beta_j}^{(j)} + \cdots \tag{43}$$

with $\beta_j = \pm 1, \pm i$ for $j = 1, 2, \ldots, L_x$.

Let p be a probability of the bit operator of i having real eigenvalues. The probability is independent of i, and two bit operators at different i and j are uncorrelated with each other. Thus, a probability of a given many-body eigenvalue being real-valued equals a probability of all $\lambda_{\beta_i}^{(i)}$ being real, which is p^{L_x}. The average and standard deviation of the number of real eigenvalues are estimated as

$$\begin{aligned} \bar{N}_{\mathrm{real}} &= (2p)^{L_x}, \\ \sigma_{N_{\mathrm{real}}} &= \sqrt{\langle N_{\mathrm{real}}^2 \rangle - \bar{N}_{\mathrm{real}}^2} = 2^{L_x}\sqrt{p^{L_x} - p^{2L_x}} \\ &\simeq (2\sqrt{p})^{L_x} \end{aligned} \tag{44}$$

for $L_x \gg 1$ and $p < 1$. Here, $\langle \cdots \rangle$ means the average over different disorder realizations. These evaluations lead to the scalings

$$\begin{aligned} \bar{N}_{\mathrm{real}} &\sim N^{\alpha}, \quad \alpha = 1 + \log_2 p < 1, \\ \sigma_{N_{\mathrm{real}}} &\sim N^{\beta}, \quad \beta = 1 + \tfrac{1}{2}\log_2 p < 1. \end{aligned} \tag{45}$$

Note that in the MBL phase with $p < 1$, $\sigma_{N_{\mathrm{real}}}$ is much larger than $\bar{N}_{\mathrm{real}}$ for large N, being consistent with the numerical observation (Fig. 10). When the on-site disorders in $\mathcal{H}_1$ become much more dominant than the Heisenberg interaction J, the probability p in the scaling forms can be determined only by W_x, W_y, and W_z (see p_0 in the caption of Fig. 11). The numerical data with the finite disorder strengths are approximately well fitted by Eq. (45) with similar values of p (Fig. 11). In the strong disorder regime, the probability distribution of N_{real} shows two peaks around $N_{\mathrm{real}} = 0$ (i.e., none of eigenvalues are real) and $N_{\mathrm{real}} = N$ (i.e., all eigenvalues are real) (Fig. 12), which are also consistent with the phenomenological explanation in Eq. (43).

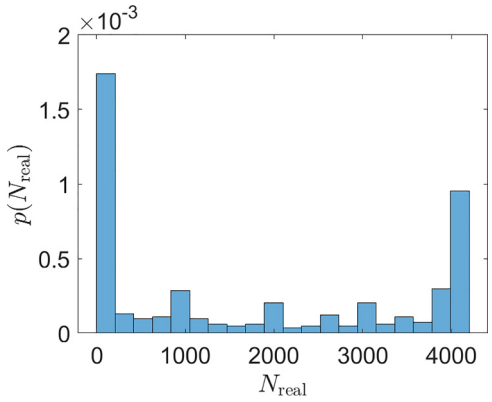

FIG. 12. Probability distribution of the number N_{real} of real eigenvalues of the interacting spin model $\mathcal{H}_1$ in the strong disorder regime ($W_x = W_z = 20$, $W_y = 10$). The distribution is obtained from the diagonalization of 400 samples with the system size $L_x = 12$. The dimensions of the Hilbert space are $N = 2^{L_x} = 4096$. The two peaks, $N_{\mathrm{real}} = 0$ and $N_{\mathrm{real}} = N$, appear in the distribution.

The level-spacing statistics of real eigenvalues show the Poisson distribution in the strong disorder regime. To illustrate this with $\sigma_{N_{\mathrm{real}}} \gg \bar{N}_{\mathrm{real}}$, we unfold the level-spacing of many-body eigenvalues by the density $\rho_c(x, y)$ of complex eigenvalues in each sample of different disorder realizations,

$$s_i \equiv (\lambda_{i+1} - \lambda_i)\bar{\rho}_r^{(k)}\left(\frac{\lambda_{i+1} + \lambda_i}{2}\right)$$

with

$$\bar{\rho}_r^{(k)}(x) \equiv \frac{N_{\mathrm{real}}^{(k)}}{\bar{N}_{\mathrm{real}}} \sum_{\lambda_i \in \mathcal{R}} \langle \delta(x - \lambda_i) \rangle. \tag{46}$$

Here, λ_i $(i = 1, 2, \ldots, 2_x^L)$ stands for the many-body eigenvalues in descending order, and $N_{\mathrm{real}}^{(k)}$ is the number of the real eigenvalues in the kth sample. The real-eigenvalue spacing thus normalized shows the Poisson distribution in the strong disorder regime with $\sigma_{N_{\mathrm{real}}} \gg N_{\mathrm{real}}$ [Fig. 9(b)]. The spacing-ratio statistics over samples with very different numbers of real eigenvalues inevitably increase statistical errors [Fig. 9(d)].

IV. DISSIPATIVE FREE FERMIONS

In the previous section, we demonstrate the universal level statistics of real eigenvalues in the ergodic phases of the bosonic many-body Hamiltonians. In this section, we study noninteracting fermionic Hamiltonians with disorder and non-Hermiticity that belong to symmetry classes AI + η_+ and AII + η_+. We calculate the DOS, the level-spacing statistics, and the number of real eigenvalues in the weak and strong disorder regimes. In both regimes, the DOS has a δ-function peak on the real axis, $\rho(E \equiv x + iy) = \rho_c(x, y) + \delta(y)\rho_r(x)$. In the metal phases, we demonstrate that the number of real eigenvalue is scaled by the square root of the dimensions of the Hamiltonians, being consistent with the random matrix theory. We also find that the real-eigenvalue spacings and spacing ratios for class AI + η_+ show the same distributions as those of the random matrices in the same symmetry class while we

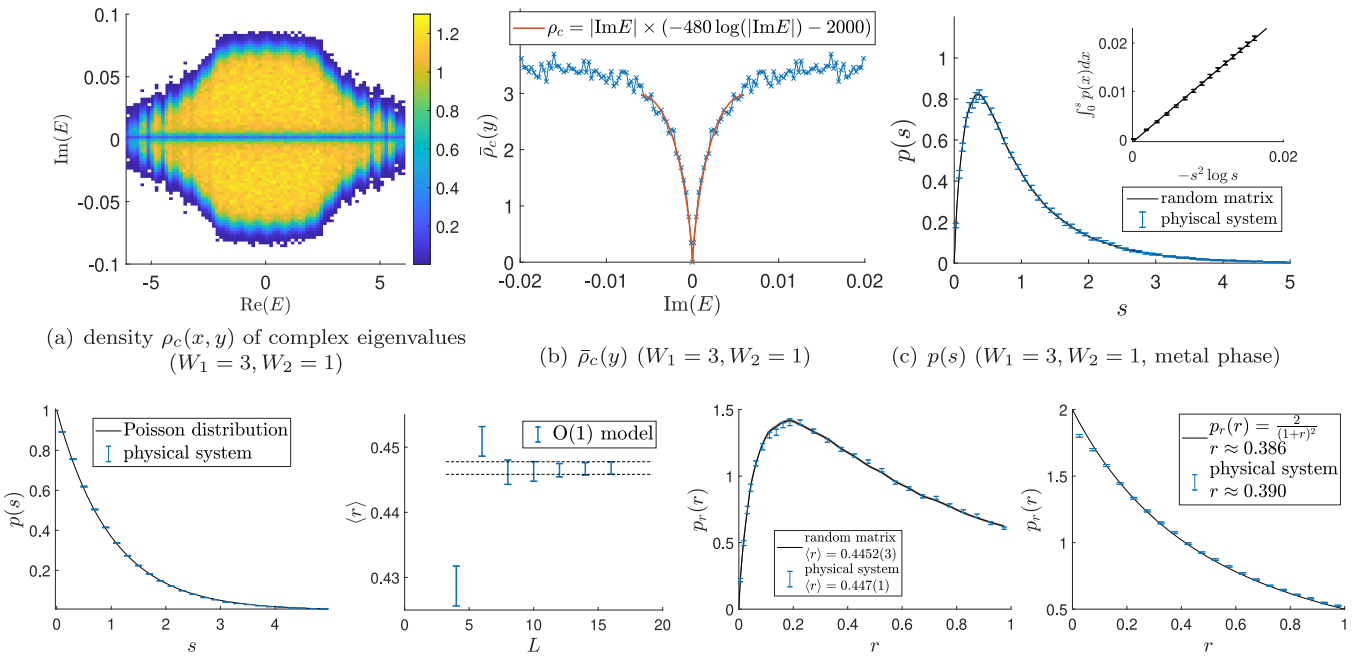

(a) density $\rho_c(x, y)$ of complex eigenvalues $(W_1 = 3, W_2 = 1)$

(b) $\bar{\rho}_c(y)$ $(W_1 = 3, W_2 = 1)$

(c) $p(s)$ $(W_1 = 3, W_2 = 1$, metal phase)

(d) $p(s)$ $(W_1 = 60, W_2 = 60$, localized phase)

(e) $\langle r\rangle - N$ $(W_1 = 3, W_2 = 1$, metal phase)

(f) $p_r(r)$ $(W_1 = 3, W_2 = 1$, metal phase)

(g) $p_r(r)$ $(W_1 = 60, W_2 = 60$, localized phase)

FIG. 13. (a) Heat map of the density $\rho_c(x, y)$ of complex eigenvalues in 3D class AI + η_+ for the weak disorder regime ($W_1 = 3$, $W_2 = 1$, $16 \times 16 \times 16$ sites). (b) Integrated density of complex eigenvalues, $\bar{\rho}_c(y) \equiv \frac{1}{2x_1}\int_{-x_1}^{x_1} \rho_c(x, y)dx$, around the real axis $y = \mathrm{Im}(E) = 0$ with $x_1 = 2$. (c) Level-spacing distribution $p(s)$ of real eigenvalues in the metal phase ($|E| < 4$, $W_1 = 3$, and $W_2 = 1$), and its comparison to $p(s)$ from non-Hermitian random matrices in the same symmetry class (black line). Inset: Asymptotic behavior of $\int_0^s p(s')ds'$ for $s \ll 1$ in the metal phase. (d) $p(s)$ in the localized phase of the 3D model (all the real energy E, $W_1 = W_2 = 60$) and its comparison to the Poisson distribution. (e) Mean value of level-spacing ratios $\langle r\rangle = \int_0^1 p_r(r)dr$ as a function of system size L. (f) Level-spacing-ratio distribution $p_r(r)$ of real eigenvalues in the metal phase ($|E| < 4$, $W_1 = 3$, $W_2 = 1$) and its comparison to $p_r(r)$ from non-Hermitian random matrices in the same symmetry class. (g) $p_r(r)$ of real eigenvalues in the localized phase (all real energy E, $W_1 = W_2 = 60$) and its comparison to $p_r(r)$ of uncorrelated real numbers. The mean value $\langle r\rangle$ of each level-spacing-ratio distribution is shown in the figures. (c)–(g) The error ranges are evaluated by the bootstrap method [69]. All the 'log' in the figures are the natural log (ln).

find discrepancies for class AII + η_+. We discuss possible reasons for these discrepancies. In the localized phases, by contrast, the level-spacings of real eigenvalues show the Poisson distribution, and the number of real eigenvalues is linearly scaled by the dimensions of the Hamiltonians.

A. 3D class AI + η_+

We study a non-Hermitian extension of the Anderson model on the three-dimensional (3D) cubic lattice:

$$\mathcal{H}_{3D} = \sum_i (c_i^\dagger(\varepsilon_i\sigma_0 + \varepsilon_i'\sigma_z)c_i + i\omega_i c_i^\dagger\sigma_y c_i) + t\sum_{\langle i,j\rangle} c_i^\dagger\sigma_0 c_j. \tag{47}$$

Here, ε_i and ε_i' describe the Hermitian disordered potentials that distribute independently and uniformly in $[-W_1/2, W_1/2]$, and ω_i describes the anti-Hermitian disordered potential that distributes uniformly in $[-W_2/2, W_2/2]$. The non-Hermitian Hamiltonian $\mathcal{H}_{3D}$ satisfies TRS,

$$\mathcal{H}_{3D} = \mathcal{H}_{3D}^*, \tag{48}$$

and pH,

$$\mathcal{H}_{3D} = \sigma_z\mathcal{H}_{3D}^\dagger\sigma_z, \tag{49}$$

where the TRS operator and the pH operator commute with each other. Thus, this model belongs to symmetry class AI + η_+.

We investigate the weak (strong) disorder regime with the parameters $t = 1$, $W_1 = 3$, $W_2 = 1$ ($W_1 = 60$, $W_2 = 60$) and with the periodic boundary conditions. We diagonalize $\mathcal{H}_{3D}$ with 240 different disorder realizations with different system sizes (the maximal system size is $16 \times 16 \times 16$). We find that eigenstates with real energy E undergo the Anderson transition in the weak disorder regime. An energy region near $E = 0$ ($|E| < 4$) is in the metal and localized phases in the weak and strong disorder regimes, respectively. We calculate the DOS, the level-spacing distribution, and the number of real eigenvalues in the weak and strong disorder regimes. In the weak disorder regime, $\rho_c(x, y)$ shows a soft gap $\rho_c(x, y) \propto -|y|\ln|y|$ around the real axis $y = 0$ [Figs. 13(a) and 13(b)], sharing the same scaling as in the random matrix theory for symmetry class AI + η_+. The mean value of the level-spacing ratios converges for the system size $L \geqslant 8$ [Fig. 13(e)]. The level-spacing distribution $p(s)$ and level-spacing-ratio distribution $p_r(r)$ of real eigenvalues, respectively match well with $p(s)$ and $p_r(r)$ from non-Hermitian random matrices in class AI + η_+ [Figs. 13(c) and 13(f)]. The number of real eigenvalues is scaled by the square root of the dimensions of

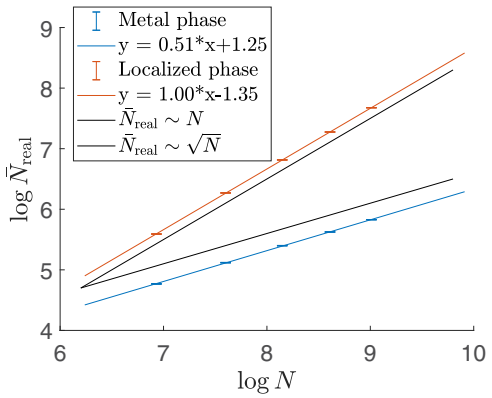

FIG. 14. Average number $\bar{N}_{\rm real}$ of real eigenvalues as a function of the dimensions N of the non-Hermitian disordered Hamiltonian in 3D class AI + η_+. The lines with the different colors are for the different disorder strengths. The blue line is for the metal phase in the weak disorder regime ($|E| \leqslant 4$, $W_1 = 3$, and $W_2 = 1$). The red line is for the localized phase in the strong disorder regime (all the real energy E, $W_1 = W_2 = 60$). For reference, the black lines are $\bar{N}_{\rm real} \propto N$ and $\bar{N}_{\rm real} \propto \sqrt{N}$, respectively. All the 'log' in the figures are the natural log (ln).

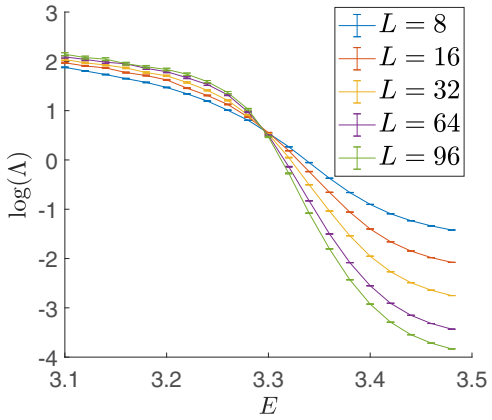

FIG. 15. Normalized localization length $\Lambda = \xi_x/L$ as a function of real energy E in the 2D non-Hermitian SU(2) model in the weak disorder regime ($W = 0.4$, $W' = 0$). The localization length ξ_x along the x direction is calculated in the quasi-1D geometry ($L_x \times L$ with $L_x \gg L$). Eigenstates with energy E and eigenstates with energy $-E$ share the same localization length. For $|E| < E_c$ ($|E| > E_c$) with $E_c \approx 3.3$, Λ increases (decreases) as L increases, and thus the system is in the metal (localized) phase. All the 'log' in the figures are the natural log (ln).

the Hamiltonian, being consistent with the scaling from the random matrix theory. In the strong disorder regime, on the other hand, the level-spacing and level-spacing-ratio statistics of real eigenvalues are consistent with those of uncorrelated real eigenvalues [Figs. 13(d) and 13(g)], and the soft gap of $\rho_c(x, y)$ near the real axis disappears (not shown here).

In the strong disorder regime, $N_{\rm real}$ is scaled linearly in N (Fig. 14). This linear scaling $\bar{N}_{\rm real} \propto N$ in the localized phase is explained as follows. A disordered Hamiltonian in the localized phase can be viewed as $(L/\xi)^d$ almost independent blocks. Here, ξ is a localization length in the localized phase, L is the linear dimensions of the system size, and d is the spatial dimensions. Each block can be regarded as an independent random matrix, and dimensions of each block are of the order of ξ^d. Thus, $N_{\rm real}$ is evaluated as

$$N_{\rm real} \sim (L/\xi)^d \sqrt{\xi^d} \propto N, \tag{50}$$

which is consistent with the numerical results.

B. 2D class AII + η_+

We study a non-Hermitian extension of the disordered SU(2) model [80] on the 2D square lattice:

$$\begin{aligned}\mathcal{H}_{\rm 2D} = &\sum_i (\varepsilon_i c_i^\dagger \sigma_0 c_i + \varepsilon_i' d_i^\dagger \sigma_0 d_i) \\ &+ \sum_{\langle i,j\rangle} t_1 [c_i^\dagger R(i,j) c_j + d_i^\dagger R'(i,j) d_j] \\ &+ \sum_{\langle i,j\rangle} t_2 [c_i^\dagger U(i,j) d_j + d_i^\dagger U'(i,j) c_j],\end{aligned} \tag{51}$$

where c_i and d_i are annihilation operators for two different orbitals defined on site i. Both operators have a pseudo-spin-1/2 degree of freedom. $\langle i, j\rangle$ denotes the nearest-neighbor square-lattice sites. σ_0 stands for the two-by-two identity matrix acting on the spin degree of freedom. ε_i and ε_i' are on-site random potentials that distribute independently and uniformly in the range $[-W/2, W/2]$. t_1 and t_2 are real numbers. $R(i, j)$, $R'(i, j)$, $U(i, j)$, and $U'(i, j)$ are SU(2) matrices that distribute uniformly with respect to the Harr measure of SU(2) [80] and satisfy the following symmetry properties:

$$R(i,j) = R^\dagger(j,i), \tag{52}$$

$$R'(i,j) = R'^\dagger(j,i), \tag{53}$$

$$U(i,j) = -U'^\dagger(j,i). \tag{54}$$

The term with t_2 is anti-Hermitian and the others are Hermitian. Let τ_z be a two-by-two matrix acting on the orbital space, satisfying $\tau_z(c_i, d_i)^T \equiv (c_i, -d_i)^T$. The Hamiltonian in Eq. (51) satisfies TRS,

$$\mathcal{H}_{\rm 2D} = \sigma_y \mathcal{H}_{\rm 2D}^* \sigma_y, \tag{55}$$

and pH,

$$\mathcal{H}_{\rm 2D} = \tau_z \mathcal{H}_{\rm 2D}^\dagger \tau_z, \tag{56}$$

where the TRS operator and the pH operator commute with each other. Thus, the Hamiltonian belongs to symmetry class AII + η_+. This Hamiltonian is a minimal model to study the interplay between the spin-orbit coupling [81] and pH.

We investigate the weak (strong) disorder regime of Eq. (51) with the parameters $t_1 = 1$, $t_2 = 0.1$, $W = 0.4$ ($W = 80$) and with the periodic boundary conditions. In the weak disorder regime, we find that eigenstates with real eigenvalues E undergo the Anderson transition at a certain mobility edge $E = E_c$. The normalized localization length $\Lambda(E, L) \equiv \xi_x(E, L)/L$ shows a scale-invariant behavior at $E = E_c$ (Fig. 15). Here, the localization length $\xi_x(E, L)$ is calculated along the x direction by the transfer matrix method in the quasi-1D geometry $L \times L_x$ ($L_x \gg L$) [48,82–84]. For the weak disorder regime, $|E| < E_c \approx 3.3$ and $|E| > E_c$ correspond to the metal and localized phases, respectively (Fig. 15). We diagonalize the Hamiltonians in Eq. (51) with 240

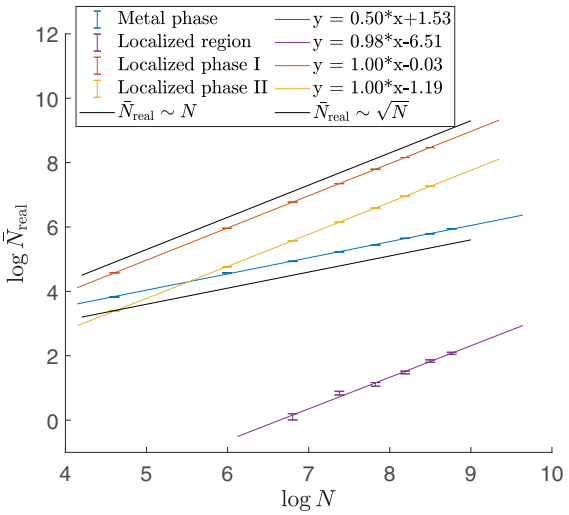

FIG. 16. Average number $\bar{N}_{\rm real}$ of real eigenvalues as a function of the dimensions N of the 2D non-Hermitian SU(2) model. The different colored lines are for the different disorder strength and energy regions. The blue line is for the metal phase ($|E| \leqslant 3$ with $W = 0.4$, $W' = 0$), the purple line is for the localized phase ($|E| \geqslant 3.5$ with $W = 0.4$, $W' = 0$), the red line is for the localized phase I (all the real energies E with $W = 80$, $W' = 0$), and the yellow line is for the localized phase II (all the real energies E with $W = 40$, $W' = 40$). For reference, the black lines are $\bar{N}_{\rm real} \propto N$ and $\bar{N}_{\rm real} \propto \sqrt{N}$, respectively. All the 'log' in the figures are the natural log (ln).

different disorder realizations for each system size (the maximal system size is 55×55 sites), where eigenstates near the mobility edge are excluded from the level statistics of real eigenvalues.

In the weak disorder regime, the density $\rho_c(x, y)$ of complex eigenvalues shows the soft gap $\rho_c(x, y) \propto |y|$ in the metal phase [$|x| = |{\rm Re}(E)| < E_c$] for $y = {\rm Im}(E)$ much smaller than the mean level-spacing [Figs. 17(a) and 17(b)]. The soft-gap behavior is consistent with the DOS of non-Hermitian random matrices in class AII + η_+. The number of real eigenvalues within the metal phase, $\bar{N}_{\rm real}^{\rm metal} \equiv \int_{-E_c}^{E_c} dx \rho_r(x)$, shows the square-root scaling with respect to the dimensions N of the Hamiltonian, $\bar{N}_{\rm real}^{\rm metal} \propto \sqrt{N}$ (Fig. 16), which is also consistent with the random matrix theory. On the other hand, the number of real eigenvalues in the localized phase, $\bar{N}_{\rm real}^{\rm loc} \equiv \int_{|x|>E_c} dx \rho_r(x)$, is scaled by N, $\bar{N}_{\rm real}^{\rm loc} \propto N$ (Fig. 16).

The mean value $\langle r \rangle$ of the level-spacing ratios in the metallic phase converges to the value $\langle r \rangle \approx 0.41$ for larger system size [Fig. 17(d)]. This value is larger than the mean value $\langle r \rangle \approx 0.37$ of non-Hermitian random matrices in class AII + η_+, suggesting a possible discrepancy of the level statistics between the physical model and the random matrices. In fact, the level-spacing distribution $p(s)$ and level-spacing-ratio distribution $p_r(r)$ in the metallic phase are also different from those of the random matrices [Figs. 17(e) and 17(g)], although the small-s behavior of $p(s)$ is consistent with the random matrix theory [inset of Fig. 17(e)]. The Kolmogorov-Smirnov distances between $p(s)$, $p_r(r)$ in the metallic phase and those of the random matrices are around 0.06 (Appendix D) while the distances are less than 0.01 in the other four symmetry classes. Similar discrepancies of the level statistics were previously reported in physical models near the mobility edge of the Anderson transition [9] or the MBL transition [85]. Nonetheless, in our study, an energy window $|E| < 3$ for the level statistics of the physical model is well within the metallic phase $|E| < E_c \approx 3.3$ (Fig. 15). No previous works found such discrepancies of $p(s)$ and $p_r(r)$ between physical models in the metallic phases and the random matrices.

A possible reason for the discrepancies is unusual level interactions in non-Hermitian random matrices in class AII + η_+. As discussed in Sec. II, the small level-spacing ratio $\langle r \rangle < \langle r \rangle_{\rm Poisson}$ and the large spectral compressibility $\chi > \chi_{\rm Poisson}$, which are also supported by the small random matrix analyses, suggest that the attractive interaction between real eigenvalues in the finite-s regime dominates the repulsive interaction in the small-s regime on average. We speculate that this unconventional level attraction makes the level statistics of the random matrices in the finite-s region unstable against details of physical models. Only for smaller level spacing $s \ll 1$, the behaviors between the physical model and random matrices are consistent. It is unclear whether $p(s)$ and $p_r(r)$ of physical models in class AII + η_+ are universal or not, and we leave this issue for future study. It is also interesting to investigate whether the non-Hermitian generalization of other random matrix ensembles, such as the power-law random banded matrix ensemble [86] and the Rosenzweig-Porter random-matrix ensemble [87,88], can describe the physical models in class AII + η_+.

In the strong disorder regime ($W = 80$), the soft gap in the DOS around the real axis $y = 0$ disappears (not shown here). The level-spacings of real eigenvalues show the Poisson distribution [Fig. 17(f)], and the level-spacing ratios of real eigenvalues show the same distribution as uncorrelated real numbers in Eq. (18) [Fig. 17(h)]. The average number of all the real eigenvalues becomes proportional to N (Fig. 16). In this phase, the Hamiltonian is dominated by the Hermitian part and almost all the eigenvalues are real, resulting in the linear scaling $\bar{N}_{\rm real} \propto N$. To confirm that this linear scaling is a general property of the Anderson localized phase, we generalize the model in Eq. (51) and study the following model $\mathcal{H}'_{\rm 2D}$:

$$\mathcal{H}'_{\rm 2D} = \mathcal{H}_{\rm 2D} + \Delta\mathcal{H},$$
$$\Delta\mathcal{H} = \sum_i \omega_i c_i^\dagger \sigma_0 d_i - \omega_i d_i^\dagger \sigma_0 c_i. \tag{57}$$

Adding $\Delta\mathcal{H}$ does not change the symmetry class of $\mathcal{H}_2$ (class AII + η_+). Here, ω_i distributes uniformly in $[-W'/2, W'/2]$. We calculate the DOS, the level-spacing distribution $p(s)$, and the number of real eigenvalues with the parameter $W' = W = 40$. Thereby, $\rho_c(x, y)$ has no soft gap around $y = 0$ [Fig. 17(c)], $p(s)$ is consistent with the Poisson distribution, and $\bar{N}_{\rm real} \equiv \int_{-\infty}^{+\infty} dx \rho_r(x)$ remains linear in N (Fig. 16).

V. CONCLUSIONS

Non-Hermitian Hamiltonians in the seven symmetry classes (classes A + η, AI, AI + $\eta_\pm$, AII, and AII + $\eta_\pm$) have TRS or pH. Real eigenvalues respect these symmetries with complex or Hermitian conjugation. We find that a subextensive number of eigenenergies of non-Hermitian random matrices in classes A + η, AI, AI + $\eta_\pm$, and AII

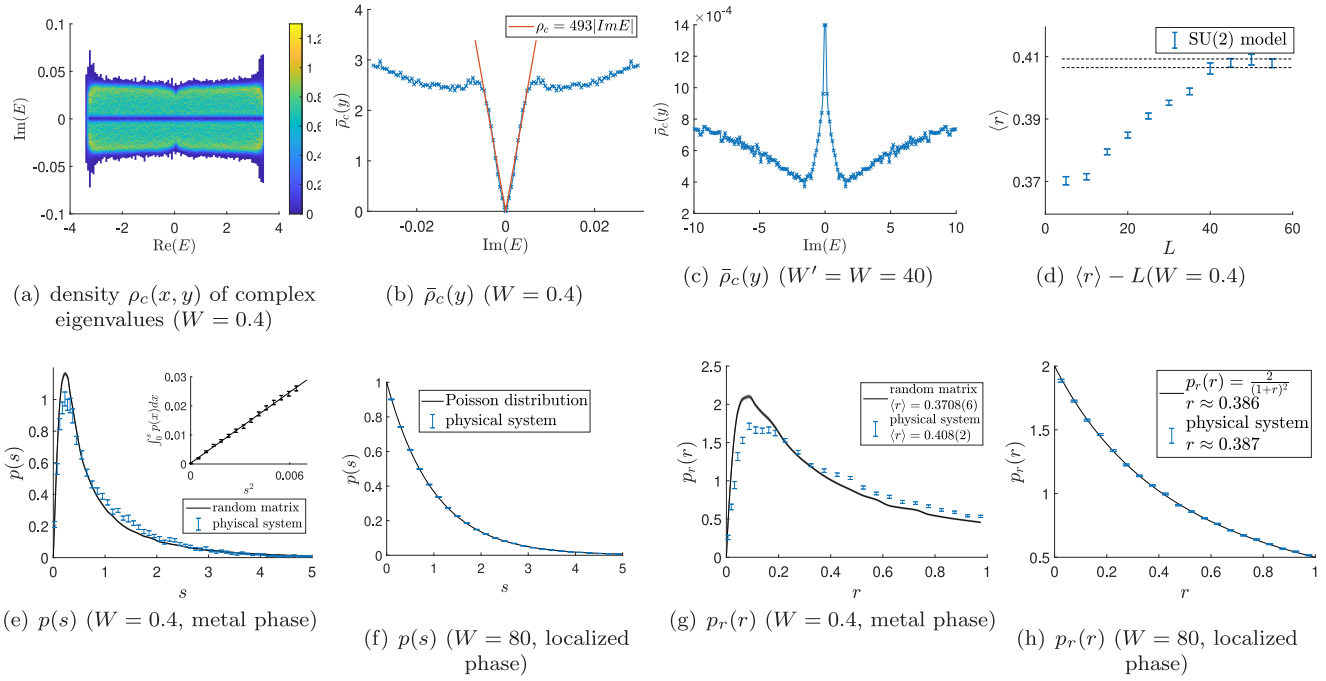

(a) density $\rho_c(x, y)$ of complex eigenvalues ($W = 0.4$)

(b) $\bar{\rho}_c(y)$ ($W = 0.4$)

(c) $\bar{\rho}_c(y)$ ($W' = W = 40$)

(d) $\langle r \rangle - L (W = 0.4)$

(e) $p(s)$ ($W = 0.4$, metal phase)

(f) $p(s)$ ($W = 80$, localized phase)

(g) $p_r(r)$ ($W = 0.4$, metal phase)

(h) $p_r(r)$ ($W = 80$, localized phase)

FIG. 17. (a) Heat map of the density $\rho_c(x, y)$ of complex eigenvalues of the 2D non-Hermitian SU(2) model in the weak disorder regime ($W = 0.4$, $W' = 0$, 55×55 sites). (b,d) Integrated density of complex eigenvalues, $\bar{\rho}_c(y) \equiv \frac{1}{2x_1} \int_{-x_1}^{x_1} \rho_c(x, y)dx$, as a function of small $y = \mathrm{Im}(E)$ around the real axis $y = 0$ (b) in the weak disorder regime ($W = 0.4$, $W' = 0$, $x_1 = 3$) and (c) in the strong disorder regime ($W = W' = 40$, $x_1 = 20$). (d) Mean value of level-spacing ratios as a function of system size in the metal phase ($|E| < 3$, $W = 0.4$, $W' = 0$). (e) Level-spacing distribution $p(s)$ of real eigenvalues in the metal phase of the non-Hermitian SU(2) model ($|E| < 3$, $W = 0.4$, $W' = 0$), and its comparison to $p(s)$ from random matrices in symmetry class AII + η_+ (red line). Inset: Asymptotic behavior of $\int_0^s p(s')ds'$ in the metal phase for $s \ll 1$. (f) $p(s)$ in the localized phase of the 2D non-Hermitian SU(2) model (all the real energies E, $W = 80$, $W' = 0$), and its comparison to the Poisson distribution. (g) Level-spacing-ratio distribution $p_r(r)$ of real eigenvalues in the metal phase of the 2D non-Hermitian SU(2) model ($|E| < 3$, $W = 0.4$, $W' = 0$) and its comparison to $p_r(r)$ from non-Hermitian random matrices in symmetry class AII + η_+. The difference between the physical model and random matrices cannot be neglected. (h) $p_r(r)$ of real eigenvalues in the localized phase (all real energy E, $W = 40$, $W' = 0$) of the 2D non-Hermitian SU(2) model and its comparison to $p_r(r)$ of uncorrelated real numbers. The mean value $\langle r \rangle = \int_0^1 p_r(r)dr$ of each level-spacing-ratio distribution is also shown in the figures. (d)–(h) The error ranges are evaluated by the bootstrap method [69].

+ η_+ are real, where the DOS on the complex plane has a δ-function peak on the real axis. We clarify the universal level-spacing distributions on the real axis in these five symmetry classes for non-Hermitian random matrices, as well as bosonic many-body Hamiltonians in the ergodic phases and fermionic noninteracting Hamiltonians in the metal phases. In classes A + η, AI, and AI + $\eta_\pm$, the level statistics of real eigenvalues show good agreement between the ergodic physical models and random matrices, while we find discrepancies in class AII + η_+. The average number of real eigenvalues in the ergodic phases universally shows the square-root scaling with respect to the dimensions of the Hamiltonians. We explain the universal asymptotic behaviors of the DOS around the real axis and the level-spacing distributions on the real axis by small random matrix analyses. We also clarify the level statistics of the physical models in the Anderson localized and MBL phases by extensive numerical calculations together with the phenomenological interpretations.

The universal level-spacing and level-spacing-ratio distributions of real eigenvalues and the scaling relationship of the number of real eigenvalues obtained in this paper provide powerful methods of studying level statistics of non-Hermitian systems with TRS and/or pH. They are also useful for detecting quantum chaos, many-body localization, and real-complex transitions in non-Hermitian systems with the symmetries.

For example, the level statistics of real eigenvalues help us answer fundamental questions on non-Hermitian disordered systems. Analyzing level spacings or level-spacing ratios of real eigenvalues in the different energy windows, we can determine the presence of mobility edges in non-Hermitian many-body systems. By the finite-size scaling analysis of spacing ratios [89], we can also evaluate the critical exponents of the Anderson transitions in non-Hermitian systems with TRS and/or pH. Comparisons of the critical exponents with systems without TRS or pH tell us whether TRS and/or pH change the universality classes of MBL transitions in non-Hermitian systems. We believe that with the help of the results in this paper, a number of spectral analysis methods and quantum chaotic studies used in Hermitian systems are ready to be applied to non-Hermitian systems with TRS and/or pH.

The real spectrum is related to the stability of non-Hermitian systems in their long-time dynamics [15,41,90,91]. The square-root scaling of the number N_{real} of real eigenvalues hints at possible dynamical instability in ergodic non-Hermitian systems. In contrast, the linear scaling of N_{real}

in the Anderson localized phase may imply that disorder can stabilize the dynamics of non-Hermitian systems. The nonuniversal scaling of the number of real eigenvalues, together with our explanation, also serves as evidence for the emergent integrability in the MBL phase of non-Hermitian systems.

The eigenstates on the real (imaginary) axis can only respect TRS (PHS†), TRS†, and pH (CS) among all the symmetries, as long as they are away from zero in the complex plane. Thus, for all 38 symmetry classes, we believe that the level-spacing distributions of real (purely imaginary) eigenvalues away from zero satisfy one of the five universal level spacing distributions found in this paper. For example, for non-Hermitian random matrices in symmetry class BDI (i.e., with TRS whose sign is $+1$ and PHS whose sign is $+1$), PHS affects the spectral statistics only around zero, and hence the real-eigenvalue spacing distribution away from zero should be the same as that in class AI. We leave testing this for all 38 symmetry classes for future work.

While we have focused on non-Hermitian Hamiltonians in this paper, our results should also be relevant to Lindbladians, which govern the open quantum dynamics of the Markovian master equation [92]. Similarly to closed quantum systems, it was conjectured that the level-spacing statistics of Lindbladians obey those of non-Hermitian random matrices in the nonintegrable phases and the Poisson statistics in the integrable phases [59,60,62]. This conjecture was previously verified for generic complex eigenvalues of Lindbladians away from the real axis. Notably, Lindbladians always respect TRS, where time reversal is effectively defined by the combination of complex conjugation and the swap operation between the bra and ket spaces. Thus, we expect that our results of the level statistics of real eigenvalues for non-Hermitian random matrices should coincide with those of nonintegrable Lindbladians in the same symmetry classes. It is also notable that the quadratic Lindbladians can be classified by the AZ† symmetry class [93], which is the same as the tenfold symmetry class studied in this paper.

Before concluding this paper, we note in passing that a non-Hermitian extension of the disordered Su-Schrieffer-Heeger model was shown to exhibit the level-spacing statistics of the Gaussian orthogonal ensemble [94]. This is due to an additional symmetry that enables a similarity transformation between this non-Hermitian model and the Hermitian Su-Schrieffer-Heeger model. Thus, in this non-Hermitian model, only the Hermitian degrees of freedom are present, and all eigenvalues are real, which are different from generic non-Hermitian random matrices studied in this paper.

ACKNOWLEDGMENTS

Z.X. thanks Haoran Chen, Lingxian Kong, and Yeyang Zhang for helpful discussions. We thank Jiachen Li for helpful comments on Appendix B. Z.X. and R.S. were supported by the National Basic Research Programs of China (No. 2019YFA0308401) and by National Natural Science Foundation of China (No. 11674011 and No. 12074008). X.L. was supported by National Natural Science Foundation of China, Grant No. 12105253. K.K. was supported by JSPS Overseas Research Fellowship, and Grant No. GBMF8685 from the Gordon and Betty Moore Foundation toward the Princeton theory program. T.O. was supported by JSPS KAKENHI Grants No. 19H00658 and No. 22H05114.

APPENDIX A: ANALYSES OF SMALL RANDOM MATRICES

Small non-Hermitian random matrices in the seven symmetry classes are written in the following unified form:

$$\mathcal{H}^{(s)} = a_0 I + \sum_{i=1}^{m} a_i L_i + \sum_{i=m+1}^{m+n} i a_i L_i. \tag{A1}$$

Here, I is the identity matrix, $L_1, L_2, \ldots, L_{m+n}$ are anticommuting Hermitian traceless matrices, $\{L_i, L_j\} = 2\delta_{i,j} I$, and $a_0, a_1, \ldots, a_{m+n}$ are real numbers. Note that

$$\mathrm{Tr}(\mathcal{H}^{(s)\dagger}\mathcal{H}^{(s)}) = \left(\sum_{i=0}^{m+n} a_i^2\right)\mathrm{Tr}(I). \tag{A2}$$

The real numbers $a_0, a_1, \ldots, a_{m+n}$ are independent of each other and obey the identical standard Gaussian distribution. Note that $\sum_{i=1}^{k} a_i^2$ obeys the χ^2 distribution with the degree k [59]. The probability of $\sum_{i=1}^{k} a_i^2 = X$ is given by

$$p(X;k) = \begin{cases} \frac{X^{\frac{k}{2}-1}e^{-\frac{X}{2}}}{2^{\frac{k}{2}}\Gamma\left(\frac{k}{2}\right)}, & X \geqslant 0, \\ 0, & X < 0. \end{cases} \tag{A3}$$

The square of the traceless part of $\mathcal{H}^{(s)}$ is proportional to I,

$$\left(\sum_{i=1}^{m} a_i L_i + \sum_{i=m+1}^{m+n} i a_i L_i\right)^2 = \left(\sum_{i=1}^{m} a_i^2 - \sum_{i=m+1}^{m+n} a_i^2\right) I. \tag{A4}$$

Thus, eigenvalues of $\mathcal{H}^{(s)}$ are given by

$$\lambda = a_0 \pm \sqrt{X - Y}, \quad X \equiv \sum_{i=1}^{m} a_i^2, \quad Y \equiv \sum_{i=m+1}^{m+n} a_i^2. \tag{A5}$$

The probability that the eigenvalues are real is given by the probability of $X \geqslant Y$:

$$p_{\lambda=\lambda^*} = \int_{-\infty}^{\infty} dX \int_{-\infty}^{+\infty} dY\, \theta(X - Y)\, p(X;m)\, p(Y;n), \tag{A6}$$

where $\theta(u)$ is the step function satisfying $\theta(u) \equiv 1$ for $u \geqslant 0$ and $\theta(u) \equiv 0$ for $u < 0$.

In terms of Pauli matrices σ_μ and τ_μ ($\mu = 0, x, y, z$) and their Kronecker products $\tau_\mu\sigma_\nu$, the traceless parts of the small random matrices in the seven symmetry classes are given as

$$\tilde{\mathcal{H}}^{(s)}_{\mathrm{AI}} = a_1\sigma_z + a_2\sigma_x + i a_3\sigma_y,$$

$$\tilde{\mathcal{H}}^{(s)}_{\mathrm{A}+\eta} = a_1\sigma_z + i a_2\sigma_x + i a_3\sigma_y,$$

$$\tilde{\mathcal{H}}^{(s)}_{\mathrm{AI}+\eta_+} = a_1\sigma_z + i a_2\sigma_y,$$

$$\tilde{\mathcal{H}}^{(s)}_{\mathrm{AII}} = i a_1\sigma_z + i a_2\sigma_x + i a_3\sigma_y,$$

$$\tilde{\mathcal{H}}^{(s)}_{\mathrm{AI}+\eta_-} = a_1\tau_z + a_2\tau_x + a_3\tau_y\sigma_y + i a_4\tau_y\sigma_x + i a_5\tau_y\sigma_z,$$

$$\tilde{\mathcal{H}}^{(s)}_{\mathrm{AII}+\eta_-} = ia_1\sigma_x + ia_2\sigma_y,$$
$$\tilde{\mathcal{H}}^{(s)}_{\mathrm{AII}+\eta_+} = a_1\tau_z + ia_2\tau_y + ia_3\tau_x\sigma_x + ia_4\tau_x\sigma_y + ia_5\tau_x\sigma_z. \tag{A7}$$

In fact, the small matrix in each class respects the following symmetries:

$$\tilde{\mathcal{H}}^{(s)}_{\mathrm{AI}} = \tilde{\mathcal{H}}^{(s)*}_{\mathrm{AI}},$$
$$\tilde{\mathcal{H}}^{(s)}_{\mathrm{A}+\eta} = \sigma_z\tilde{\mathcal{H}}^{(s)\dagger}_{\mathrm{A}+\eta}\sigma_z,$$
$$\tilde{\mathcal{H}}^{(s)}_{\mathrm{AI}+\eta_+} = \tilde{\mathcal{H}}^{(s)*}_{\mathrm{AI}+\eta_+}, \quad \tilde{\mathcal{H}}^{(s)}_{\mathrm{AI}+\eta_+} = \sigma_z\tilde{\mathcal{H}}^{(s)\dagger}_{\mathrm{AI}+\eta_+}\sigma_z,$$
$$\tilde{\mathcal{H}}^{(s)}_{\mathrm{AII}} = \sigma_y\tilde{\mathcal{H}}^{(s)*}_{\mathrm{AII}}\sigma_y,$$
$$\tilde{\mathcal{H}}^{(s)}_{\mathrm{AI}+\eta_-} = \tilde{\mathcal{H}}^{(s)*}_{\mathrm{AI}+\eta_-}, \quad \tilde{\mathcal{H}}^{(s)}_{\mathrm{AI}+\eta_-} = \sigma_y\tilde{\mathcal{H}}^{(s)\dagger}_{\mathrm{AI}+\eta_-}\sigma_y,$$
$$\tilde{\mathcal{H}}^{(s)}_{\mathrm{AII}+\eta_-} = \sigma_y\tilde{\mathcal{H}}^{(s)*}_{\mathrm{AII}+\eta_-}\sigma_y, \quad \tilde{\mathcal{H}}^{(s)}_{\mathrm{AII}+\eta_-} = \sigma_z\tilde{\mathcal{H}}^{(s)\dagger}_{\mathrm{AII}+\eta_-}\sigma_z,$$
$$\tilde{\mathcal{H}}^{(s)}_{\mathrm{AII}+\eta_+} = \sigma_y\tilde{\mathcal{H}}^{(s)*}_{\mathrm{AII}+\eta_+}\sigma_y, \quad \tilde{\mathcal{H}}^{(s)}_{\mathrm{AII}+\eta_+} = \tau_z\tilde{\mathcal{H}}^{(s)\dagger}_{\mathrm{AII}+\eta_+}\tau_z. \tag{A8}$$

The number m of the real degrees of freedom and the number n of the imaginary degrees of freedom for the small random matrices in each symmetry class are summarized in Table II. The probability of real eigenvalues is finite for $\mathcal{H}^{(s)}$ in classes AI, A + η, AI + η_+, AI + η_-, and AII + η_+ because of $m \neq 0$; on the other hand, the probability of real eigenvalues is zero for $\mathcal{H}^{(s)}$ in classes AII and AII + η_- because of $m = 0$.

1. Real-eigenvalue spacing

With a finite probability, the small random matrices in classes AI, A + η, AI + $\eta_\pm$, and AII + η_+ have a pair of real eigenvalues. The distance s between the two real eigenvalues is given by

$$s = 2\sqrt{\sum_{i=1}^{m} a_i^2 - \sum_{i=m+1}^{m+n} a_i^2}. \tag{A9}$$

The probability of $(s/2)^2 = X$ under the condition that the eigenvalues are real is calculated as follows:

$$P(X) = \frac{\int_{-\infty}^{\infty} dX' \int_{-\infty}^{\infty} dY' \delta(X' - Y' - X) p(X'; m) p(Y'; n)}{\int_{-\infty}^{\infty} dX' \int_{-\infty}^{\infty} dY' \theta(X' - Y') p(X'; m) p(Y'; n)}$$
$$= \frac{\int_0^{\infty} dx (x+X)^{\frac{m}{2}-1} e^{-\frac{x+X}{2}} x^{\frac{n}{2}-1} e^{-\frac{x}{2}}}{\int_0^{\infty} dx \int_0^{\infty} dX (x+X)^{\frac{m}{2}-1} e^{-\frac{x+X}{2}} x^{\frac{n}{2}-1} e^{-\frac{x}{2}}}$$
$$= \begin{cases} \frac{1}{2} e^{-\frac{X}{2}}, & (m,n) = (2,1), \\ \frac{1}{2(\sqrt{2}-1)} e^{\frac{X}{2}} \mathrm{erfc}(\sqrt{X}), & (m,n) = (1,2), \\ \frac{1}{\pi} K_0(\frac{X}{2}), & (m,n) = (1,1), \\ \frac{e^{-\frac{X}{2}} [\sqrt{\pi} e^X \mathrm{erfc}(\sqrt{X}) + 2\sqrt{X}]}{2(2\sqrt{2}-1)\sqrt{\pi}}, & (m,n) = (3,2), \\ \frac{e^{-\frac{X}{2}} [2\sqrt{X} - \sqrt{\pi} e^X (2X-1) \mathrm{erfc}(\sqrt{X})]}{2\sqrt{\pi}(4\sqrt{2}-5)}, & (m,n) = (1,4), \end{cases}$$

with $\int_0^{\infty} dX P(X) = 1$. Here, $\mathrm{erfc}(u) \equiv \frac{2}{\sqrt{\pi}} \int_u^{\infty} e^{-t^2} dt$ is the complementary error function and $K_\nu(u)$ is the modified Bessel function of the second kind. Then, the probability of the distance being s under the condition that the eigenvalues are real is given by

$$P_s(s) = \frac{s}{2} P\left(\left(\frac{s}{2}\right)^2\right), \tag{A10}$$

with $\int_0^{\infty} P_s(s) ds = 1$. Note that the real-eigenvalue spacing distribution function $p(s)$ in the main text is defined for the distance normalized by the mean value of the distance: $\int_0^{\infty} p(s) s ds = 1$. Thus, we have

$$p(s) \equiv \bar{s} P_s(\bar{s}s), \tag{A11}$$

with the mean value

$$\bar{s} \equiv \int_0^{\infty} s P_s(s) ds. \tag{A12}$$

From Eqs. (A10) and (A11), we obtain the probability distribution functions of the normalized distances between the two real eigenvalues as follows:

$$p(s) = \begin{cases} \frac{1}{2}\pi s e^{-\frac{\pi}{4}s^2}, & (m,n) = (2,1), \\ \frac{1}{4}(\sqrt{2}+1)\bar{s}_2^2 s e^{\frac{1}{8}\bar{s}_2^2 s^2} \mathrm{erfc}(\frac{\bar{s}_2 s}{2}), & (m,n) = (1,2), \\ \frac{8s\Gamma(\frac{3}{4})^4 K_0(\frac{2s^2\Gamma(\frac{3}{4})^4}{\pi^2})}{\pi^3}, & (m,n) = (1,1), \\ \frac{\bar{s}_3^2 s e^{-\frac{\bar{s}_3^2 s^2}{2}} (\sqrt{\pi} e^{\bar{s}_3^2 s^2} \mathrm{erfc}(\bar{s}_3 s) + 2\bar{s}_3 s)}{(2\sqrt{2}-1)\sqrt{\pi}}, & (m,n) = (3,2), \\ \frac{\bar{s}_4^2 s e^{-\frac{1}{8}\bar{s}_4^2 s^2} (\bar{s}_4 s - \sqrt{\pi} e^{\frac{1}{4}\bar{s}_4^2 s^2} (\frac{1}{2}\bar{s}_4^2 s^2 - 1) \mathrm{erfc}(\frac{\bar{s}_4 s}{2}))}{4(4\sqrt{2}-5)\sqrt{\pi}}, & (m,n) = (1,4), \end{cases} \tag{A13}$$

with

$$\bar{s}_2 \equiv \frac{2(1+\sqrt{2})(2 - \sqrt{2}\sinh^{-1}(1))}{\sqrt{\pi}} \approx 2.053, \tag{A14}$$
$$\bar{s}_3 \equiv \frac{6 - \sqrt{2}\sinh^{-1}(1)}{(2\sqrt{2}-1)\sqrt{\pi}} \approx 1.467, \tag{A15}$$
$$\bar{s}_4 \equiv \frac{20 - 14\sqrt{2}\sinh^{-1}(1)}{(4\sqrt{2}-5)\sqrt{\pi}} \approx 2.190. \tag{A16}$$

Note that $p(s)$ takes the following asymptotic forms for $s \ll 1$:

$$p(s) \sim \begin{cases} s, & (m,n) = (2,1), (1,2), (3,2), (1,4), \\ -s\ln(s), & (m,n) = (1,1). \end{cases} \tag{A17}$$

2. Density of states

We calculate the DOS of the small random matrices. For $m \neq 0$, the DOS $\rho(E = x + iy)$ is decomposed into the density $\rho_c(x,y)$ of complex eigenvalues and the density $\rho_r(x)$ of real eigenvalues, $\rho(E) = \rho_c(x,y) + \delta(y)\rho_r(x)$, while for $m = 0$, the density of real eigenvalues always vanishes, $\rho(E) = \rho_c(x,y)$. The density $\rho_c(x,y)$ of complex eigenvalues is the probability of E being $x + iy$. For $m \neq 0$, it is given by

$$\begin{aligned} \rho_c(x,y) &= \frac{2|y|e^{-\frac{x^2}{2}}}{\sqrt{2\pi}} \int_{-\infty}^{\infty} dX \int_{-\infty}^{\infty} dY\, \delta(Y - X - y^2) \\ &\quad \times p(Y;n)\, p(X;m) \\ &= \begin{cases} \sqrt{2}|y|e^{\frac{y^2}{2} - \frac{x^2}{2}} \mathrm{erfc}(|y|), & (m,n) = (2,1), \\ \sqrt{2}|y|e^{-\frac{y^2}{2} - \frac{x^2}{2}}, & (m,n) = (1,2), \\ \sqrt{\frac{2}{\pi}}|y| K_0(\frac{y^2}{2}) e^{-\frac{x^2}{2}}, & (m,n) = (1,1), \\ \sqrt{\frac{1}{2}}|y|e^{-\frac{y^2}{2} - \frac{x^2}{2}}, & (m,n) = (3,2), \\ \sqrt{\frac{1}{2}}(2y^2+1)|y|e^{-\frac{y^2}{2} - \frac{x^2}{2}}, & (m,n) = (1,4), \end{cases} \end{aligned} \tag{A18}$$

with the normalization $\int_{-\infty}^{\infty} dx \int_{-\infty}^{\infty} dy \rho(x,y) = 2$. Here, the constant 2 is the number of different eigenvalues of small matrices. Note also that we have $\int_{-\infty}^{\infty} dx \int_{-\infty}^{\infty} dy \rho_c(x,y) \neq \int_{-\infty}^{\infty} dx \int_{-\infty}^{\infty} dy \rho(x,y) = 2$ under this normalization condition. For $m = 0$, the DOS in the complex plane $\rho(x,y) = \rho_c(x,y)$ is given by

$$\begin{aligned} \rho_c(x,y) &= \frac{2|y|e^{-\frac{x^2}{2}}}{\sqrt{2\pi}} \int_{-\infty}^{+\infty} dY\, \delta(Y - y^2)\, p(Y;n) \\ &= \frac{1}{2^{\frac{n-1}{2}}\sqrt{\pi}\Gamma\left(\frac{n}{2}\right)} |y|^{n-1} e^{-\frac{y^2}{2} - \frac{x^2}{2}} \\ &= \begin{cases} \frac{1}{\sqrt{2\pi}}|y|e^{-\frac{y^2}{2} - \frac{x^2}{2}}, & (m,n) = (0,2), \\ \frac{1}{\pi}|y|^2 e^{-\frac{y^2}{2} - \frac{x^2}{2}}, & (m,n) = (0,3), \end{cases} \end{aligned} \tag{A19}$$

with the same normalization $\int_{-\infty}^{\infty} dx \int_{-\infty}^{\infty} dy \rho(x,y) = 2$. For $|y| \ll 1$, the density $\rho_c(x,y)$ of complex eigenvalues takes the following asymptotic forms for each symmetry class:

$$\rho_c(x,y) \sim \begin{cases} |y|, & (m,n) = (2,1), (1,2), (3,2), \\ & \quad (1,4), (0,2), \\ |y|^2, & (m,n) = (0,3), \\ -|y|\ln(|y|), & (m,n) = (1,1). \end{cases} \tag{A20}$$

APPENDIX B: RANDOM MATRIX ENSEMBLES

1. Class AI

For a random matrix in class AI, let $\mathcal{U}_T$ be the identity matrix I. In this choice, $\mathcal{H}$ is a real matrix. The probability distribution function in the Gaussian ensemble is given by

$$p(\mathcal{H})d\mathcal{H} = C_N \exp\left(-\beta \sum_{ij} \mathcal{H}_{ij}^2\right) \prod_{ij} d\mathcal{H}_{ij}, \tag{B1}$$

where β is a constant and C_N is a normalization constant. With $\mathcal{U}_T = I$, the probability distribution function in the Bernoulli ensemble is given by

$$H_{ij} = \begin{cases} 1 & \text{with the probability } 1/2, \\ -1 & \text{with the probability } 1/2. \end{cases} \tag{B2}$$

Notably, the probability distribution in the Bernoulli ensemble is not invariant under unitary transformations.

2. Class AI + η_+

For a random matrix in class AI + η_+, let us choose $\mathcal{U}_T = I$ and $\mathcal{U}_\eta = \sigma_z \otimes I_{\frac{N}{2}\times\frac{N}{2}}$ with the identity matrix $I_{\frac{N}{2}\times\frac{N}{2}}$. Then, $\mathcal{H}_{\mathrm{AI}+\eta_+}$ generally takes

$$\mathcal{H}_{\mathrm{AI}+\eta_+} = \begin{pmatrix} A & B \\ -B^T & C \end{pmatrix}, \tag{B3}$$

where A, B, C are $\frac{N}{2} \times \frac{N}{2}$ real matrices with

$$A_{ij} = A_{ji}, C_{ij} = C_{ji}. \tag{B4}$$

The probability distribution function in the Gaussian ensemble is

$$\begin{aligned} p(\mathcal{H})d\mathcal{H} = C_N \exp\Bigg\{ -\beta \Bigg[& 2\sum_{i,j} B_{ij}^2 + 2\sum_{i>j} \left(A_{ij}^2 + C_{ij}^2\right) \\ & + \sum_i \left(A_{ii}^2 + C_{ii}^2\right) \Bigg] \Bigg\} \prod_{i,j} dB_{ij} \prod_{i \geqslant j} dA_{ij} dC_{ij}. \end{aligned} \tag{B5}$$

The probability distribution function in the Bernoulli ensemble is

$$\begin{aligned} & B_{ij}, A_{ij} (i \geqslant j), C_{ij} (i \geqslant j) \\ & \quad = \begin{cases} 1 & \text{with the probability } 1/2, \\ -1 & \text{with the probability } 1/2, \end{cases} \end{aligned} \tag{B6}$$

with Eq. (B4).

3. Class AI + η_-

For a random matrix in class AI+ η_-, let us choose $\mathcal{U}_T = I$ and $\mathcal{U}_\eta = \sigma_y \otimes I_{\frac{N}{2}\times\frac{N}{2}}$. Then, $\mathcal{H}_{\mathrm{AI}+\eta_-}$ takes a form of

$$\mathcal{H}_{\mathrm{AI}+\eta_-} = \begin{pmatrix} A & B \\ C & A^T \end{pmatrix}, \tag{B7}$$

where A, B, C are $\frac{N}{2} \times \frac{N}{2}$ real matrices satisfying,

$$B_{ij} = -B_{ji}, C_{ij} = -C_{ji}. \tag{B8}$$

The probability distribution function in the Gaussian ensemble is

$$p(\mathcal{H})d\mathcal{H} = C_N \exp\left\{-2\beta\left[\sum_{i,j} A_{ij}^2 + \sum_{i>j}\left(B_{ij}^2 + C_{ij}^2\right)\right]\right\} \times \prod_{i,j} dA_{ij} \prod_{i>j} dB_{ij} dC_{ij}. \tag{B9}$$

The probability distribution function in the Bernoulli ensemble is

$$A_{ij}, B_{ij}(i>j), C_{ij}(i>j) = \begin{cases} 1 & \text{with the probability } 1/2, \\ -1 & \text{with the probability } 1/2, \end{cases} \tag{B10}$$

with Eq. (B8).

4. Class A + η

For a random matrix in class A with pH, let $\mathcal{U}_\eta$ be $\sigma_z \otimes I_{\frac{N}{2}\times\frac{N}{2}}$. Then, $\mathcal{H}_{\mathrm{A}+\eta}$ is given by

$$\mathcal{H}_{\mathrm{A}+\eta} = \begin{pmatrix} A & B \\ -B^\dagger & C \end{pmatrix}, \tag{B11}$$

where A, B, C are $\frac{N}{2} \times \frac{N}{2}$ matrices satisfying

$$A_{ij} = A_{ji}^*, C_{ij} = C_{ji}^*. \tag{B12}$$

The probability distribution function in the Gaussian ensemble is given by

$$p(\mathcal{H})d\mathcal{H} = C_N \exp\left\{-\beta\left[\sum_i \left(A_{ii}^2 + C_{ii}^2\right) + 2\sum_{i>j}\left(|A_{ij}|^2 + |C_{ij}|^2\right) + 2\sum_{i,j}|B_{ij}|^2\right]\right\} \times \prod_{i>j} dA_{ij} dA_{ij}^* dC_{ij} dC_{ij}^* \prod_i dA_{ii} dC_{ii} \prod_{i,j} dB_{ij} dB_{ij}^*. \tag{B13}$$

The probability distribution function in the Bernoulli ensemble is given by

$$A_{ii}, C_{ii} = \begin{cases} 1 & \text{with the probability } 1/2, \\ -1 & \text{with the probability } 1/2, \end{cases} \tag{B14}$$

and

$$A_{ij}(i>j), C_{ij}(i>j), B_{ij} = \begin{cases} 1+i & \text{with the probability } 1/4, \\ -1+i & \text{with the probability } 1/4, \\ 1-i & \text{with the probability } 1/4, \\ -1-i & \text{with the probability } 1/4, \end{cases} \tag{B15}$$

and Eq. (B8).

5. Class AII

For a random matrix in class AII, let $\mathcal{U}_T$ be $\sigma_y \otimes I_{\frac{N}{2}\times\frac{N}{2}}$. Then, $\mathcal{H}_{\mathrm{AII}}$ is given by

$$\mathcal{H}_{\mathrm{AII}} = \begin{pmatrix} A & B \\ -B^* & A^* \end{pmatrix}, \tag{B16}$$

with $\frac{N}{2} \times \frac{N}{2}$ matrices A and B. The probability distribution function in the Gaussian ensemble is

$$p(\mathcal{H})d\mathcal{H} = C_N \exp\left[-2\beta\sum_{ij}(|A_{ij}|^2 + |B_{ij}|^2)\right] \times \prod_{ij} dA_{ij} dA_{ij}^* dB_{ij} dB_{ij}^*. \tag{B17}$$

The probability distribution function in the Bernoulli ensemble is

$$A_{ij}, B_{ij} = \begin{cases} 1+i & \text{with the probability } 1/4, \\ -1+i & \text{with the probability } 1/4, \\ 1-i & \text{with the probability } 1/4, \\ -1-i & \text{with the probability } 1/4. \end{cases} \tag{B18}$$

6. Class AII + η_+

For a random matrix in class AII+ η_+, let us choose $\mathcal{U}_T = \tau_0\sigma_y \otimes I_{\frac{N}{4}\times\frac{N}{4}}$ and $\mathcal{U}_\eta = \tau_z\sigma_0 \otimes I_{\frac{N}{4}\times\frac{N}{4}}$ with the identity matrix $I_{\frac{N}{4}\times\frac{N}{4}}$. Then, $\mathcal{H}_{\mathrm{AII}+\eta_+}$ generally takes

$$\mathcal{H}_{\mathrm{AI}+\eta_+} = \begin{pmatrix} A^1 & A^2 & B^1 & B^2 \\ -A^{2*} & A^{1*} & -B^{2*} & B^{1*} \\ -B^{1\dagger} & B^{2T} & C^1 & C^2 \\ -B^{2\dagger} & -B^{1T} & -C^{2*} & C^{1*} \end{pmatrix}, \tag{B19}$$

where A^μ, B^μ, C^μ ($\mu = 1, 2$) are $\frac{N}{4} \times \frac{N}{4}$ matrices satisfying

$$A_{ij}^1 = A_{ji}^{1*}, C_{ij}^1 = C_{ji}^{1*}, A_{ij}^2 = -A_{ji}^2, C_{ij}^2 = -C_{ji}^2. \tag{B20}$$

The probability distribution function in the Gaussian ensemble is

$$p(\mathcal{H})d\mathcal{H} = C_N \exp\left\{-\beta\left[2\sum_i\left(\left(A_{ii}^1\right)^2 + \left(C_{ii}^1\right)^2\right) + 4\sum_{\mu=1,2}\sum_{i>j}\left(\left|A_{ij}^\mu\right|^2 + \left|C_{ij}^\mu\right|^2\right) + 4\sum_{\mu=1,2}\sum_{i,j}\left|B_{ij}^\mu\right|^2\right]\right\} \times \prod_{i>j} dA_{ij}^1 dA_{ij}^{1*} dA_{ij}^2 dA_{ij}^{2*} dC_{ij}^1 dC_{ij}^{1*} dC_{ij}^2 dC_{ij}^{2*} \times \prod_i dA_{ii}^1 dC_{ii}^1 \prod_{i,j} dB_{ij}^1 dB_{ij}^{1*} dB_{ij}^2 dB_{ij}^{2*}. \tag{B21}$$

The probability distribution function in the Bernoulli ensemble is

$$A_{ii}^1, C_{ii}^1 = \begin{cases} 1 & \text{with the probability } 1/2, \\ -1 & \text{with the probability } 1/2, \end{cases} \tag{B22}$$

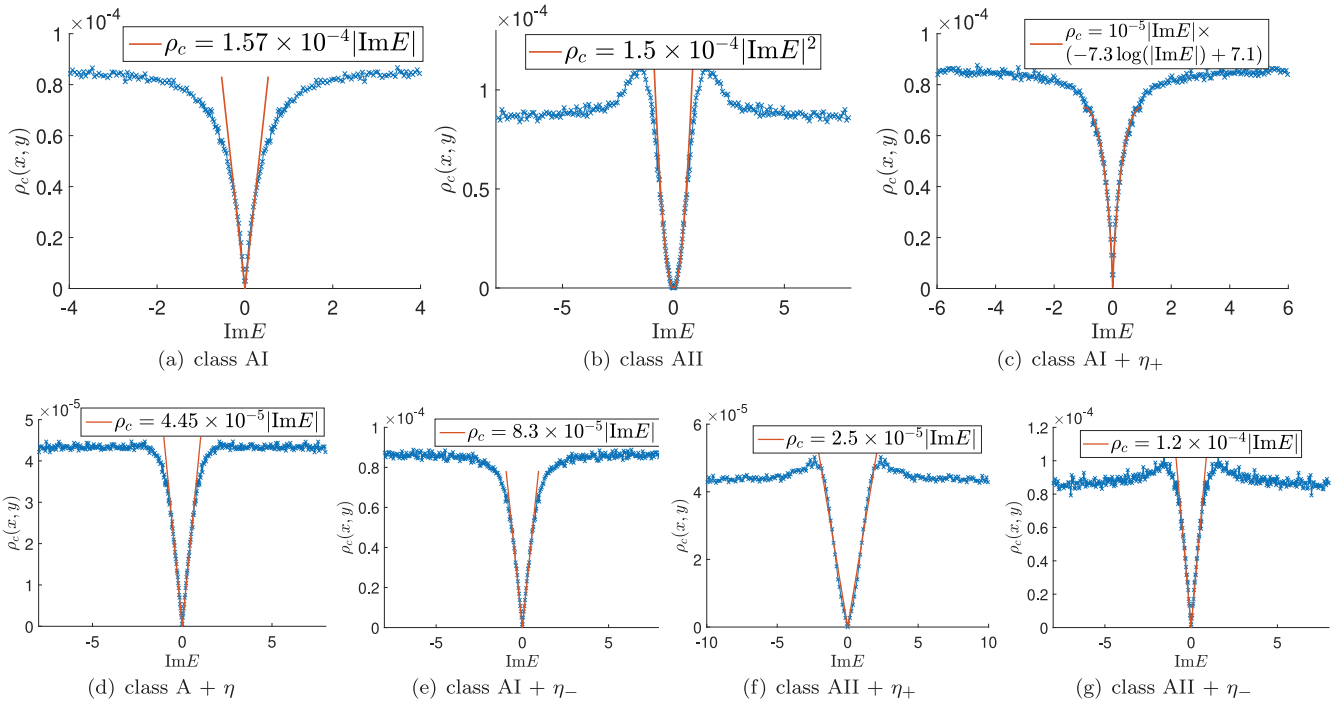

(a) class AI (b) class AII (c) class AI + η_+

(d) class A + η (e) class AI + η_- (f) class AII + η_+ (g) class AII + η_-

FIG. 18. Density $\rho_c(x, y)$ of complex eigenvalues for non-Hermitian random matrices in the Bernoulli ensemble for classes (a) AI, (b) AII, (c) AI + η_+, (d) A + η, (e) AI + η_-, (f) AII + η_+, and (g) AII + η_-. Here, $\rho_c(x, y)$ is shown as a function of $y = \mathrm{Im}(E)$ for fixed $x = \mathrm{Re}(E)$ near the real axis $y = 0$ of complex energy E. The data are obtained from diagonalizations of 5000 samples of 4000 × 4000 random matrices in each symmetry class. Note that $\rho_c(x, y)$ is almost independent of x as long as E is away from the boundary of a circle inside which the complex eigenvalues E distribute. All the 'log' in the figures are the natural log (ln).

$$A^{\mu}_{ij}(i > j), C^{\mu}_{ij}(i > j), B^{\mu}_{ij} = \begin{cases} 1+i & \text{with the probability } 1/4, \\ -1+i & \text{with the probability } 1/4, \\ -1-i & \text{with the probability } 1/4, \\ -1-i & \text{with the probability } 1/4 \end{cases} \tag{B23}$$

for $\mu = 1, 2$ with Eq. (B20).

7. Class AII + η_-

For a random matrix in class AII+ η_-, let us choose $\mathcal{U}_T = \sigma_y \otimes I_{\frac{N}{2}\times\frac{N}{2}}$ and $\mathcal{U}_\eta = \sigma_z \otimes I_{\frac{N}{2}\times\frac{N}{2}}$. Then, $\mathcal{H}_{\mathrm{AII}+\eta_-}$ is given by

$$\mathcal{H}_{\mathrm{AII}+\eta_-} = \begin{pmatrix} A & B \\ -B^* & A^* \end{pmatrix}, \tag{B24}$$

where A, B are $\frac{N}{2} \times \frac{N}{2}$ matrices satisfying

$$A_{ij} = A^*_{ji}, B_{ij} = B_{ji}. \tag{B25}$$

The probability distribution function in the Gaussian ensemble is given by

$$p(\mathcal{H})d\mathcal{H} = C_N \exp\left\{-\beta\left[\sum_i 2\left(A^2_{ii} + |B_{ii}|^2\right) + 4\sum_{i>j}(|A_{ij}|^2 + |B_{ij}|^2)\right]\right\} \times \prod_{i>j} dA_{ij}dA^*_{ij} \prod_i dA_{ii} \prod_{i\geqslant j} dB_{ij}dB^*_{ij}. \tag{B26}$$

The probability distribution function in the Bernoulli ensemble is given by

$$A_{ii} = \begin{cases} 1 & \text{with the probability } 1/2, \\ -1 & \text{with the probability } 1/2, \end{cases} \tag{B27}$$

$$A_{ij}(i > j), B_{ij}(i \geqslant j) = \begin{cases} 1+i & \text{with the probability } 1/4, \\ -1+i & \text{with the probability } 1/4, \\ 1-i & \text{with the probability } 1/4, \\ -1-i & \text{with the probability } 1/4, \end{cases} \tag{B28}$$

with Eq. (B25).

8. Level statistics in the Bernoulli ensemble

We diagonalize non-Hermitian random matrices in the Bernoulli ensemble for the seven symmetry classes and obtain the universal properties of the DOS as well as the level statistics of real eigenvalues in the Bernoulli ensemble. The DOS in each symmetry class shows the same property as the DOS in the Gaussian ensemble. The soft-gap behaviors of the density $\rho_c(x, y)$ of complex eigenvalues around the real axis ($y = 0$) are consistent with the DOS in the Gaussian ensemble (Fig. 18). For non-Hermitian random matrices in classes AII and AII + η_-, no real eigenvalues appear. By contrast, the average numbers of real eigenvalues in classes AI, A + η, AI + $\eta_\pm$, and AII + η_+ are proportional to $\sqrt{N}$ in the Bernoulli ensemble (Fig. 19). In these five symmetry classes, both the level-spacing distribution $p(s)$ and the level-spacing-ratio distribution $p_r(r)$ of real eigenvalues in

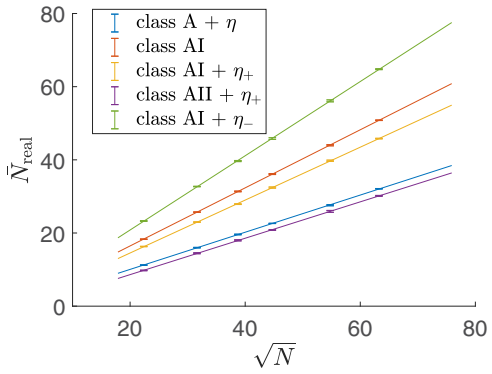

FIG. 19. Average number $\bar{N}_{\rm real}$ of real eigenvalues of non-Hermitian random matrices in the Bernoulli ensemble as a function of $\sqrt{N}$ for the five symmetry classes. Here, N is the dimensions of the random matrices. The error bars in the plot stand for the standard deviations of $\bar{N}_{\rm real}$. The plots clearly demonstrate the square-root scaling $\bar{N}_{\rm real} \propto \sqrt{N}$ in all five symmetry classes. For each symmetry class and matrix size, $\bar{N}_{\rm real}$ from the Bernoulli ensemble is almost the same as $\bar{N}_{\rm real}$ from the Gaussian ensemble.

the Bernoulli ensemble are consistent with the distribution functions in the Gaussian ensemble (Figs. 20 and 21). These results demonstrate the universality of the soft gap of the DOS around the real axis, the level-spacing and level-spacing-ratio distributions of real eigenvalues, and the scaling relation of the average number of real eigenvalues.

APPENDIX C: GENERALIZED GAUSSIAN ENSEMBLE

1. Probability distribution functions

Suppose that $\mathcal{H}$ is a non-Hermitian random matrix in one of the seven symmetry classes (i.e., classes A + η, AI, AI + $\eta_{\pm,}$, AII, and AI + $\eta_{\pm}$). Then,

$$\mathcal{H}' = \frac{x}{2}(\mathcal{H} + \mathcal{H}^\dagger) + \frac{1-x}{2}(\mathcal{H} - \mathcal{H}^\dagger) \tag{C1}$$

is a non-Hermitian random matrix in the same symmetry class as $\mathcal{H}$ when x is a real number satisfying $x \neq 0, 1$. Thus, we can generalize the Gaussian ensemble in each symmetry class into the generalized Gaussian ensemble. $\mathcal{H}'$ in the generalized Gaussian ensemble is realized with the same probability as $\mathcal{H}$ in the Gaussian ensemble,

$$p'(\mathcal{H}')d\mathcal{H}' = p(\mathcal{H})d\mathcal{H}. \tag{C2}$$

The inverse transform of Eq. (C1) is given by

$$\mathcal{H} = \frac{1}{2x}(\mathcal{H}' + \mathcal{H}'^\dagger) + \frac{1}{2(1-x)}(\mathcal{H}' - \mathcal{H}'^\dagger). \tag{C3}$$

As Eq. (C1) is a linear transform, the Jacobian matrix of the transform depends only on x,

$$d\mathcal{H}' = C_x d\mathcal{H}, \tag{C4}$$

where C_x is an x-dependent constant. The probability distribution in the generalized Gaussian ensemble is

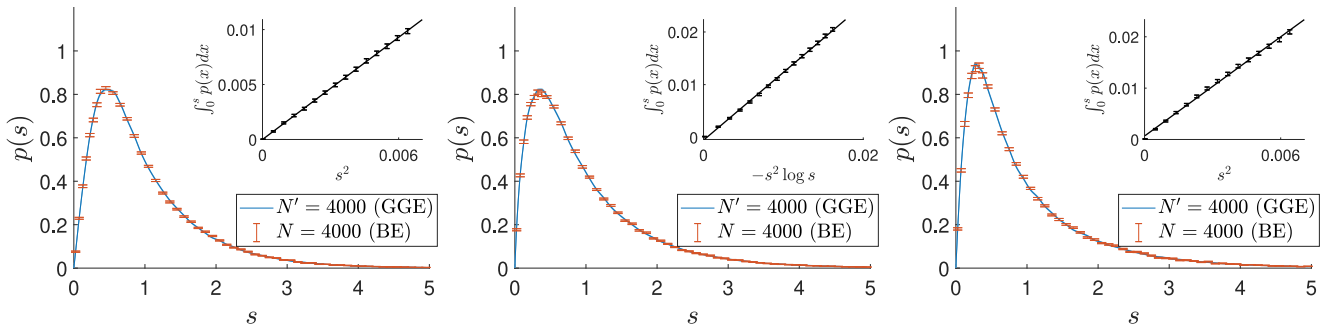

(a) $p(s)$ in class AI (b) $p(s)$ in class AI + η_+ (c) $p(s)$ in class A + η

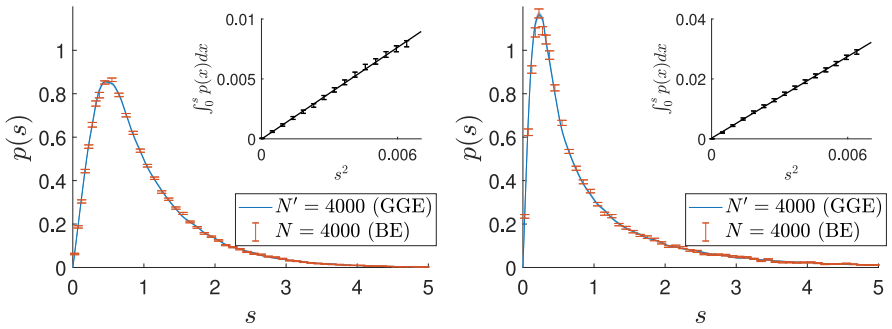

(d) $p(s)$ in class AI + η_- (e) $p(s)$ in class AII + η_+

FIG. 20. Real-eigenvalue spacing distribution functions $p(s)$ of 4000 × 4000 non-Hermitian random matrices in the Bernoulli ensemble (BE) for the five symmetry classes and their comparisons to $p(s)$ obtained from non-Hermitian random matrices in the generalized Gaussian ensemble (GGE) with $\beta_2/\beta_1 = 16$. Insets: Asymptotic behaviors of the distribution functions for $s \ll 1$, where the cumulative distribution function $\int_0^s p(s')ds'$ is plotted as a function of either s^2 or $-\ln(s)s^2$. The error ranges are evaluated by the bootstrap method [69]. The error ranges of $p(s)$ of the GGE random matrices are much smaller than those of the BE random matrices and not shown here (see also Fig. 4). All the 'log' in the figures are the natural log (ln).

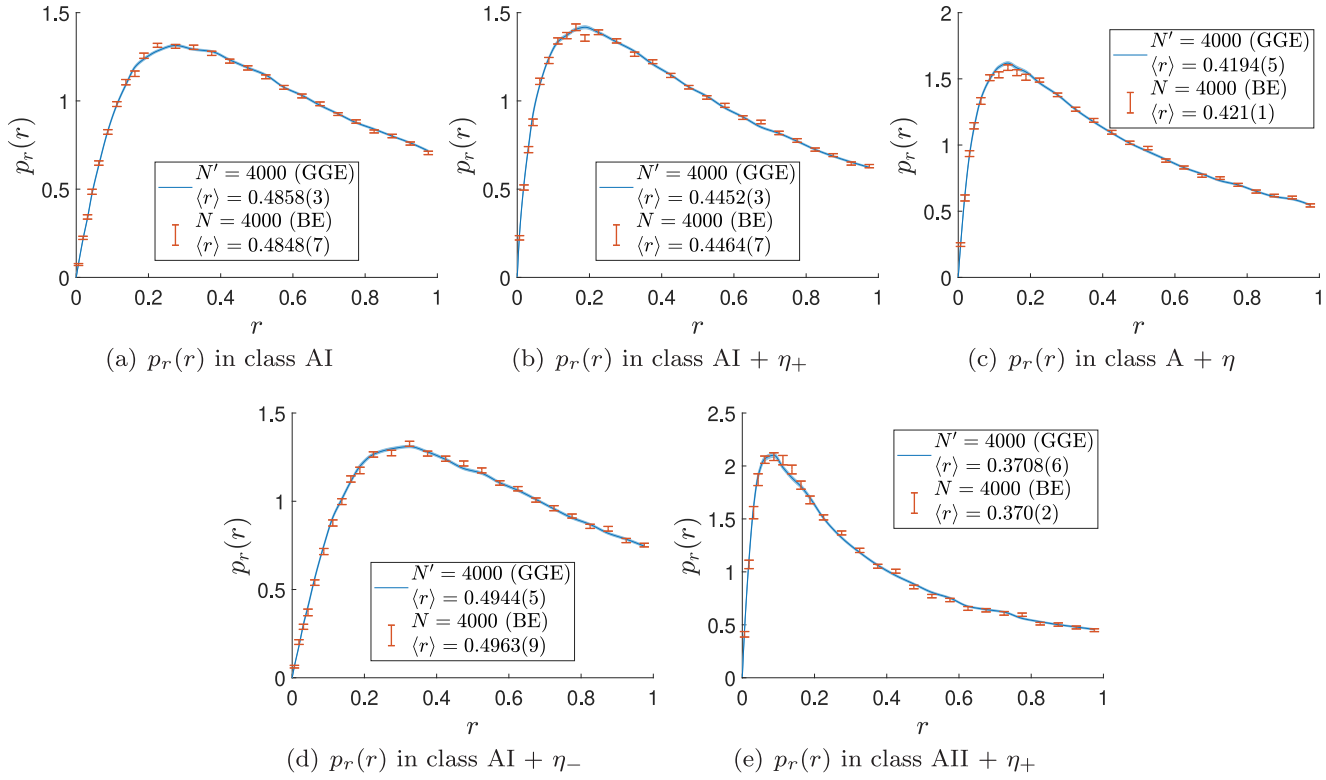

(a) $p_r(r)$ in class AI (b) $p_r(r)$ in class AI + η_+ (c) $p_r(r)$ in class A + η

(d) $p_r(r)$ in class AI + η_- (e) $p_r(r)$ in class AII + η_+

FIG. 21. Level-spacing-ratio distributions $p_r(r)$ of real eigenvalues obtained from 4000×4000 non-Hermitian random matrices in the Bernoulli ensemble for the five symmetry classes and their comparisons to $p_r(r)$ obtained from non-Hermitian random matrices in the generalized Gaussian ensemble with $\beta_2/\beta_1 = 16$. The mean value $\langle r\rangle = \int_0^1 p_r(r)dr$ of each distribution is also shown in each figure. The error ranges are evaluated by the bootstrap method [69]. The error ranges of $p_r(r)$ of the GGE random matrices are much smaller than those of the BE random matrices and not shown here (see also Fig. 5).

given by

$$\begin{aligned} p'(\mathcal{H}')d\mathcal{H}' &= p(\mathcal{H})d\mathcal{H} \\ &= C_N^{-1} e^{-\beta \mathrm{Tr}(\mathcal{H}^\dagger \mathcal{H})} d\mathcal{H} \\ &= C_N^{-1} C_x^{-1} e^{-\mathrm{Tr}[\frac{\beta}{4}(\mathcal{H}+\mathcal{H}^\dagger)^2 - \frac{\beta}{4}(\mathcal{H}-\mathcal{H}^\dagger)^2]} d\mathcal{H}' \\ &= C_N^{-1} C_x^{-1} e^{-\mathrm{Tr}[\frac{\beta}{4x^2}(\mathcal{H}'+\mathcal{H}'^\dagger)^2 - \frac{\beta}{4(1-x)^2}(\mathcal{H}'-\mathcal{H}'^\dagger)^2]} d\mathcal{H}', \end{aligned} \tag{C5}$$

which reduces to Eq. (12) with $C^{-1}_{N,(\beta_1,\beta_2)} \equiv C_N^{-1} C_x^{-1}$, $\beta_1 \equiv \frac{\beta}{4x^2}$, and $\beta_2 \equiv \frac{\beta}{4(1-x)^2}$.

2. Level statistics

We show that level-spacing and level-spacing ratio distributions, $p(s)$ and $p_r(r)$, in the generalized Gaussian ensemble (GGE) with $\beta_2 > \beta_1$ converge faster than those in the Gaussian ensemble (GE). Figures 3(d) and 3(i) show that $p(s)$ and $p_r(r)$ in class AII + η_+ converge more slowly than those in the other symmetry classes. Thus, we focus on $p(s)$ and $p_r(r)$ in class AII + η_+ and compare their convergence in the GGE and GE. For the other four symmetry classes, random matrices in the GGE have the same properties.

We find that for $N \times N$ non-Hermitian random matrices in the GGE with different parameter β_1, β_2, the average number of real eigenvalues $\bar{N}_{\mathrm{real}}$ is approximately scaled by

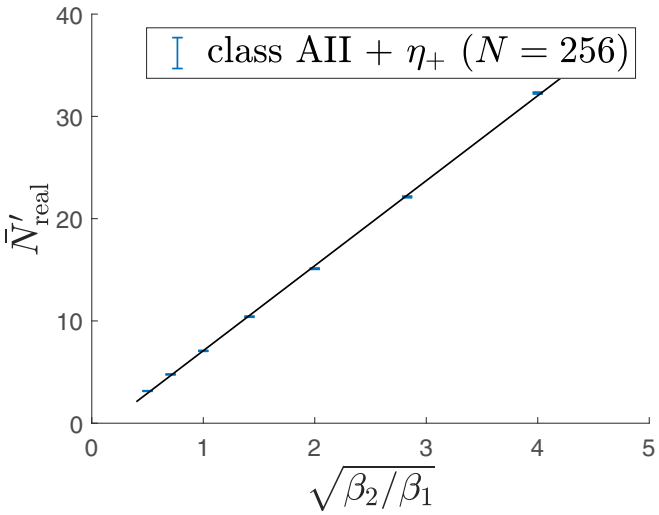

FIG. 22. Average number $\bar{N}'_{\mathrm{real}}$ for real eigenvalues of 256×256 non-Hermitian random matrices in the generalized Gaussian ensemble as a function of β_2/β_1 (class AII + η_+). Here, β_1 and β_2 are the parameters of the generalized Gaussian ensemble in Eq. (12). The plot clearly demonstrates $\bar{N}'_{\mathrm{real}} \propto \sqrt{\beta_2/\beta_1}$. For random matrices with different sizes and in the other four symmetry classes, the same scaling relation also holds true.

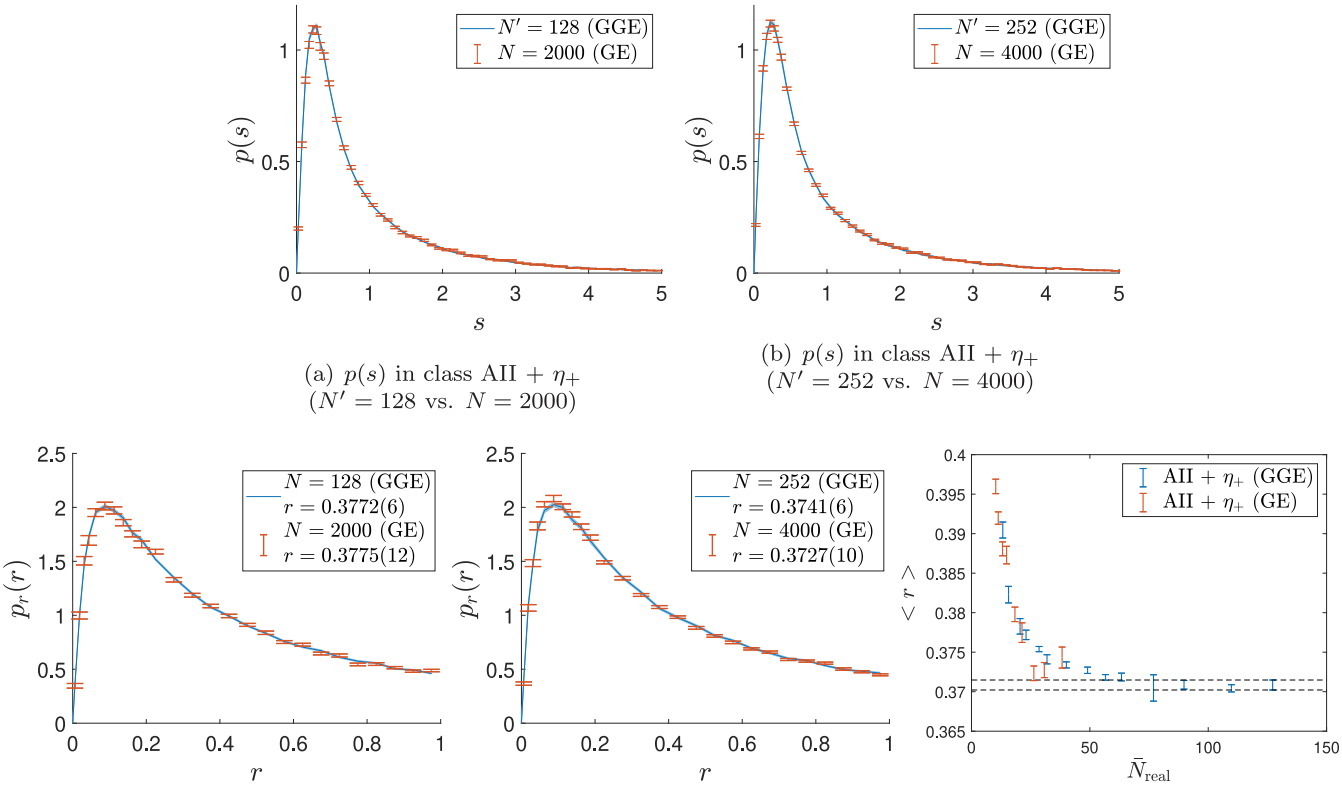

(a) $p(s)$ in class AII + η_+ ($N' = 128$ vs. $N = 2000$)

(b) $p(s)$ in class AII + η_+ ($N' = 252$ vs. $N = 4000$)

(c) $p_r(r)$ in class AII + η_+ ($N' = 128$ vs. $N = 2000$)

(d) $p_r(r)$ in class AII + η_+ ($N' = 252$ vs. $N = 4000$)

(e) $\langle r \rangle$ in class AII + η_+

FIG. 23. (a)–(d) Comparison between level-spacing-ratio distributions $p_r(r)$ and level-spacing distributions $p(s)$ of real eigenvalues obtained from $N' \times N'$ non-Hermitian random matrices in the generalized Gaussian ensemble and $N \times N$ non-Hermitian random matrices in the Gaussian ensemble for class AII + η_+. (e) Mean value of the level-spacing ratio $\langle r \rangle = \int_0^1 p_r(r)dr$ as a function of the average number $\bar{N}_{\rm real}$ of real eigenvalues in the GE and GGE for class AII + η_+. For $\bar{N}_{\rm real} \gtrsim 70$ ($N' > 1000$), the error bars of $\langle r \rangle$ for different sizes overlap with one another. The error ranges are evaluated by the bootstrap method [69]. The error ranges of the distributions of the GGE random matrices are much smaller than those of the GE random matrices and not shown here (see also Figs. 4 and 5).

(see Fig. 22)

$$\bar{N}_{\rm real} \propto \sqrt{\frac{\beta_2}{\beta_1}}, \tag{C6}$$

which is compatible with Eq. (13). When the average numbers of real eigenvalues of two GGE random matrices with different β_2/β_1 and different N are approximately the same, we also numerically find that the level-spacing and level-spacing ratio distributions, $p(s)$ and $p_r(r)$, from the two matrices are the same In Fig. 23, we compare $p(s)$ and $p_r(r)$ from 252×252 (128×128) GGE random matrices with $\beta_2/\beta_1 = 16$ and those from 4000×4000 (2000×2000) GE random matrices. The error bars for almost all the data points overlap with each other, and the average number of real eigenvalues is approximately the same (e.g., $\sqrt{252 \times 16} = \sqrt{4032} \approx \sqrt{4000}$). In the limit of $N \to \infty$, $p(s)$ and $p_r(r)$ in the GGE with different β_2/β_1 converge to the same universal distribution. For the same matrix size N of the random matrices, $p(s)$ and $p_r(r)$ converge faster in the GGE with larger β_2/β_1, as shown in Fig. 23(e). The square-root scaling of $N_{\rm real}$ with respect to the dimensions N of the matrices and the soft gap of density of complex eigenvalues around the real axis are also universally observed in random matrices of the GGE (not shown).

APPENDIX D: KOLMOGOROV-SMIRNOV DISTANCE

It is more feasible to use cumulative distribution functions than probability distribution functions, when comparing ergodic phases of physical systems with random matrices. Here, we calculate the Kolmogorov-Smirnov (KS) distance from the cumulative spacing distribution function $\int_0^s p(s')ds'$ and cumulative spacing-ratio distribution function $\int_0^r p_r(r')dr'$ among physical systems and random matrices in different symmetry classes (Tables III and IV). In the calculations, we first obtain the empirical cumulative distribution function $F_e(x)$ from a set of real random variables $\{x_1, x_2, \ldots, x_n\}$ for the spacing and spacing ratio,

$$F_e(x) \equiv \frac{1}{n} \sum_i^n \theta(x_i - x), \tag{D1}$$

with the step function θ. This function $F_e(x)$ corresponds to the cumulative level-spacing and level-spacing-ratio distribution function of real eigenvalues. The KS distance between the two empirical cumulative distribution functions $F_{e1}(x)$ and $F_{e2}(x)$ is defined by the maximum value of the difference

TABLE III. Kolmogorov-Smirnov (KS) distance among level-spacing distribution functions $p(s)$ of real eigenvalues obtained from 4000×4000 non-Hermitian random matrices in the five symmetry classes (classes A+η, AI, AI + $\eta_\pm$, and AII + η_+), and KS distance between $p(s)$ obtained from the physical systems in the ergodic phases and $p(s)$ obtained from the random matrices in the five classes. The first column specifies the random matrices (RM) and Hamiltonians of the physical models. The physical models are the 2D disordered free fermions in class AII + η_+ ($\mathcal{H}_{2D}$), the 3D disordered free fermions in class AI + η_+ ($\mathcal{H}_{3D}$), the hard-core boson model with the nonreciprocal hopping ($\mathcal{H}_{HN}$), and the four interacting spin models ($\mathcal{H}_1, \mathcal{H}_2, \mathcal{H}_3, \mathcal{H}_4$). The second column denotes the symmetry classes to which the random matrices or the Hamiltonians in the first column belong. The first row labels the RM in the five symmetry classes. The KS distances between $p(s)$ from the first column and $p(s)$ from the first row are shown. For each system in the first column, the shortest distance to random matrices is highlighted with the bold characters.

System	Class	AI	AI + η_+	A + η_+	AI + η_-	AII + η_+
RM	AI	**0**	0.052	0.089	0.011	0.165
RM	AI + η_+	0.052	**0**	0.038	0.063	0.114
RM	A + η_+	0.089	0.038	**0**	0.098	0.077
RM	AI + η_-	0.011	0.063	0.098	**0**	0.174
RM	AII + η_+	0.165	0.114	0.077	0.174	**0**
$\mathcal{H}_{HN}$	AI	**0.010**	0.043	0.079	0.020	0.155
$\mathcal{H}_1$	AI	**0.009**	0.045	0.081	0.018	0.157
$\mathcal{H}_{3D}$	AI + η_+	0.050	**0.003**	0.040	0.060	0.115
$\mathcal{H}_3$	AI + η_+	0.055	**0.004**	0.036	0.066	0.111
$\mathcal{H}_2$	A + η_+	0.093	0.043	**0.005**	0.102	0.073
$\mathcal{H}_4$	AI + η_-	0.010	0.062	0.097	**0.003**	0.174
$\mathcal{H}_{2D}$	AII + η_+	0.118	0.066	**0.032**	0.129	0.052

between the two functions over all x,

$$D_{e1,e2} \equiv \sup_x |F_{e1}(x) - F_{e2}(x)|. \tag{D2}$$

Tables III (Table IV) summarizes the KS distance among $p(s)$ [$p_r(r)$] from 4000×4000 random matrices in the generalized Gaussian ensemble with $\beta_2/\beta_1 = 16$ for the five symmetry classes. Table III (Table IV) also give the KS distance between $p(s)$ [$p_r(r)$] from the physical systems in the ergodic phases with the maximal system size, and $p(s)$ [$p_r(r)$] from the random matrices in the five symmetry classes. Tables III and IV show that in classes AI, AI + $\eta_\pm$, and A + η, the probability distribution functions $p(s)$ and $p_r(r)$ from the physical systems in the ergodic phases have the shortest distance to $p(s)$ and $p_r(r)$ from the random matrices in the same symmetry class, and the shortest distances are less than 0.01. Tables III and IV also show that $p(s)$ and $p_r(r)$ of the physical systems in class AII + η_+ have the shortest KS distance with $p(s)$ and $p_r(r)$ of the random matrices in class A + η but have the larger distance (>0.05) with $p(s)$ and $p_r(r)$ of the random matrices in class AII + η_+.

TABLE IV. Kolmogorov-Smirnov (KS) distance among level-spacing-ratio distribution functions $p_r(r)$ of real eigenvalues obtained from 4000×4000 non-Hermitian random matrices in the five symmetry classes (classes A+η, AI, AI + $\eta_\pm$, and AII + η_+), and KS distance between $p_r(r)$ obtained from the physical systems in the ergodic phases and $p_r(r)$ obtained from the random matrices in the five classes. The notation is the same as Table III.

System	Class	AI	AI + η_+	A + η_+	AI + η_-	AII + η_+
RM	AI	**0**	0.070	0.114	0.016	0.194
RM	AI + η_+	0.070	**0**	0.044	0.085	0.125
RM	A + η_+	0.114	0.044	**0**	0.129	0.083
RM	AI + η_-	0.016	0.085	0.129	**0**	0.209
RM	AII + η_+	0.194	0.125	0.083	0.209	**0**
$\mathcal{H}_{HN}$	AI	**0.007**	0.067	0.110	0.021	0.191
$\mathcal{H}_1$	AI	**0.003**	0.071	0.114	0.017	0.195
$\mathcal{H}_{3D}$	AI + η_+	0.069	**0.006**	0.045	0.084	0.126
$\mathcal{H}_3$	AI + η_+	0.067	**0.004**	0.047	0.083	0.128
$\mathcal{H}_2$	A + η_+	0.119	0.049	**0.006**	0.134	0.081
$\mathcal{H}_4$	AI + η_-	0.015	0.085	0.128	**0.004**	0.208
$\mathcal{H}_{2D}$	AII + η_+	0.138	0.069	**0.025**	0.154	0.062

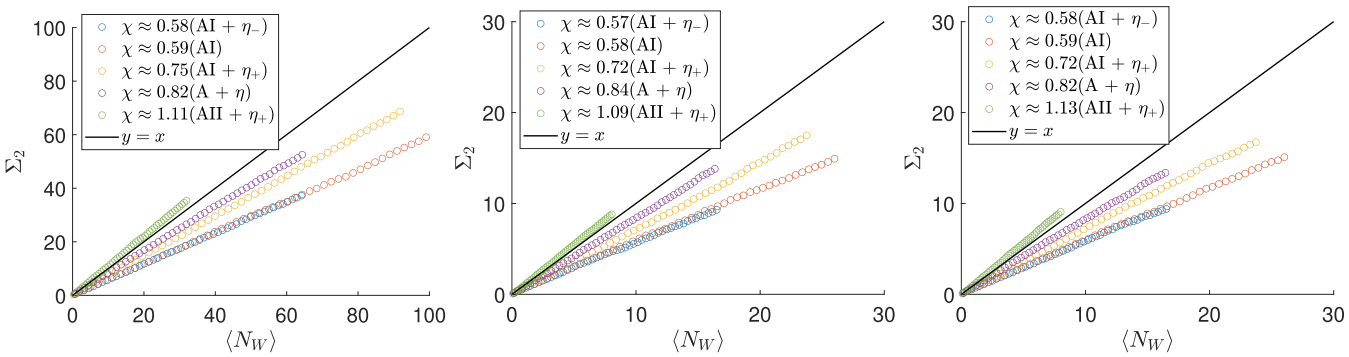

(a) generalized Gaussian ensemble ($\beta_2/\beta_1 = 16$) (b) Gaussian ensemble (c) Bernoulli ensemble

FIG. 24. Variance Σ_2 and mean value $\langle N_W \rangle$ of the number of real eigenvalues of non-Hermitian random matrices in the five symmetry classes. Σ_2 and $\langle N_W \rangle$ within different energy windows are obtained from 4000×4000 non-Hermitian random matrices in the (a) generalized Gaussian ensemble with $\beta_2/\beta_1 = 16$, (b) Gaussian ensemble, and (c) Bernoulli ensemble. The scaling relation $\Sigma_2 \simeq \chi \langle N_W \rangle$ holds for all five symmetry classes. The spectral compressibility χ is obtained by the linear fitting of the data points for each symmetry class.

APPENDIX E: NUMBER VARIANCE AND SPECTRAL COMPRESSIBILITY

For an ensemble of non-Hermitian random matrices, we count the number $N_W(E)$ of real eigenvalues in an energy window $[-E, E]$ with $E \geqslant 0$ in each sample. We evaluate the mean value $\langle N_W(E)\rangle$ and the variance $\Sigma_2(E) = \langle N_W(E)^2\rangle - \langle N_W(E)\rangle^2$ of the number in the energy window for different E. In our evaluation, only less than 50% of all the real eigenvalues are included in the energy window. Note also that in classes AI + η_- and AII + η_+, we regard each Kramers pair as one real eigenvalue, and we characterize the level interaction between neighboring Kramers pairs by $\Sigma_2(E)$ and $\langle N_W(E)\rangle$.

In all random matrix ensembles studied in this paper (i.e., generalized Gaussian ensemble with $\beta_2/\beta_1 = 16$, Gaussian ensemble, and Bernoulli ensemble), we have the scaling relation

$$\Sigma_2(E) \simeq \chi N_W(E) \tag{E1}$$

for all five symmetry classes (Fig. 24). The spectral compressibility χ in each symmetry class takes the same value for the different ensembles, suggesting the universality of χ. While χ is less than $\chi_{\text{Poisson}} = 1$ in classes AI, AI + $\eta_\pm$, and A + η_+, χ is larger than $\chi_{\text{Poisson}} = 1$ in class AII + η_+. This unusual relation $\chi > \chi_{\text{Poisson}} = 1$ in class AII + η_+ indicates that attractive interactions are more dominant than repulsive interactions in this symmetry class, which has no analogs in Hermitian random matrices and also non-Hermitian random matrices in the other four symmetry classes.

[1] M. L. Mehta, *Random Matrices* (Elsevier, Amsterdam, 2004).

[2] E. P. Wigner, On the statistical distribution of the widths and spacings of nuclear resonance levels, Math. Proc. Cambridge Philos. Soc. **47**, 790 (1951).

[3] O. Bohigas, M. J. Giannoni, and C. Schmit, Characterization of Chaotic Quantum Spectra and Universality of Level Fluctuation Laws, Phys. Rev. Lett. **52**, 1 (1984).

[4] F. Haake, *Quantum Signatures of Chaos* (Springer, Berlin, 1991).

[5] L. D'Alessio, Y. Kafri, A. Polkovnikov, and M. Rigol, From quantum chaos and eigenstate thermalization to statistical mechanics and thermodynamics, Adv. Phys. **65**, 239 (2016).

[6] B. L. Al'tshuler, I. K. Zharekeshev, S. A. Kotochigova, and B. I. Shklovskii, Repulsion between energy levels and the metal-insulator transition, Zh. Eksp. Theo. Fiz **94**, 343 (1988) [Sov. Phys. JETP **67**, 625 (1988)].

[7] B. I. Shklovskii, B. Shapiro, B. R. Sears, P. Lambrianides, and H. B. Shore, Statistics of spectra of disordered systems near the metal-insulator transition, Phys. Rev. B **47**, 11487 (1993).

[8] A. D. Mirlin, Statistics of energy levels and eigenfunctions in disordered systems, Phys. Rep. **326**, 259 (2000).

[9] F. Evers and A. D. Mirlin, Anderson transitions, Rev. Mod. Phys. **80**, 1355 (2008).

[10] V. Oganesyan and D. A. Huse, Localization of interacting fermions at high temperature, Phys. Rev. B **75**, 155111 (2007).

[11] A. Pal and D. A. Huse, Many-body localization phase transition, Phys. Rev. B **82**, 174411 (2010).

[12] M. Serbyn and J. E. Moore, Spectral statistics across the many-body localization transition, Phys. Rev. B **93**, 041424(R) (2016).

[13] D. A. Abanin, E. Altman, I. Bloch, and M. Serbyn, Colloquium: Many-body localization, thermalization, and entanglement, Rev. Mod. Phys. **91**, 021001 (2019).

[14] J.-y. Choi, S. Hild, J. Zeiher, P. Schauß, A. Rubio-Abadal, T. Yefsah, V. Khemani, D. A. Huse, I. Bloch, and C. Gross, Exploring the many-body localization transition in two dimensions, Science **352**, 1547 (2016).

[15] C. M. Bender and S. Boettcher, Real Spectra in Non-Hermitian Hamiltonians Having $\mathcal{PT}$ Symmetry, Phys. Rev. Lett. **80**, 5243 (1998).

[16] K. G. Makris, R. El-Ganainy, D. N. Christodoulides, and Z. H. Musslimani, Beam Dynamics in $\mathcal{PT}$ Symmetric Optical Lattices, Phys. Rev. Lett. **100**, 103904 (2008).

[17] A. Guo, G. J. Salamo, D. Duchesne, R. Morandotti, M. Volatier-Ravat, V. Aimez, G. A. Siviloglou, and D. N. Christodoulides, Observation of $\mathcal{PT}$-Symmetry Breaking in Complex Optical Potentials, Phys. Rev. Lett. **103**, 093902 (2009).

[18] C. E. Rüter, K. G. Makris, R. El-Ganainy, D. N. Christodoulides, M. Segev, and D. Kip, Observation of parity-time symmetry in optics, Nat. Phys. **6**, 192 (2010).

[19] L. Feng, M. Ayache, J. Huang, Y.-L. Xu, M.-H. Lu, Y.-F. Chen, Y. Fainman, and A. Scherer, Nonreciprocal Light Propagation in a Silicon Photonic Circuit, Science **333**, 729 (2011).

[20] J. M. Zeuner, M. C. Rechtsman, Y. Plotnik, Y. Lumer, S. Nolte, M. S. Rudner, M. Segev, and A. Szameit, Observation of a Topological Transition in the Bulk of a Non-Hermitian System, Phys. Rev. Lett. **115**, 040402 (2015).

[21] M. Pan, H. Zhao, P. Miao, S. Longhi, and L. Feng, Photonic zero mode in a non-Hermitian photonic lattice, Nat. Commun. **9**, 1308 (2018).

[22] J. Li, A. K. Harter, J. Liu, L. de Melo, Y. N. Joglekar, and L. Luo, Observation of parity-time symmetry breaking transitions in a dissipative Floquet system of ultracold atoms, Nat. Commun. **10**, 855 (2019).

[23] V. V. Konotop, J. Yang, and D. A. Zezyulin, Nonlinear waves in $\mathcal{PT}$-symmetric systems, Rev. Mod. Phys. **88**, 035002 (2016).

[24] M.-A. Miri and A. Alù, Exceptional points in optics and photonics, Science **363**, eaar7709 (2019).

[25] T. E. Lee, Anomalous Edge State in a Non-Hermitian Lattice, Phys. Rev. Lett. **116**, 133903 (2016).

[26] Y. Xu, S.-T. Wang, and L.-M. Duan, Weyl Exceptional Rings in a Three-Dimensional Dissipative Cold Atomic Gas, Phys. Rev. Lett. **118**, 045701 (2017).

[27] G. Harari, M. A. Bandres, Y. Lumer, M. C. Rechtsman, Y. D. Chong, M. Khajavikhan, D. N. Christodoulides, and M. Segev, Topological insulator laser: Theory, Science **359**, eaar4003 (2018).

[28] Z. Gong, Y. Ashida, K. Kawabata, K. Takasan, S. Higashikawa, and M. Ueda, Topological Phases of Non-Hermitian Systems, Phys. Rev. X **8**, 031079 (2018).

[29] S. Yao and Z. Wang, Edge States and Topological Invariants of Non-Hermitian Systems, Phys. Rev. Lett. **121**, 086803 (2018).
[30] S. Yao, F. Song, and Z. Wang, Non-Hermitian Chern Bands, Phys. Rev. Lett. **121**, 136802 (2018).
[31] K. Kawabata, S. Higashikawa, Z. Gong, Y. Ashida, and M. Ueda, Topological unification of time-reversal and particle-hole symmetries in non-Hermitian physics, Nat. Commun. **10**, 297 (2019).
[32] K. Kawabata, K. Shiozaki, M. Ueda, and M. Sato, Symmetry and Topology in Non-Hermitian Physics, Phys. Rev. X **9**, 041015 (2019).
[33] S. Longhi, Topological Phase Transition in non-Hermitian Quasicrystals, Phys. Rev. Lett. **122**, 237601 (2019).
[34] Q.-B. Zeng and Y. Xu, Winding numbers and generalized mobility edges in non-Hermitian systems, Phys. Rev. Res. **2**, 033052 (2020).
[35] L. Li, C. H. Lee, and J. Gong, Topological Switch for Non-Hermitian Skin Effect in Cold-Atom Systems with Loss, Phys. Rev. Lett. **124**, 250402 (2020).
[36] N. Hatano and D. R. Nelson, Localization Transitions in Non-Hermitian Quantum Mechanics, Phys. Rev. Lett. **77**, 570 (1996).
[37] K. B. Efetov, Quantum disordered systems with a direction, Phys. Rev. B **56**, 9630 (1997).
[38] J. Feinberg and A. Zee, Non-Hermitian localization and delocalization, Phys. Rev. E **59**, 6433 (1999).
[39] N. Hatano and J. Feinberg, Chebyshev-polynomial expansion of the localization length of Hermitian and non-Hermitian random chains, Phys. Rev. E **94**, 063305 (2016).
[40] B. Xu, T. Ohtsuki, and R. Shindou, Integer quantum magnon Hall plateau-plateau transition in a spin-ice model, Phys. Rev. B **94**, 220403(R) (2016).
[41] R. Hamazaki, K. Kawabata, and M. Ueda, Non-Hermitian Many-Body Localization, Phys. Rev. Lett. **123**, 090603 (2019).
[42] A. F. Tzortzakakis, K. G. Makris, and E. N. Economou, Non-Hermitian disorder in two-dimensional optical lattices, Phys. Rev. B **101**, 014202 (2020).
[43] C. Wang and X. R. Wang, Level statistics of extended states in random non-Hermitian Hamiltonians, Phys. Rev. B **101**, 165114 (2020).
[44] Y. Huang and B. I. Shklovskii, Anderson transition in three-dimensional systems with non-Hermitian disorder, Phys. Rev. B **101**, 014204 (2020).
[45] Y. Huang and B. I. Shklovskii, Spectral rigidity of non-Hermitian symmetric random matrices near the Anderson transition, Phys. Rev. B **102**, 064212 (2020).
[46] K. Kawabata and S. Ryu, Nonunitary Scaling Theory of Non-Hermitian Localization, Phys. Rev. Lett. **126**, 166801 (2021).
[47] X. Luo, T. Ohtsuki, and R. Shindou, Universality Classes of the Anderson Transitions Driven by Non-Hermitian Disorder, Phys. Rev. Lett. **126**, 090402 (2021).
[48] X. Luo, T. Ohtsuki, and R. Shindou, Transfer matrix study of the Anderson transition in non-Hermitian systems, Phys. Rev. B **104**, 104203 (2021).
[49] X. Luo, Z. Xiao, K. Kawabata, T. Ohtsuki, and R. Shindou, Unifying the Anderson transitions in Hermitian and non-Hermitian systems, Phys. Rev. Res. **4**, L022035 (2022).
[50] J. Ginibre, Statistical Ensembles of Complex, Quaternion, and Real Matrices, J. Math. Phys. **6**, 440 (1965).
[51] R. Grobe, F. Haake, and H.-J. Sommers, Quantum Distinction of Regular and Chaotic Dissipative Motion, Phys. Rev. Lett. **61**, 1899 (1988).
[52] R. Grobe and F. Haake, Universality of Cubic-level Repulsion for Dissipative Quantum Chaos, Phys. Rev. Lett. **62**, 2893 (1989).
[53] N. Lehmann and H.-J. Sommers, Eigenvalue Statistics of Random Real Matrices, Phys. Rev. Lett. **67**, 941 (1991).
[54] A. Edelman and E. Kostlan, How many zeros of a random polynomial are real?, Bull. Am. Math. Soc. **32**, 1 (1995).
[55] J. Feinberg and A. Zee, Non-hermitian random matrix theory: Method of hermitian reduction, Nucl. Phys. B **504**, 579 (1997).
[56] H. J. Sommers, A. Crisanti, H. Sompolinsky, and Y. Stein, Spectrum of Large Random Asymmetric Matrices, Phys. Rev. Lett. **60**, 1895 (1988).
[57] E. Kanzieper and G. Akemann, Statistics of Real Eigenvalues in Ginibre's Ensemble of Random Real Matrices, Phys. Rev. Lett. **95**, 230201 (2005).
[58] P. J. Forrester and T. Nagao, Eigenvalue Statistics of the Real Ginibre Ensemble, Phys. Rev. Lett. **99**, 050603 (2007).
[59] R. Hamazaki, K. Kawabata, N. Kura, and M. Ueda, Universality classes of non-Hermitian random matrices, Phys. Rev. Res. **2**, 023286 (2020).
[60] G. Akemann, M. Kieburg, A. Mielke, and T. Prosen, Universal Signature from Integrability to Chaos in Dissipative Open Quantum Systems, Phys. Rev. Lett. **123**, 254101 (2019).
[61] P. Ribeiro and T. Prosen, Integrable Quantum Dynamics of Open Collective Spin Models, Phys. Rev. Lett. **122**, 010401 (2019).
[62] L. Sá, P. Ribeiro, and T. Prosen, Complex Spacing Ratios: A Signature of Dissipative Quantum Chaos, Phys. Rev. X **10**, 021019 (2020).
[63] L. Sá, P. Ribeiro, and T. Prosen, Integrable nonunitary open quantum circuits, Phys. Rev. B **103**, 115132 (2021).
[64] J. Li, T. Prosen, and A. Chan, Spectral Statistics of Non-Hermitian Matrices and Dissipative Quantum Chaos, Phys. Rev. Lett. **127**, 170602 (2021).
[65] A. M. García-García, L. Sá, and J. J. M. Verbaarschot, Symmetry Classification and Universality in Non-Hermitian Many-Body Quantum Chaos by the Sachdev-Ye-Kitaev Model, Phys. Rev. X **12**, 021040 (2022).
[66] A. Altland and M. R. Zirnbauer, Nonstandard symmetry classes in mesoscopic normal-superconducting hybrid structures, Phys. Rev. B **55**, 1142 (1997).
[67] D. Bernard and A. LeClair, A Classification of Non-Hermitian Random Matrices, in *Statistical Field Theories*, NATO Science Series Vol. 73, edited by A. Cappelli and G. Mussardo (Kluwer Academic Publishers, Springer, Dordrecht, 2002), pp. 207–214.
[68] H. Zhou and J. Y. Lee, Periodic table for topological bands with non-Hermitian symmetries, Phys. Rev. B **99**, 235112 (2019).
[69] W. H. Press, S. A. Teukolsky, W. T. Vetterling, and B. P. Flannery, *Numerical Recipes: The Art of Scientific Computing* (Cambridge University Press, Cambridge, 2007).
[70] Tiny apparent imaginary parts of real eigenvalues stem from the machine inaccuracy of a numerical subroutine program. We can estimate their upper bound (error bound) by numerical diagonalization of Hermitian random matrices based on the same subroutine program. By the diagonalization, we observe that when eigenvalues of an N-by-N Hermitian random matrix in the Gaussian ensemble are in a range of $[-\Lambda, \Lambda]$ with $\Lambda = O(1)$,

the upper bound of the imaginary parts of the eigenvalues is of the order of 10^{-15}–10^{-14} for $100 \leqslant N \leqslant 4000$. Based on this observation, we set the cutoff C of the imaginary part to $C = 10^{-13}$. To be specific, we first normalize an N-by-N non-Hermitian random matrix in the Gaussian ensemble such that its complex eigenvalues E are distributed within a circle of the order of 1 [i.e., $|E| \lesssim O(1)$]. Then, we regard any complex eigenvalue of the random matrix whose imaginary parts are less than $C = 10^{-13}$ as real. The cutoff C is much larger than the error bound, so that it shall not miss any real eigenvalues of the matrix. The probability P of complex eigenvalues being mistaken as real depends on N and is negligible for $N < 10^4$. To evaluate this probability P, let us suppose that complex eigenvalues E of the non-Hermitian random matrix are distributed uniformly within the circle [i.e., $|E| \lesssim O(1)$]. Then, the probability p that a given complex eigenvalue of the random matrix is mistaken as real is of the order of $C = 10^{-13}$, and the probability P that complex eigenvalues are mistaken as real is estimated as $P = 1 - (1 - p)^N \simeq Np$. This probability is negligible for $N < 10^4$ because $p \sim C = 10^{-13}$. This justifies our setting of the cutoff C in this paper, where N is typically less than 10^4.

[71] M. A. M. de Aguiar and Y. Bar-Yam, Spectral analysis and the dynamic response of complex networks, Phys. Rev. E **71**, 016106 (2005).

[72] Y. Y. Atas, E. Bogomolny, O. Giraud, and G. Roux, Distribution of the Ratio of Consecutive Level Spacings in Random Matrix Ensembles, Phys. Rev. Lett. **110**, 084101 (2013).

[73] G. Marinello and M. P. Pato, Statistical properties of eigenvalues of an ensemble of pseudo-Hermitian Gaussian matrices, Phys. Scr. **94**, 115201 (2019).

[74] E. Chertkov, B. Villalonga, and B. K. Clark, Numerical Evidence for Many-Body Localization in Two and Three Dimensions, Phys. Rev. Lett. **126**, 180602 (2021).

[75] X. Yu, D. J. Luitz, and B. K. Clark, Bimodal entanglement entropy distribution in the many-body localization transition, Phys. Rev. B **94**, 184202 (2016).

[76] A. K. Kulshreshtha, A. Pal, T. B. Wahl, and S. H. Simon, Behavior of l-bits near the many-body localization transition, Phys. Rev. B **98**, 184201 (2018).

[77] M. Goihl, M. Gluza, C. Krumnow, and J. Eisert, Construction of exact constants of motion and effective models for many-body localized systems, Phys. Rev. B **97**, 134202 (2018).

[78] T. E. Lee and C.-K. Chan, Heralded Magnetism in Non-Hermitian Atomic Systems, Phys. Rev. X **4**, 041001 (2014).

[79] A. J. Daley, Quantum trajectories and open many-body quantum systems, Adv. Phys. **63**, 77 (2014).

[80] Y. Asada, K. Slevin, and T. Ohtsuki, Anderson Transition in Two-Dimensional Systems with Spin-Orbit Coupling, Phys. Rev. Lett. **89**, 256601 (2002).

[81] F. Geissler, F. Crépin, and B. Trauzettel, Random Rashba spin-orbit coupling at the quantum spin Hall edge, Phys. Rev. B **89**, 235136 (2014).

[82] A. MacKinnon and B. Kramer, One-Parameter Scaling of Localization Length and Conductance in Disordered Systems, Phys. Rev. Lett. **47**, 1546 (1981).

[83] A. MacKinnon and B. Kramer, The scaling theory of electrons in disordered solids: Additional numerical results, Z. Phys. B **53**, 1 (1983).

[84] K. Slevin and T. Ohtsuki, Critical exponent for the Anderson transition in the three-dimensional orthogonal universality class, New J. Phys. **16**, 015012 (2014).

[85] P. Sierant and J. Zakrzewski, Level statistics across the many-body localization transition, Phys. Rev. B **99**, 104205 (2019).

[86] A. D. Mirlin, Y. V. Fyodorov, F.-M. Dittes, J. Quezada, and T. H. Seligman, Transition from localized to extended eigenstates in the ensemble of power-law random banded matrices, Phys. Rev. E **54**, 3221 (1996).

[87] N. Rosenzweig and C. E. Porter, "Repulsion of Energy Levels" in Complex Atomic Spectra, Phys. Rev. **120**, 1698 (1960).

[88] V. E. Kravtsov, I. M. Khaymovich, E. Cuevas, and M. Amini, A random matrix model with localization and ergodic transitions, New J. Phys. **17**, 122002 (2015).

[89] C. L. Bertrand and A. M. García-García, Anomalous Thouless energy and critical statistics on the metallic side of the many-body localization transition, Phys. Rev. B **94**, 144201 (2016).

[90] Y. C. Hu and T. L. Hughes, Absence of topological insulator phases in non-Hermitian PT-symmetric Hamiltonians, Phys. Rev. B **84**, 153101 (2011).

[91] K. Kawabata and M. Sato, Real spectra in non-Hermitian topological insulators, Phys. Rev. Res. **2**, 033391 (2020).

[92] H.-P. Breuer and F. Petruccione, *The Theory of Open Quantum Systems* (Oxford University Press, Oxford, 2002).

[93] S. Lieu, M. McGinley, and N. R. Cooper, Tenfold Way for Quadratic Lindbladians, Phys. Rev. Lett. **124**, 040401 (2020).

[94] K. Mochizuki, N. Hatano, J. Feinberg, and H. Obuse, Statistical properties of eigenvalues of the non-Hermitian Su-Schrieffer-Heeger model with random hopping terms, Phys. Rev. E **102**, 012101 (2020).